



UNIL | Université de Lausanne

Unicentre

CH-1015 Lausanne

<http://serval.unil.ch>

Year : 2015

Advanced quantitative Magnetic Resonance Imaging to study the physiopathology of Multiple Sclerosis

BONNIER Guillaume

BONNIER Guillaume, 2015, Advanced quantitative Magnetic Resonance Imaging to study the physiopathology of Multiple Sclerosis

Originally published at : Thesis, University of Lausanne

Posted at the University of Lausanne Open Archive <http://serval.unil.ch>

Document URN : urn:nbn:ch:serval-BIB_DDCB86EBA1F18

Droits d'auteur

L'Université de Lausanne attire expressément l'attention des utilisateurs sur le fait que tous les documents publiés dans l'Archive SERVAL sont protégés par le droit d'auteur, conformément à la loi fédérale sur le droit d'auteur et les droits voisins (LDA). A ce titre, il est indispensable d'obtenir le consentement préalable de l'auteur et/ou de l'éditeur avant toute utilisation d'une oeuvre ou d'une partie d'une oeuvre ne relevant pas d'une utilisation à des fins personnelles au sens de la LDA (art. 19, al. 1 lettre a). A défaut, tout contrevenant s'expose aux sanctions prévues par cette loi. Nous déclinons toute responsabilité en la matière.

Copyright

The University of Lausanne expressly draws the attention of users to the fact that all documents published in the SERVAL Archive are protected by copyright in accordance with federal law on copyright and similar rights (LDA). Accordingly it is indispensable to obtain prior consent from the author and/or publisher before any use of a work or part of a work for purposes other than personal use within the meaning of LDA (art. 19, para. 1 letter a). Failure to do so will expose offenders to the sanctions laid down by this law. We accept no liability in this respect.



UNIL | Université de Lausanne

Faculté de biologie
et de médecine

Advanced quantitative Magnetic Resonance Imaging to study the physiopathology of Multiple Sclerosis

Thèse de doctorat ès sciences de la vie (PhD)
présentée à la
Faculté de biologie et de médecine de l'Université de Lausanne
par

Guillaume BONNIER

présenté le 22 Mai 2015
à la Faculté de Biologie et Medecine
programme doctoral en Science de la Vie
université de Lausanne

pour l'obtention du grade de Docteur ès Sciences
par

acceptée sur proposition du jury:

Prof. Du Pasquier Renaud, président du jury
Prof. Thiran Jean-Philippe, directeur de thèse
Dr Granziera Cristina, co-directrice de thèse
Prof. Radü Ernst Wilhelm, Expert
Dr Krueger Gunnar, Expert

Lausanne, UNIL, 2015



UNIL | Université de Lausanne

Faculté de biologie
et de médecine

Ecole Doctorale

Doctorat ès sciences de la vie

Imprimatur

Vu le rapport présenté par le jury d'examen, composé de

Président	Monsieur Prof. Renaud Du Pasquier
Directeur de thèse	Monsieur Prof. Jean-Philippe Thiran
Co-directeur de thèse	Madame Dre Cristina Granziera
Experts	Monsieur Prof. Ernst Wilhelm Radü
	Monsieur Dr Gunnar Krueger

le Conseil de Faculté autorise l'impression de la thèse de

Monsieur Guillaume Bonnier

Master de l' Ecole Supérieure de Chimie Physique Electronique de Lyon

intitulée

**Advanced quantitative Magnetic Resonance Imaging to study
the pathophysiology of Multiple Sclerosis**

Lausanne, le 28 août 2015

pour le Doyen
de la Faculté de biologie et de médecine

Prof. Renaud **Du Pasquier**

Acknowledgements

This thesis would not have been realized without the support of many people. I wish to express my gratitude to all these people for their comments and many interesting suggestions and encouragement I received during these years.

First, I thank my supervisor, Prof. Jean-Philippe Thiran, for his encouragement and support. I also would like to thank my co-supervisor Dr. Cristina Granziera for her support and especially for her patience and presence to discuss and improve my work each time I needed. Her advice, remarks and critical comments on my work have played an important role in the content and presentation of this thesis. The work environment was very pleasant and I was very lucky to work with such a person.

I am thankful to the jury of my thesis: Prof. Ernst Radue, Dr. Gunnar Krueger and the president of the jury Dr. Renaud Du Pasquier. They made me proud of my achievements in this thesis and supported me to go further in my research career. I especially thank Dr. Krueger who initiated me into the biomedical research field.

I would like to thank all my colleagues: Tobias Kober for his help but mainly for the special humor we share, Alexis Roche for his valuable advice in statistics and many other fields but also for the very instructive and fun coffee breaks we had, Bénédicte Mortamet for her delicacy in this world of brutal physics and for the "CPE connexion" unbreakable link, Davide Piccini for his jokes of course, and Kieran O'Brien for his incomparable New Zealand accent. I shall not forget Chems, Tom, Pavel, Maryna and Mario Joao for the perfect working atmosphere and the barbecues!

I reserve a special word to thank "ma Elda" for her help and support during before and during this thesis but before all for her love...and her delicious tortillas. Je t'aime guapa! I also have to mention Cléo, who reminds me every day what really matters, to be happy...and to eat.

The warmest thanks to my uncles, aunts and cousins from Marseille...and especially Dominique et Alain for their support during my final presentation but also the party ;-)

Finally I would like to thank my parents for their love and support during all these years and the next ones. They gave me the opportunity to do and achieve what I wanted without ever questioning my choices, I thank you for that and I hope I'll be as good with Cléo as you were with me. And to finish I want to thank my little sister, for her unconditional love and franchise whatever happen and how far we are, merci minote! Je vous aime...

Lausanne, 17 Avril 2015

G. B.

Preface

Multiple sclerosis (MS) is one of the most common disease of the central nervous system affecting young adults. MS affects indeed about 2 million of people of any age and gender although it has a special preference for young people, for women and for those in northern latitudes. MS symptoms can vary among patients including visual, motor, sensory and cognitive deficit leading to significant impact on personal and social daily-life of patients.

Historically, MS has been described for the first time in 1868 by Jean-Martin Charcot, a professor at the university of Paris, who observed the characteristic scars or "plaques" of MS during an autopsy. Seminal studies performed in the late 19th and early 20th centuries showed MS was characterized by demyelinated lesions around veins and inflammatory activity. During the 20th century, the development of several scientific domains, such as biology, led to attribute MS damage to a dysfunction of the immune system. Though the exact causes of MS remain unclear, several treatments and therapies have been developed so far to attenuate neurological damage by reducing the pathological immune response. In the 1980's, the emergence of Magnetic Resonance Technology provided images of MS pathology (focal "plaques") leading to more rapid diagnosis and a better monitoring of the disease and treatment effects. The development of Magnetic Resonance Imaging (MRI) provided new insights on the changes due to MS in the whole-brain, which included cortical and subcortical gray matter in addition to the classical white matter "plaques". Furthermore, it became clear that the normal appearing tissue was also altered in MS patients compared to healthy population.

Nowadays, MRI is a fundamental part of MS diagnosis and is mainly used for lesions detection and qualitative estimation of lesions volume. However, though advances in conventional MRI improved images sensitivity to measure mechanisms such as inflammation or tissue loss, they lack of sensitivity to detect diffuse pathology and suffer from a poor correlation with clinical symptoms. In this context, in the last decades new advanced techniques have emerged such as diffusion imaging, relaxometry, magnetization transfer imaging and magnetic resonance spectroscopy, providing more specific and sensitive tools to assess diffuse pathology. And recently, it became clear that the combination of different MR contrasts or modalities would improve our understanding of the underlying processes leading to neurodegeneration.

This dissertation presents a new approach combining several advanced MRI techniques to study the overall effects of MS pathology in brain tissue at early stages of the disease. We performed an extensive analysis to detect and identify diffuse and focal changes in normal appearing tissue, MS lesions and basal ganglia, but also to reveal the dynamics of these changes in these regions.

Preface

The pathogenesis of MS is very complex and multifactorial, with both genetic susceptibility and environmental causes involved. Although they remain unclear, we know that these causes lead to the propagation of the immune response and provokes brain damage observed in MRI. In the first chapter, we briefly describe the MS pathogenesis and the different courses of the disease, as well as the role of conventional and non-conventional MRI in our understanding of MS pathology.

In Chapter 2, we present our approach combining relaxometry and magnetization transfer imaging to detect and identify subtle and diffuse tissue alteration in MS patients. We performed a comparative analysis on a group of relapsing-remitting MS patients with minor deficit and a group of controls. We also correlate our MRI observations with clinical symptoms characterized by motor and cognitive scores.

In Chapter 3, we used our approach to classify MS lesions according to the different mechanisms occurring in these plaques.

In the Chapter 4, we focused on basal ganglia by using a new technique to estimate the partial volume. The deep gray matter nuclei are indeed very challenging regions considering the presence of mixture of brain tissue. Therefore, we propose to measure the proportion of tissue in each voxel and to extract their characteristic MR signal in order to provide additional information on the altered tissue.

Finally, the Chapter 5 present the results of a longitudinal study performed over 2 years. We measured the dynamics of MS mechanisms in the normal appearing tissue and MS lesions based on multi-contrast analysis. Last, we exploit the information of advanced MRI to predict patients clinical outcome at 2 years follow up.

Abstract

Multiple sclerosis (MS) is the most common disabling neurological disease of young adults around the world, affecting about 2 million of people of any age and gender. Typical symptoms can vary among patients and include visual, motor, sensory and cognitive deficits which may significantly impact patients personal and social life. Described for the first time in 1868 by Jean-Martin Charcot, MS has been intensely studied since then and is now defined as a chronic inflammatory autoimmune demyelinating disease of the central nervous system. In the 1980's, the emergence of Magnetic Resonance Technology provided new insights on brain pathology in MS, and improved the monitoring of available pharmacological therapies. Nowadays, magnetic resonance imaging (MRI) is a fundamental part of MS diagnosis, and in the last decades new advanced MRI techniques have emerged providing more specific and sensitive tools to assess not only local pathology (plaques) but also diffuse alteration in the brain tissue.

In this thesis, we present an approach combining new advanced MRI techniques including relaxometry and magnetization transfer imaging, to analyse brain tissue micro-structure properties in MS patients. We show how to take advantage of the complementarity of quantitative and semi-quantitative MRI sensitivity, to identify the physio-pathological processes underlying tissue alterations in normal appearing tissue, MS lesions and deep gray matter nuclei. We then extend our multi-contrast approach to model the heterogeneity of tissue damage in MS lesions through a classification framework, and present an innovative technique based on partial volume estimation, to provide additional information on the micro-properties of the tissue in thalamus and basal ganglia. Last, we show the potential of our approach to monitor MS disease over time, and to identify complex mechanisms such as repair and degeneration activity.

Our work provides evidence of the potential of multi-contrast advanced MRI to study the physiopathology of MS over the whole brain, even at early stages of the disease. Though these state-of-the art MRI techniques require more sophisticated hardware and software than conventional MRI, recent advances in acquisitions speed and robustness render them strong candidates for clinical applications in next future.

Key words: Multiple Sclerosis, Advanced MRI, Quantitative imaging techniques, Micro-structure analysis, Multi-contrast.

Résumé

La Sclérose en Plaques (SEP) est la maladie neurologique chez les jeunes adultes la plus commune dans le monde, touchant 2 millions de personnes de tout âge et genre. Les symptômes classiques peuvent varier parmi les patients incluant des déficits visuel, moteur, sensoriel et cognitif qui ont un impact significatif sur leur quotidien et leur vie sociale. Décrites pour la première fois en 1868 par Jean-Martin Charcot, la SEP, qui a été depuis intensément étudié, est une maladie auto-immune et inflammatoire chronique affectant le système nerveux central. Dans les années 1980, l'émergence de la technologie de résonance magnétique a fourni une nouvelle vision des modifications du tissu cérébral provoqués par la maladie, et a amélioré le suivi des traitements et des thérapies développées jusqu'alors. De nos jours, l'Imagerie par Résonance Magnétique (IRM) est devenue fondamentale lors du diagnostic de la SEP, de plus ces dernières années l'émergence de nouvelles techniques avancées a permis le développement d'analyses plus spécifiques et sensibles aux pathologies diffuse de la SEP.

Dans cette thèse, nous présentons une nouvelle approche combinant de nouvelles techniques avancées d'imagerie dont la relaxometrie et l'imagerie par transfert magnétique, afin d'analyser les propriétés micro-structurelles du tissu cérébral chez les personnes atteintes de SEP. Nous montrons comment profiter de la complémentarité des contrastes IRM pour identifier les processus physiopathologiques sous-jacents dans les tissu d'apparence normale, les lésions et les noyaux gris. Nous étendons ensuite notre approche en modélisant l'hétérogénéité des lésions de la SEP à l'aide d'une méthode de classification, puis nous présentons une technique innovante basée sur l'estimation du volume partiel qui fourni de nouvelles informations sur la microstructure du thalamus et des noyaux gris centraux. Enfin, ces travaux révèlent le potentiel de notre approche pour assurer le suivi de la maladie, et ainsi identifier des mécanismes complexes tels que la dégénérescence et la capacité de réparation du cerveau. En conclusion, nos travaux prouvent le potentiel de ses nouvelles techniques IRM pour étudier la physiopathologie de la SEP dans toutes les parties du cerveau, même aux premiers stades de la maladie. Bien que ces nouvelles techniques d'acquisition requièrent des méthodes de traitement plus sophistiquées, les récentes avancées en termes de rapidité et de robustesse des acquisitions IRM en font de sérieux candidats pour les applications cliniques des années à venir.

Mots clefs : Sclérose en Plaques, IRM avancé, Techniques d'imagerie quantitative, Analyse de la micro-structure, Multi-contrast.

Contents

Acknowledgements	i
Preface	iii
Abstract (English/Français)	v
List of figures	xiii
List of tables	xvii
1 Neuromaging in Multiple Sclerosis	1
1.1 Introduction	1
1.2 Multiple sclerosis	1
1.2.1 Pathogenesis of MS	1
1.2.2 Clinical onset and diagnosis	2
1.2.3 MS subtypes	3
1.3 Magnetic Resonance Imaging in Multiple Sclerosis	4
1.3.1 Conventional MRI in MS	5
1.3.2 Non-conventionall MRI in MS	7
1.3.3 Mulitmodal approach	11
1.3.4 Conclusion	11
2 Multi-contrast MRI for normal appearing tissue analysis	13
2.1 Introduction	14
2.2 Method	14
2.2.1 Study population	14
2.2.2 Clinical assessment	15
2.2.3 MRI techniques	15
2.2.4 MRI contrasts	17
2.2.5 Image analysis and tissue segmentation	19
2.2.6 Statistical analysis	20
2.3 Results	22
2.4 Discussion	25
2.5 Conclusion	26

3	Multi-contrast MRI quantification of focal inflammation and degeneration in multiple sclerosis	27
3.1	Introduction	28
3.2	Method	28
3.2.1	Lesion segmentation	28
3.2.2	Lesion classification	29
3.2.3	Statistical analysis	30
3.3	Results	31
3.4	Discussion	33
3.5	Conclusion	34
4	A new approach for deep gray matter analysis using partial volume estimation	35
4.1	Introduction	36
4.2	Method	36
4.2.1	Image processing	36
4.2.2	Qualitative assessment	37
4.2.3	Quantitative assessment	38
4.3	Results	39
4.3.1	Qualitative assessment	39
4.3.2	Quantitative group comparison using global ROI averaging, T1 tissue intensities and concentrations	40
4.4	Discussion	42
4.5	Conclusion	44
5	Longitudinal analysis of multi-contrast advanced MRI	45
5.1	Introduction	46
5.2	Methods	46
5.2.1	Tissue and lesions segmentation and images registration	47
5.2.2	Image processing and lesions classification	47
5.2.3	Statistical analysis	47
5.3	Results	49
5.3.1	Normal appearing tissue and volume analysis	49
5.3.2	Lesions	50
5.3.3	Regression analysis	52
5.4	Discussion	53
5.5	Conclusion	55
6	Conclusion : Achievements and Perspectives	57
6.1	Achievements	57
6.2	Perspectives	58

A Appendix	61
A.1 Preliminary analysis on lesions classification	61
A.2 Longitudinal analysis of RRMS patients and controls	64
Bibliography	84
Curriculum Vitæ	85

List of Figures

1.1	Clinical course of MS subtypes.	4
1.2	T1-w MPRAGE, T2-w FLAIR of MS patients with lesions (red arrows). Lesion appear brighter on T2-w images, and darker on T1-w images.	6
1.3	T1, T2 and MTR images of MS patients with lesions. On T1 and T2 quantitative maps, lesion appears bright while it appears darker on MTR image.	8
2.1	Example of MR images from MS advanced protocol : MP2RAGE uniform image, MPRAGE, DIR, 3D FLAIR images as well as MP2RAGE T1, T2, T2*, and MTR maps for one healthy control subject (first two rows) and one MS patient (last two rows). Examples of lesions are shown by red arrows in the images from the MS patient.	18
2.2	Biophysical basis of MRI contrasts. ++: increase; - : decrease. Big red arrow: large increase; small red arrow: small increase. Big blue arrow: large decrease; small blue arrow: small decrease.	19
2.3	Example of tissue segmentation and lobe parcellation using in-house software MorphoBox. The segmentation was obtained using MPRAGE image as input.	20
2.4	Histograms and boxplots of T2 and T2* in RRMS patients and HC. (A) (Top): T2* and T2 mean histograms in NAWM (temporal lobe) for HC (blue) and MS patients (red); (B) (Below): Boxplots of T2* and T2 in NAWM (temporal lobe) for HC (left) and MS patients (right).	23
2.5	Mean z-scores of T1, MTR, T2, and T2* of MS lesions per patient. Each column represents a patient.	24
3.1	Pipeline for MS lesions classification using multi-contrast approach. Computation of lesion fingerprint using z-score measurement.	30
3.2	List of the 12 combinations of MS lesions z-scores for T1, T2, T2* and MTR q/sq MRI from the least (combination 1) to the most (combination 12) severe stage. The presence of irreversible tissue loss was considered a sign of higher severity than inflammation.	31
3.3	Distribution of lesions among combinations and distribution of combination among patients. Combinations 1 (non significant z-score in all contrasts) and 4 (isolated high T1 z-score) count more than 50% of all lesions and are the combinations mostly found in all patients.	32

List of Figures

4.1	Comparison between 2 axial slices of GM concentration maps (first row) and Statistical Parametric Mapping (SPM) GM probabilistic maps (second row) at 3T. The SPM map mainly shows binary concentrations, and some parts (pointed out by red arrows) of the thalamus and putamen disappear compared with concentration maps.	38
4.2	GM concentration map using T1 maps of 3 healthy subjects at 3T and histological slice with an outline of nuclei of the thalamus on a coronal Myelin-Nissl-stained section (right).	39
4.3	Comparison between GM concentration map of 3 healthy subjects at 7T and an histological slice from a healthy human subject . The concentration map were estimated using the whole-brain T1 map. In the zoomed area of GM concentration map we can observe the gray matter bridge present in the histological slice between the caudate and the putamen.	40
4.4	Boxplots of the WM and GM of the thalamus for RRMS patients and controls using the proposed PV method. It shows significant increase in the T1 of the GM components between the RRMS patients and HC.	41
4.5	Boxplots of the WM and GM of the putamen for RRMS patients and controls using PV method. This method showed no significant increase in the T1 of the GM and WM components neither concentration ratio between the RRMS patients and HC.	41
4.6	Boxplot of mean T1 in the thalamus and putamen using global averaging method. This method showed significant increase of T1 in both ROIs in RRMS patients compared with HC.	42
5.1	Evolution of lesions among the different group based on qMRI combination.	51
5.2	Example of new lesions on q/sq MRI contrasts. Though we found significant difference between normal appearing tissue and HC in regions where lesions will appear (red square), we can not see any evidence of changes in q/sq MRI before lesions appearance.	52
6.1	Pipeline for deviation maps computation. The inputs are the q/sq MRI concentration maps, as well as the normative ranges of WM and GM in each brain structure.	58
6.2	Deviation maps of T1, T2 and MTR contrast. In order to adapt the colormap to the T1 and T2 contrasts, the MTR deviation map shows the opposite of the MTR z-score ($z_{MTR} = -z$). The color code shows in dark blue the negative z-scores (decrease of T1, T2 and an increase of MTR), in light blue a positive z-score, and in yellow to red a high z-score (increase of T1, T2 and decrease of MTR). Based on this color code, the analysis of the lesions shows strong changes in T1, T2 and MTR z-scores within the lesions but also in the surrounding area.	59

A.1	Distribution of all lesions according to their T1, T2 and MTR z-score. The distribution shows no cluster. The red dashed lines delimit the threshold manually set for lesion classification.	62
A.2	Distribution of lesions z-scores according to their type, size and location. Cortical lesions appeared to have lower z-score, due to their low contrast. No sign of correlation between T1, T2, T2* and MTRz-score value and lesions size and location.	63
A.3	Boxplot of the difference of T1 of normal appearing tissue in patients between time-points. T1 relaxation times increase in WM and GM of the temporal lobe and in the WM of the cerebellum.	64
A.4	Boxplot of the difference of T1 of normal appearing tissue of controls between time-points. T1 relaxation times increase in WM and GM of the temporal lobe and in the WM of the cerebellum.	65
A.5	Boxplot of T2 difference of normal appearing tissue in patients between time-points. T2 relaxation times decrease in pallidum, putamen and WM of the parietal, frontal and parietal lobes but increases in the caudate and MG of the frontal lobe.	66
A.6	Boxplot of T2 difference of normal appearing tissue in controls between time-points. T2 relaxation times decrease in pallidum, putamen and WM of the parietal, frontal and parietal lobes but increases in the caudate and MG of the frontal lobe.	67
A.7	Boxplot of T2* and MTR differences of normal appearing tissue between time-points. T2* relaxation times increases in caudate, putamen and WM of the cerebellum, while MTR decreases in the GM of the occipital lobe.	68
A.8	Evolution of lesions among the different group based on qMRI combination.	69
A.9	Difference between T1, T2 and MTR in RRMS patients at TP1 in regions where lesions appear at TP2 and T1, T2, MTR of the healthy normal appearing tissue in the corresponding lobes (HC), and T1, T2, MTR at TP1 in the normal appearing tissue surrounding the region (NA).	70
A.10	Difference between T1, T2, T2* and MTR in RRMS patients at TP1 in regions where lesions expand at TP2 and the T1, T2, T2* and MTR in healthy normal appearing tissue in the corresponding lobes (HC) and T1, T2, T2* and MTR in the normal appearing tissue surrounding the region (NA).	70

List of Tables

1.1	2010 revised McDonald MS diagnostic criteria. The diagnosis of MS requires elimination of more likely diagnose and demonstration of dissemination of lesions in space (DIS) and time (DIT).	3
2.1	Demographic characteristics of HC and RRMS patients.	14
2.2	Clinical tests (mean \pm std)	15
2.3	Detailed MS Advanced protocol sequences parameters. Total acquisition time 1h08'.	17
2.4	Regression analysis. Each line corresponds to the corrected p-values, and adjusted-R ² of each model (n=7) subjected to regression and cross-validation analysis. (***: p< 0.001), (** : p< 0.01), (* : p< 0.05).	25
3.1	Regression analysis of clinical scores using lesions characteristics. Each line corresponds to the corrected p-values, and adjusted-R ² of each model (n=7) subjected to regression and cross-validation analysis. (***: p< 0.001), (** : p< 0.01), (* : p< 0.05).	33
5.1	Paired two-sampled t-tests p-values for RRMS patients in significant ROIs for all contrast between TP1 and TP2. n.s : non significant.	50
5.2	Paired two-sampled t-tests p-values for controls in significant ROIs for all contrast between TP1 and TP2. n.s : non significant.	50
5.3	Regression results using MRI data from Time-point 1 to predict clinical scores from Time-point 2.	53

1 Neuromaging in Multiple Sclerosis

1.1 Introduction

Multiple sclerosis (MS) is the most common disabling neurological disease of young adults around the world. MS affects about 2 million of people of any age and gender, though it's most commonly diagnosed in women between the age of 20 and 50 years [1]. Typical symptoms include visual, motor, sensory and cognitive deficits as well as fatigue, leading to physical and cognitive disability. Therefore, MS has a significant personal, social and economic impact for patients and healthcare services. MS is a chronic inflammatory autoimmune demyelinating disease of the central nervous system (CNS). It affects the brain and the spinal cord through focal and diffuse alteration of brain tissue. Traditionally, MS has been characterized by the presence of focal demyelination; yet in the last decades, magnetic resonance imaging (MRI) studies revealed substantial cortical damage as well as diffuse changes in normal appearing (NA) tissue. Although MRI provided new insight in the pathophysiology of MS, the underlying mechanisms of brain degeneration remain unclear. The recent development of advanced MR techniques such as T1, T2, T2* relaxometry, magnetisation transfer imaging, diffusion imaging and spectroscopy may provide new and sensitive ways to characterize tissue biology and pathology in vivo in MS, in order to improve diagnostic, prognostic and follow-up methods.

1.2 Multiple sclerosis

1.2.1 Pathogenesis of MS

MS pathophysiology is complex and multifactorial. In fact, both genetic susceptibility and environmental factors contribute to the development of MS in a complex interplay. In an initial step, inflammatory cells cross into the CNS due to blood brain barrier leaks [2], then the immune response is propagated through the brain. A non specific immune response, the innate response, provokes first the production of small proteins so-called cytokines, which modulate an adaptive immune response [3]. The innate system plays a role both in the initiation and progression of MS by influencing the effector function of specialised defender

cells: the T and B cells. The adaptive response is in fact initiated by the presentation of a specific antigen to T lymphocytes using antigen presenting cells such as B cells, dendritic cells, microglia and macrophages. The propagation of these molecules and cytokines promotes inflammatory process and induce demyelination. Some studies observed a positive correlation of T-cells, macrophages and microglia with the extent of axonal damage [4], [5]. These results suggest that the myelin breakdown leaves axons vulnerable to pro-inflammatory mediators direct attacks. Myelin loss may also contribute to the disease process by activating microglia, which mediate neuronal damage [6]. There is also evidence that the loss of oligodendrocytes which provide trophic support to axons, leads to degeneration despite intact surrounding myelin and a lack of inflammation [7], [8]. These damages manifest by the appearance of focal lesions, which develop around small veins and venules in several regions of the brain, with a variable degree of inflammation, gliosis and axonal degeneration [9]. In addition to this degenerative aspect, the presence of newly formed myelin indicates signs of remyelination in MS lesions reflecting brain plasticity [10]. In the last decade, cortical demyelination has also emerged as a critical aspect of the pathogenesis of MS [11–14], as well as diffuse inflammation [15] and progressive neuroaxonal loss in NA tissue [7]. The complex interaction and overlap of these underlying processes induced by immune-mediated renders the clinical disease course of MS difficult to monitor and predict.

1.2.2 Clinical onset and diagnosis

Inflammatory and neurodegenerative processes in MS lead to physical and cognitive disabilities. MS symptoms can vary among patients and include muscle weakness, balance problems, loss of coordination and mobility, visual and sensory problems, speech difficulties, bowel, bladder and sexual dysfunction, as well as cognitive impairment. In this context, early diagnosis is important since treatment can slow the disease, improve patient daily life and decrease long-term disability. To date, MS is diagnosed based on the revised McDonald criteria 2010 [16], which rely on clinical and MRI data. These tests are based on the principles of dissemination in space (DIS) and dissemination in time (DIT) of the disease, and the exclusion of other diseases with similar characteristics. DIS and DIT are established using serial MR images. They allow to predict clinically definite MS diagnosis in 70% of patients who have experienced only a single clinically isolated syndrome (CIS) [17]. Recently, new guidelines have proposed to diagnose MS in a CIS patient using a single MRI scan [18].

1.2. Multiple sclerosis

Clinical (attack)	Lesions	Additional criteria
2 or more	Objective clinical evidence of more than 2 lesions or objective clinical evidence of 1 lesion with reasonable historical evidence of a prior attack	None. Clinical evidence alone will suffice, additional evidence desirable but must be consistent with MS
2 or more	Objective clinical evidence of 1 lesion	DIS; OR await further clinical attack implicating a different CNS site
1	Objective evidence of at least 2 lesions	DIT; OR await a second clinical attack
1	Objective clinical evidence of 1 lesion	DIS; OR await further clinical attack implicating a different CNS site AND DIT; OR await a second clinical attack
0 (progression from onset)		One year of disease progression (retrospective or prospective) AND at least two of : DIS in the brain based on at least 1 T2 lesion in periventricular, juxtacortical or infratentorial regions; DIS in the spinal cord based on at least 2 lesions or positive CSF

Table 1.1: 2010 revised McDonald MS diagnostic criteria. The diagnosis of MS requires elimination of more likely diagnose and demonstration of dissemination of lesions in space (DIS) and time (DIT).

1.2.3 MS subtypes

The complex pathogenesis of MS and the variety of symptoms among patients, make the clinical disease course of MS unpredictable. To date, four different clinical MS forms have been described (see Figure 1.1) [19]:

- Relapsing remitting (RRMS) affects 85% of MS patients and is characterized by episodes of exacerbations of symptoms followed by periods of remission.
- Secondary progressive (SPMS) develops in more than 50% of untreated patients affected by RRMS. The course of the disease continues to worsen with or without periods of remission or levelling of symptoms severity.
- Primary progressive (PPMS) is a form of MS which is more resistant to drugs typically used in MS therapy. The symptoms continue to worsen gradually without remission or relapse episodes with occasional plateaus. However few MS patients are affected by this subtype (10%).
- Progressive relapsing MD (PRMS) is the rarest form of MS (<5%). Its course is progressive

from the start without any period of remission.

The disease progression is usually assessed by neurological examination and disability rating scales such as the Expanded Disability Status Scale (EDSS) [20]. Nevertheless, these methods lack of sensitivity and specificity to monitor the disease course on short period of time. In this context, magnetic resonance imaging is an objective and sensitive tool, which may provide appropriate and reliable criteria to diagnose and monitor disease progression.

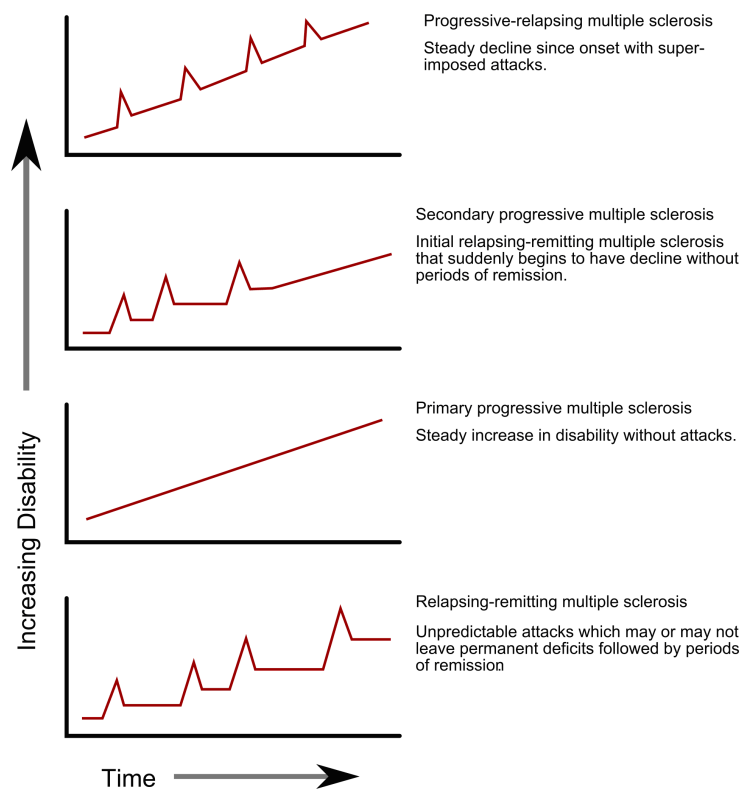


Figure 1.1: Clinical course of MS subtypes.

1.3 Magnetic Resonance Imaging in Multiple Sclerosis

Magnetic resonance imaging (MRI) plays an important role both for MS clinical management and the investigation of its pathophysiology. Conventional MRI techniques are routinely used for MS clinical diagnosis and patients follow-up. Nevertheless, they suffer from a number of limitations such as limited sensitivity to diffuse damage as well as low correlations with clinical tests. In this context, new emerging techniques such as diffusion imaging, relaxometry or magnetization transfer imaging propose a novel approach to assess at a time focal and diffuse pathology and support with new biomarkers correlating with clinical performances.

1.3.1 Conventional MRI in MS

Conventional MRI (cMRI) techniques are sequences used routinely on a standard clinical MRI scanner. In MS, they are mainly used for lesion detection and monitoring, but also for qualitative atrophy measurements. These sequences include proton density (PD), T2-weighted (T2-w), T1-weighted (T1-w), Fluid Attenuated Inversion Recovery (FLAIR) images and Gadolinium-enhanced T1-weighted imaging. Conventional MRI techniques have been developed to improve diagnosis and prognosis in MS by revealing mainly focal expression of MS pathology. Although to date, atrophy measurement are not a part of clinical routine, recent improvements in cMRI post-processing methods allow to perform off-line longitudinal volumetric analysis and atrophy rates of specific brain structures or the whole brain.

Conventional MR physics

MR technology is based on nuclear magnetic resonance of atoms within the body induced by the application of radio waves. The signal intensity on an MR image is determined by basic parameters characterizing tissue properties: the proton density (PD), and the relaxation times T1, T2 and T2*. The proton density is the concentration of protons in the tissue in the form of water and macromolecules (proteins, macrophages, etc). The relaxation times T1, T2 and T2* define the way that the protons revert back to their resting states after the initial RF pulse. They are representatives of the structural characteristics of the tissue. T1, T2 and PD weighted images are basic pulse sequences in MRI and are widely used in clinical application of MS. Recently, the FLAIR sequence has replaced the PD image. FLAIR images are T2-w with the CSF signal suppressed (see Figure 1.2). Recent improvements in MR field also allowed to provide high resolution (1mm³) images at high field (3T), and improve detection and identification of pathology of MS in the brain.

Focal inflammation and neurodegeneration in conventional MRI

cMRI allows visualisation of the structure of the brain, and the areas of focal damage due to the increased water content relative to the surrounding tissue. PD and T2-w images are standard sequences in clinical practice to detect MS lesions which appear as focal areas of signal increase. MS lesions observed from these sequences can occur throughout the entire CNS, but tend to predominate in the periventricular WM. In this area, due to the suppression of CSF signal in FLAIR, the lesions can be better distinguished from CSF spaces than in PD/T2-w images. T1-w images are mainly used to differentiate anatomical structures thanks to the high contrast between each tissue, where high proton density areas appear bright and low density dark. On T1-w images increased water such as oedema appear as hypointense. However, only 10-30% of lesions seen on T2-w images can be visualised on T1-w images, which suggests that these T2-w lesions invisible on T1-w may reflect inflammatory process. On the opposite side, the chronic T1 hypointensities so-called "black holes" indicate areas with severe tissue destruction which may reflect marked oedema with or without matrix destruction during acute phase of MS [21, 22]. During the active stage of MS, there is an increased permeability of the blood brain barrier and the contrast agent Gadolinium (Gd) is used with T1-w imaging to

identify areas of acute inflammation and distinguish active and inactive lesions. T1-w is indeed sensitive to paramagnetic substances such as Gd which appear bright. Gd-enhanced T1-w images provide an important tool to detect and distinguish acute/active and chronic/non-active lesions, but this method remain invasive and strongly affected by several factors such as Gd dose, image acquisition parameters and treatment during acute attacks [23].

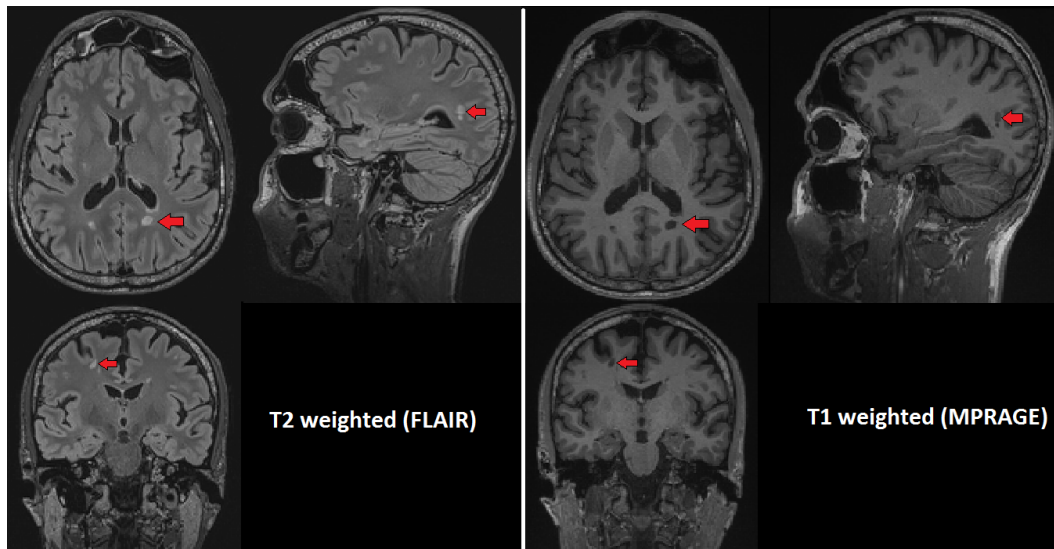


Figure 1.2: T1-w MPRAGE, T2-w FLAIR of MS patients with lesions (red arrows). Lesion appear brighter on T2-w images, and darker on T1-w images.

Recently, new approaches using cMRI have emerged based on serial analysis of images [24] or their subtraction [25], to relate signal changes to lesions evolution.

Global neurodegeneration in conventional MRI

Cerebral atrophy is a common feature of MS reflecting loss of neurons and the connections between them. Atrophy can be generalized or focal. In the last decade, brain volumetry has become an emerging technique based on conventional MRI data to provide sensitive and reproducible assessments of brain volumetry over time and hence atrophy rates. Several methods exist to assess brain atrophy based on segmentation or registration techniques [26,27]. Although it has been recognised as a feature of advanced or severe MS, some studies measured atrophy already in CIS and early stage patients [27]. A number of gray and white matter (WM) regions are affected by atrophy such as cerebral lobes, brainstem, cerebellum, thalamus and specific WM tracts [28]. Recent studies evidenced gray matter (GM) atrophy expressed by diffuse and focal thinning of cortex [29, 30]. A small cohort study showed cortical thinning in frontal and temporal cortex of early disease or mild disability patients [29] and a larger study reported significant correlations between cortical atrophy in the anterior cingulate cortex, insula and temporal gyrus with lesion load [30]. Cortical atrophy has also been shown to be the best predictor of future disability in MS patients [28,31]. Despite atrophy is related to neurodegeneration, the underlying mechanisms appear to differ depending

1.3. Magnetic Resonance Imaging in Multiple Sclerosis

on its location. Inflammation appeared more pronounced in WM areas compared with GM areas [28,32]. This suggests that atrophy in WM is mainly reflecting focal loss of myelin and axon following inflammation [28, 33, 34]. Yet, a longitudinal study suggested that WM volume may transiently increase due to presence of oedema, despite an increase of lesion load, masking sometimes the real brain volume loss [35]. Conventional MRI techniques provide measures of inflammation (T2-w lesions, gadolinium-enhancing T1-w lesions), in acute and chronic disease, and new post-processing methods applied to conventional sequences support with measures of degeneration (global brain atrophy) as well as with metrics of focal tissue loss (chronic black holes on T1-w images). Combined, they provide a unique insight into the dynamics of MS lesion development and the long-term pathological consequences on CNS tissues. However, cMRI showed weak associations with clinical status which may reflect its lack of sensitivity to detect diffuse disease. In this context, non-conventional techniques have emerged and may improve the detection of diffuse MS pathology and the correlation with clinical disabilities.

1.3.2 Non-conventionall MRI in MS

Non-conventional quantitative MRI techniques (qMRI) have raised in the last decades, and provided new insights into MS pathology. The signal intensity in conventional MRI is influenced by intrinsic contrast mechanisms, such as density of water proton and proton relaxation (T1, T2, T2*), but also by characteristics unrelated to tissue properties such as scan parameters, variation in the magnetic field and image scaling [36]. Quantitative imaging provides information on the tissue properties that is theoretically independent of hardware and sequence parameters. Quantification, therefore, allows comparisons across different sites, between different patients and different time-points [37]. In addition, qMRI provide biophysical parameters maps which are more specific for the microscopic structure of tissue than the mixed contrast images of conventional MRI. Advanced MR sequences require more sophisticated methods and post-processing approaches to compute parameters maps, which limit their use to research field. However recent advances in acquisition speed and robustness make them more suitable to clinical applications.

Relaxometry

Magnetic resonance relaxometry is a promising approach to assess tissue properties and composition *in vivo*. This quantitative method provides a more detailed characterization of tissue microstructure by establishing a more direct link between MRI signal and tissue microstructural properties. The term microstructure comprise neuronal bodies, unmyelinated and myelinated axons, glia cells, vessels, and extracellular-extravascular spaces. The biophysical parameters related to MR sequences are the proton density and the relaxation times T1, T2 and T2*.

T1 relaxation time (T1-rt) in brain tissue is mainly influenced by free water protons and the degree of structural organization (i.e. amount of macromolecules such as myelin, lipids,

Chapter 1. Neuromaging in Multiple Sclerosis

proteins). Myelin shortens T1 as the lipid composing myelin sheath do not contribute to signal. In this context, an increase in T1-rt may indicate a loss of structure or myelin and/or an increase in water content (see Figure 1.3). Conversely, greater density of macromolecules and reduced water content as well as iron accumulation tend to reduce T1 [38].

T2-rt measures the loss of spin coherence and therefore, mainly reflect the dynamic state of water protons and their interaction with macromolecules. An increase in T2-rt characterizes a loss of macromolecules and/or increased water content. On the contrary, a decrease in T2-rt reflects an increase of protons bound to macromolecules. As for T1, iron accumulation also causes a shorter T2 [39] (see Figure 1.3).

The effective T2*-rt transverse describes the loss of transverse magnetization due to T2 relaxation and magnetic field inhomogeneities (R2' component [40]). Possible sources are tissue-dependent differences in magnetic susceptibility or the presence of paramagnetic or ferromagnetic ions like iron. For these reasons, an increase in T2* most often indicates a loss of macromolecules, while a decrease suggests an increase of macromolecular compounds or iron that translate into an increase in R2'.

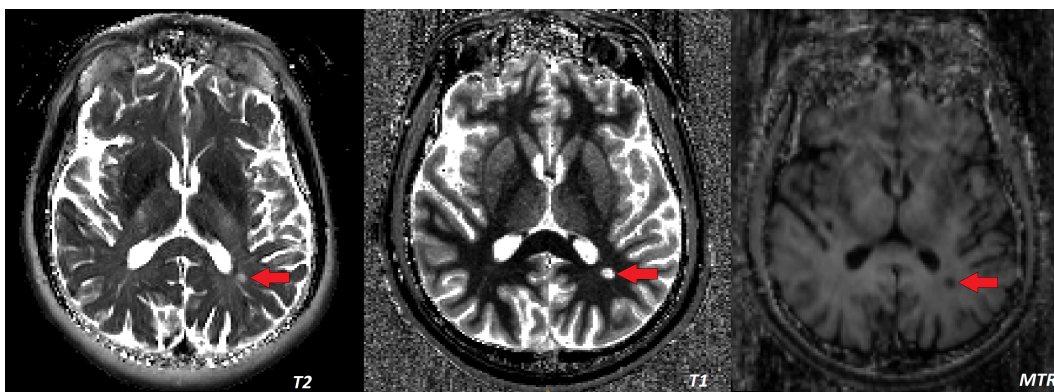


Figure 1.3: T1, T2 and MTR images of MS patients with lesions. On T1 and T2 quantitative maps, lesion appears bright while it appears darker on MTR image.

In the last decades, single scan relaxometry acquisitions have been extensively used in MS research (for review see [41, 42]). Several studies used quantitative imaging to assess diffuse processes such as inflammation and degeneration in normal-appearing (NA) tissue in MS patients. Neema and Whittall observed an increase of the T2-rt in the normal appearing white matter (NAWM) of a heterogeneous cohort of MS patients compared to healthy controls [43, 44], while Bakshi showed T2 increase in the deep GM [45]. These findings suggest diffuse inflammatory process in NA tissue. On the other hand, Vrenken used T1 mapping to observe global changes in the NA gray and WM in RR and SP MS patients with long disease duration [46], and Manfredonia et al. investigated global T1 changes in early stages of the disease and their correlation with disability [47]. The prolongation of T1-rt due to tissue or axonal/myelin loss appeared less pronounced compared to inflammation [48]. In addition, T1rt is more affected (longer) by axonal loss than myelin loss. Therefore, previous results reporting prolongation of

1.3. Magnetic Resonance Imaging in Multiple Sclerosis

T1-rt in NAWM and NAGM as well as WM/GM lesions might indicate the presence of different degrees of inflammation or degeneration.

Magnetization transfer imaging

Magnetization transfer (MT) imaging targets cross-relaxation and exchange between macromolecules and water. MT contrast is evoked by implementing additional off-resonance radio-frequency RF pulses into MRI sequences. Such an MT pulse reduces the longitudinal magnetization of the macromolecules, but has little effect on the free water. This saturation is then transferred to the water [49] and observed as an attenuated signal compared to the absence of pulses. In vivo MT measurements are quantified by a two pool model. Most relevant parameters are the macromolecular fraction and the forward transfer rate. The bound pool is larger in WM (11%) than in GM (4%), much smaller in blood, and practically absent in cerebro-spinal fluid (CSF) [50] (see Figure 1.3). Several metrics can be obtained from MTI scans. The first analysis step is the creation of MTR maps, derived from the two sets of images acquired with and without off resonance pulse. The MT ratio are derived by removing the signal of the free protons voxel-by-voxel according to the equation :

$$MTR = \frac{M_0 - M_T}{M_0} \quad (1.1)$$

with M_0 and M_T the T2* images acquired without and with MT pulse, respectively. MTR expresses macromolecular tissue integrity and provides both morphological and pathological information with a higher specificity than conventional MRI [51].

MT ratio which informs about myelin integrity and water content [52], has been widely used to perform histogram analysis of NA tissue in MS patients. Despite a limited difference found by Vrenken in MTR measure of NA tissue between controls and MS patients [53], Catalaa and others found a significant decrease of MTR in NA tissue of MS subjects compared to healthy controls [54]. Levesque and Tardif also used MTR to analyze lesion tissue in MS patients and observed a lower MTR in both subcortical and cortical lesions compared to healthy tissue [55, 56]. In all these studies, relative MTR decrease has been interpreted as the result of myelin loss. Nevertheless, inflammation and oedema also influence MTR [52], and should be take into account when interpreting MTR images.

Diffusion imaging

Diffusion imaging is based on the microscopic Brownian motion of water molecules. In a tissue, diffusion is 'hindered' by the semipermeable cell membranes, which couple the diffusivity in extra- and intracellular subspaces. In the axon bundles of WM, diffusion is anisotropic. The simplest model to describe the directional dependence of diffusion is an ellipsoid, the diffusion tensor (DT) [57]. The main diffusion direction is that along the parallel axons. The mean diffusion over all directions is mean diffusivity (MD). The degree of anisotropy is a scalar measure for axonal coherence, and is known as the fractional anisotropy (FA). Increased

MD and reduced FA are the hallmarks of demyelination. Pathological studies evaluated the physiological correlates of these diffusion indices [58], and a post-mortem study showed strong correlation between MD and FA with myelin content in chronic MS patients [59]. Abnormalities in diffusivity patterns have been observed in focal MS lesion and NA brain tissue (NABT). Several studies showed increase of MD and decrease of FA at various degrees in lesions compare with NABT [60, 61]. An histopathological study showed that MD reflects the advanced alteration of the tissue in chronic T1 hypointensities, where there is an irreversible tissue disruption, gliosis and axonal loss [21]. Conversely, a longitudinal study in patient revealed a progressive increase of MD only in a subgroup of Gd-enhancing lesions which were all showing MD increase at the beginning [62]. These results suggest that MD is sensitive to the different mechanisms in MS lesions such as neurodegeneration but also oedema, demyelination and remyelination. Unlike MD, FA appears higher in non-enhancing of lesions compared with Gd-enhancing lesions, reflecting a sensitivity to demyelination, axonal injury and large amount of inflammatory cells [61, 63]. Diffusion imaging provided also new insights on diffuse pathology in NABT. Several studies found abnormalities in diffusion metrics in the periphery of T2 lesions in the NAWM and NAGM, as well as in regions of NAWM close to newly appeared lesions [61, 64]. Global analysis also reported higher average MD and lower average FA in MS patients compared with healthy controls [65]. Diffusion tensor imaging properties, such as mean brain diffusivity or apparent diffusion coefficient in NABT and lesions, have also been suggested as strong predictors of clinical outcome [66]. Correlation between diffusion metrics in T2 lesions and disability were observed [67].

Magnetic resonance spectroscopy

Magnetic resonance spectroscopy (MRS) complements magnetic resonance imaging (MRI) as a non-invasive technique. Proton MRS uses the signal from hydrogen protons to determine the concentration of brain metabolites such as N-acetyl aspartate (NAA), choline (Cho), creatine (Cr) and lactate in the tissue examined. Hydrogen MRS has now become a routinely used clinical tool in the brain, and is widely used to study MS as it proposes potential specific biomarkers of demyelination, inflammation and neuronal/axonal integrity [68]. NAA, found exclusively in neurons, is a marker of neuronal viability and its decrease may reflect inflammatory conditions but also axonal or neuronal loss. Cho resonance have been associated with a protein expressing cells proliferation, and is also an important indicator, with Cr, of disease state such as demyelination. Lactate is absent in normal brain tissue and its presence is indicative of metabolic disorders. The combination of these different measurements provide specific information on the nature of mechanisms underlying brain tissue alteration. MRS studies showed indeed a diminished NAA peak and increased Cho and free-lipid peaks in acute MS lesions, suggesting demyelination and axonal loss [69–71]. The MRS was also used to evaluate neuronal damage in NAWM, where lower NAA-Cr ratio in patients was observed [69, 72]. In addition, correlations with clinical disability showed that MRS metabolic measurements were better predictors than conventional MRI [72, 73].

1.3.3 Multitmodal approach

The brain quantitative imaging techniques detailed above provide complementary information that is critical to understand the complexity of MS pathophysiology. However, to date, most qMRI studies applied a single contrast approach, which leads to important limitations when the results need to be interpreted [74]. In fact unicontrast studies can not discriminate single underlying mechanism. For example, magnetization transfer imaging alone cannot discriminate between myelin alterations and variation of water content in tissues [52]. As another example, DTI studies showed reduced fractional anisotropy (FA) in NAWM of early MS patients that was interpreted as axonal loss [75, 76]. Nevertheless, this interpretation may be misleading since loss of anisotropy can derive from the loss of the branched-shape of microglia cells that is typical of their activated-inflammatory form [77]. Thus, another possible explanation is that reduced FA might point to inflammatory rather than degenerative phenomena. In the last five years, multimodal approaches in MRI have become a popular method to study pathophysiology of neurodegenerative disease. The combination of different MR modalities or contrasts provided MR parameters sensitive to complementary tissue characteristics (atrophy, iron, microstructure damage...) which have a great potential to detect and identify pathological changes. In addition, multi-contrast approaches also show strong potential to improve disability prediction.

In MS, a number of studies tried to address the limitation of unicontrast ones by combining relaxometry, MTR measurements [78], and DTI [79]. Hasan et al. used T2 relaxometry and diffusion tractography maps to assess widespread pathology of RRMS patients. They focused their analysis on neocortical and corpus callosum regions, and observed increase in T2 and diffusivities suggesting inflammation. Their multimodal approach also improve correlation with disability scores [79]. In another study, Reich et al. proposed a multi-contrast approach associating relaxometry, diffusion and magnetization transfer imaging. They analysed the corticospinal tract of advanced MS patients, and found abnormalities along this tract such as MTR decreases or asymmetry [78].

1.3.4 Conclusion

MRI plays now a key role in the diagnosis and monitoring of MS by characterizing brain tissue properties in vivo and reducing the gap with clinical findings. The complex mechanisms underlying MS pathology are still unclear, but the ongoing advances in MRI technology should extend our understanding of disease effects on tissue microstructure. In this thesis, we combined advanced MRI techniques, including relaxometry, magnetization transfer imaging and new imaging techniques such as 3D Fluid Attenuated Inversion Recovery (FLAIR) and Double Inversion Recovery (DIR) sequences, to assess brain tissue microstructure properties of MS patients at early stage of the disease. We performed our analysis on NA tissue, MS lesions, but also focused on deep GM structures. In the next chapter, we present our multi-contrast approach applied to analyse diffuse changes in NA tissue.

2 Multi-contrast MRI for normal appearing tissue analysis

Abstract

In patients with multiple sclerosis (MS), conventional magnetic resonance imaging (MRI) provides only limited insights into the nature of brain damage with modest clinical-radiological correlation. In this chapter, we applied recent advanced MRI techniques to study brain micro-structural alterations in a early relapsing-remitting MS (RRMS) patients cohort with minor deficits. Further, we investigated the potential use of advanced MRI to predict functional performances in these patients. Brain relaxometry (T1, T2, T2*) and magnetisation transfer imaging were performed at 3T in 36 RRMS patients and 18 healthy controls (HC). Multi-contrast analysis was used to assess for micro-structural alterations in normal-appearing (NA) tissue and lesions. A generalized linear model was computed to predict clinical performance in patients using multi-contrast MRI data, conventional MRI measures as well as demographic and behavioural data as covariates. Results showed that quantitative T2 and T2* relaxometry were significantly increased in temporal normal appearing white matter (NAWM) of patients compared to HC, indicating subtle micro-edema ($T2 : p = 0.03$; $T2^* : p = 0.004$). Furthermore, significant T1 and magnetisation transfer ratio (MTR) variations in lesions (*mean T1 z-score: 4.42 and mean MTR z-score: -4.09*) suggested substantial tissue loss. Finally, combinations of multi-contrast and conventional MRI data significantly predicted cognitive fatigue ($p = 0.01$, $Adj-R^2 = 0.4$), attention ($p = 0.0004$, $Adj-R^2 = 0.6$), and disability ($p = 0.03$, $Adj-R^2 = 0.4$). In conclusion, advanced MRI techniques at 3T unraveled the nature of brain tissue damage in early MS and substantially improved clinical-radiological correlations in patients with minor deficits, as compared to conventional measures of disease.

The content of this chapter has been published in [80].

2.1 Introduction

MS is characterized by the presence of focal lesions in WM and GM, but also by diffuse inflammation and degeneration in normal-appearing (NA) tissue [81, 82]. Conventional MRI, which plays a major role in identifying focal inflammation and diagnosing MS, has important limits in assessing underlying pathology. As a consequence, this method provides only modest correlations with patient functional performance, particularly during early phases of the disease [41]. In this context, quantitative and semi-quantitative (q/sq) MRI techniques [42, 83] may provide new biomarkers of disease severity and help to improve the clinical-radiological mismatch in MS treatment. To this end, pathological processes such as demyelination, oedema formation, tissue loss, and iron accumulation lead to variable changes in quantitative measures of proton relaxation times (T1, T2, and T2*) as well as in semi-quantitative parameters such as the magnetisation transfer ratio (MTR) [43, 45, 54–56]. Thanks to recent MRI developments [84, 85], it is now possible to combine multiple q/sq MRI sequences in a clinically applicable protocol and gather more specific information about the nature of tissue pathology in MS.

In this chapter, we investigated whether the combination of advanced T1, T2, and T2* relaxometry and magnetisation transfer imaging may be employed (i) to assess the nature of brain tissue changes occurring early in MS and (ii) to improve the correlation between imaging and clinical performance.

2.2 Method

2.2.1 Study population

We enrolled 36 patients with relapsing-remitting MS (RRMS), 24 women / 12 men, age = 34.8 ± 9.2 years (mean \pm standard deviation (SD)) and 18 age-matched healthy controls (HC), 9 women / 9 men, age = 33 ± 9.7 years. All patients were < 6 years from initial symptoms (33.3 ± 21 months, range 2 to 70 months) and disease diagnosis (27.1 ± 18 months, range 0 to 59 months) (see Table 2.1). Thirty patients (83%) were under immunomodulatory treatment (high dosage IFN beta or fingolimod) for at least 3 months. No patient had received corticosteroid therapy within the three months preceding the enrollment. The study was approved by the ethics committee of the Lausanne University Hospital (CHUV). Written, informed consent was obtained from each subject.

Demographic data	HC	RRMS patient
Number of subjects	18	36
Age (mean years \pm std)	33 ± 9.7	34.8 ± 9.2
Gender(females:males)	9:9	24:12
Months since intial symptoms		27.1 ± 18

Table 2.1: Demographic characteristics of HC and RRMS patients.

2.2.2 Clinical assessment

Each subject underwent a neurological examination including the following cognitive and behavioural tests: (i) Brief Repeatable Battery of Neuropsychological Tests (BRB-N) [86], which examine verbal and spatial memory, sustained attention, information processing speed, and verbal fluency on semantic cues; (ii) the Hospital Anxiety and Depression scale (HAD) [87] and (iii) the Fatigue Scale for Motor and Cognitive functions (FSMC) [88], which quantifies depressive mood symptoms and fatigue. The Expanded Disability Status Scale (EDSS [20]) and the Multiple Sclerosis Functional Composite (MSFC [89]) scores were assessed by a certified neurologist (C. Granziera, CG) to quantify motor performance. (see Table 2.2).

Disability and motor tests	Assessed function	HC	RRMS patient
<i>BRB-N</i>			
SRT-LTS	Verbal memory	66.06 ± 6.72	64.14 ± 7.12
SRT-CTRL	Verbal memory	63.19 ± 8.76	59.64 ± 11.94
SRT-D	Verbal memory	11.75 ± 1	11.54 ± 0.79
SDMT	Attention	56.88 ± 12.24	58.54 ± 9.89
WLG	Execution	27.56 ± 7.23	28.64 ± 5.65
<i>Mood and fatigue</i>			
HADA	Anxiety	5.38 ± 2.45	6.50 ± 4.32
HADD	Depression	1.38 ± 1.26	3.07 ± 2.62
FSMC Cognitive	Cognitive fatigue	16.13 ± 5.30	23.00 ± 9.17
FSMC motor	Motor fatigue	14.19 ± 4.25	22.39 ± 11.01
EDSS	Disability		1.55 ± 0.21
MSFC	Disability		-0.08 ± 0.24

Table 2.2: Clinical tests (mean ± std)

2.2.3 MRI techniques

All MR images were acquired on a 3T Siemens Trio (Siemens, Erlangen, Germany) equipped with a 32-channel head coil. The acquisition protocol consisted of (see Table 2.3):

- High-resolution 3D magnetization-prepared acquisition with gradient echo (MPRAGE) (TR/TE = 2300/2.89 ms, voxel size = 1.0x1.0x1.2 mm³, FoV = 256x240x192 mm³, acquisition time = 5:12 min) for automatic brain tissue and atlas-based segmentation as reported previously [90–92]; signal-to-noise ratio (SNR) measurements on a MPRAGE image were performed based on [93, 94];
- High-resolution 3D fluid attenuated inversion recovery (FLAIR) (TR/TE/TI = 5000/394/1800 ms, voxel size = 1.0x1.0x1.2 mm³, FoV = 256x240x212 mm³, acquisition time = 6:27 min);

Chapter 2. Multi-contrast MRI for normal appearing tissue analysis

- High-resolution 3D double inversion recovery (DIR) (TR/TE/TI = 10000/218/3650 ms, voxel size = 1.1x1.0x1.2 mm³, FoV = 256x240x192 mm³, inversion times 450/3652 ms, acquisition time = 12:52 min);
- Magnetization Prepared 2 Rapid Acquisition Gradient Echoes MP2RAGE [85] (TR/TE = 5000/2.89 ms, voxel size = 1x1x1.2 mm³, FoV = 256x240x192 mm³, acquisition time = 8:22 min) for lesion count [95] and whole-brain T1 relaxometry;
- T2 relaxometry (TR/TE = 5000/9 ms, 21 echos, 30 slices: voxel size = 1x1x4 mm³, FoV = 256x240x192 mm³, acquisition time = 3 min) using a new nonlinear inverse reconstruction algorithm that directly estimates a T2 and spin-density map from a train of undersampled spin echoes [84];
- T2* relaxometry (TR/TE = 47/1.23 ms, 32 gradient echoes, voxel size = 1.6x1.6x1.6 mm³, FoV = 217x217x179 mm³, acquisition time = 11:16 min) with and without magnetization transfer (MT) pulse (MT pulse flip angle: 220 deg; duration: 4000 ms; pulse offset: 2000 Hz; spoiler moment: 25000 us*mT/m).

In order to correct for susceptibility induced macroscopic field inhomogeneities, which were already diminished by isotropic high-spatial resolution, we used a 3D Sinc Correction [96] that was extended to include a non-linear correction term based on the underlying B0 map [97]; The B0 map was calculated as the weighted mean phase difference [98] of the temporally unwrapped phase followed by a median and Gaussian filters to remove phase inconsistencies [99]. R2' maps were computed from T2 and T2* maps according to

$$R2' = \frac{1}{T2^*} - \frac{1}{T2} \quad (2.1)$$

MTR maps were derived from the T2* data by

$$MTR = \frac{M_0 - M_T}{M_0} \quad (2.2)$$

with M0 and MT the images acquired without and with MT pulse, respectively. MT images were registered to images without MT pulse. Before any processing, image quality was assessed for each modality by visual inspection. Table 2.1 lists all sequences properties of the protocol, and the Figure 2.1 provides an example of all images and maps in one HC and one MS subject. Total scan time was approximatively 1h08 mins.

Sequence	Parameters	Time
T2* (MT)	TR/TE = 47/1.23 ms; 32 echoes, δ TE = 1.23 ms; Voxel size = $1.6 \times 1.6 \times 1.6 \text{ mm}^3$; FoV = $136 \times 136 \times 112$	11' 16"
T2	TR = 5000 ms, 21 echoes with δ TE = 9 ms; Voxel size = $1.1 \times 1.1 \times 4.0 \text{ mm}^3$, FoV = $160 \times 192 \times 30$	3' 15"
MP2RAGE	TR/TE = 5000/2.89, IT1 = 700 ms, IT2 = 2500 ms; Voxel size = $1.0 \times 1.0 \times 1.2 \text{ mm}^3$, FA = 4°; FoV = $256 \times 240 \times 176$	8' 22"
3D FLAIR	TR/TE/TI = 5000/394/1800 ms; Voxel size = $1.0 \times 1.0 \times 1.2 \text{ mm}^3$; FoV = $256 \times 240 \times 176$	6' 27"
3D DIR	TR/TE/TI = 10000/218/3650 ms; Voxel size = $1.1 \times 1.0 \times 1.2 \text{ mm}^3$; FoV = $240 \times 256 \times 160$	12' 52"
MPRAGE	TR/TE = 2300/2.98 ms; Voxel size = $1.0 \times 1.0 \times 1.2 \text{ mm}^3$; FoV = $256 \times 240 \times 160$	5' 12"

Table 2.3: Detailed MS Advanced protocol sequences parameters. Total acquisition time 1h08'.

2.2.4 MRI contrasts

T1 relaxation time (rt) in brain tissue is mainly influenced by free water protons and the degree of structural organization (i.e. amount of macromolecules such as myelin, lipids, proteins). In this context, an increase in T1rt may indicate a loss of structure and/or an increase in water content. Conversely, greater density of macromolecules and reduced water content as well as iron accumulation tend to reduce T1 [38].

T2-rt measures the loss of spin coherence and therefore, mainly reflect the dynamic state of water protons and their interaction with macromolecules. An increase in T2-rt characterizes a loss of macromolecules and/or increased water content. On the contrary, a decrease in T2-rt reflects an increase of protons bound to macromolecules. As for T1, iron accumulation also causes a shorter T2 [39].

The effective T2*-rt transverse describe the loss of transverse magnetization due to T2 relaxation and magnetic field inhomogeneities (R2' component [40]). Possible sources are tissue-dependent differences in magnetic susceptibility or the presence of paramagnetic or ferromagnetic ions like iron. For these reasons, an increase in T2* most often indicates a loss of macromolecules, while a decrease suggests an increase of macromolecular compounds or iron that translate into an increase in R2'.

MT images are based on the interaction between free protons and immobilized protons bound to macromolecules, so that a lower MTR indicates a reduced spin exchange between macromolecules and surrounding bulk water suggesting neuroaxonal damage or myelin breakdown [100] and/or water increase. (see Figure 2.2)

Chapter 2. Multi-contrast MRI for normal appearing tissue analysis

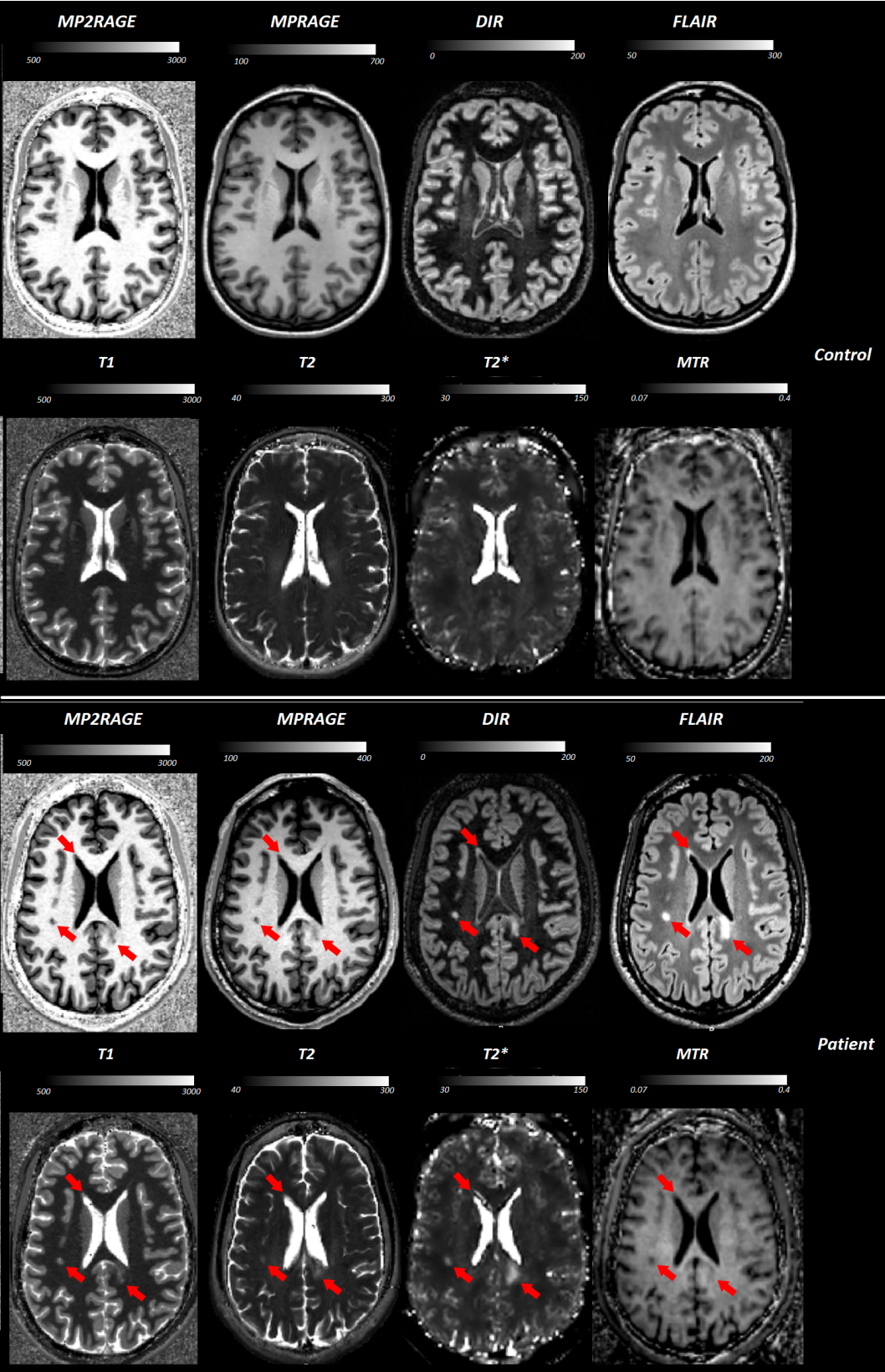


Figure 2.1: Example of MR images from MS advanced protocol : MP2RAGE uniform image, MPRAGE, DIR, 3D FLAIR images as well as MP2RAGE T1, T2, T2*, and MTR maps for one healthy control subject (first two rows) and one MS patient (last two rows). Examples of lesions are shown by red arrows in the images from the MS patient.

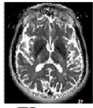
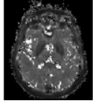

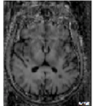
 T2 map	Extracellular water	++	→	T2 rt	↑
	Iron concentration	++	→	T2 rt	↓
	Macromolecules	--	→	T2 rt	↑
 T2* map	Extracellular water	++	→	T2* rt	↑
	Iron concentration	++	→	T2* rt	↓
	Macromolecules	--	→	T2* rt	↑
 T1 map	Macromolecules	--	→	T1 rt	↑
	Extracellular water	++	→	T1 rt	↑
	Iron concentration	++	→	T1 rt	↓
 MTR	Macromolecules	--	→	MT ratio	↓
	Extracellular water	++	→	MT ratio	↓

Figure 2.2: Biophysical basis of MRI contrasts. ++: increase; -: decrease. Big red arrow: large increase; small red arrow: small increase. Big blue arrow: large decrease; small blue arrow: small decrease.

2.2.5 Image analysis and tissue segmentation

We used the Elastix c++ library [101] to perform (i) rigid registration with BSpline interpolation of the T2 maps to the T1 maps (from the MP2RAGE); (ii) rigid registration of T2* maps, MPRAGE, FLAIR, and DIR images to one of the inverted contrasts of the MP2RAGE sequence. By doing this, we obtained all images in the MP2RAGE space. Regions of interest (ROIs) were derived from the MPRAGE image using in-house software based on variational expectation-maximization tissue classification [102]. The following ROIs were automatically segmented: whole brain WM and cortical GM, thalamus and basal ganglia (caudate, putamen and globus pallidus), cerebellar WM and GM. In addition, we computed lobar WM and GM (temporal, occipital, frontal, parietal areas) (see Figure 2.3).

An experienced neurologist (Cristina Granziera, CG) and a radiologist (D. Rotzinger, DR) manually counted MS lesions by consensus in 3D FLAIR, 3D DIR, and MP2RAGE images for all MS subjects and HC, as performed previously [92]. A trained technician generated manual contours for each lesion in the three different contrasts (re-checked by DR). In order to maximize the sensitivity of lesion count and volume, lesion masks from each contrast were merged into a single mask (lesion union mask), as reported in [92]. The lesion union mask and the ROIs masks were then registered to the T1, T2, T2*, and MTR maps to obtain parametric values in lesions and NA tissue in each ROI. The volume of each ROI was also automatically obtained using the in-house software [103] and normalized by total intracranial volume.

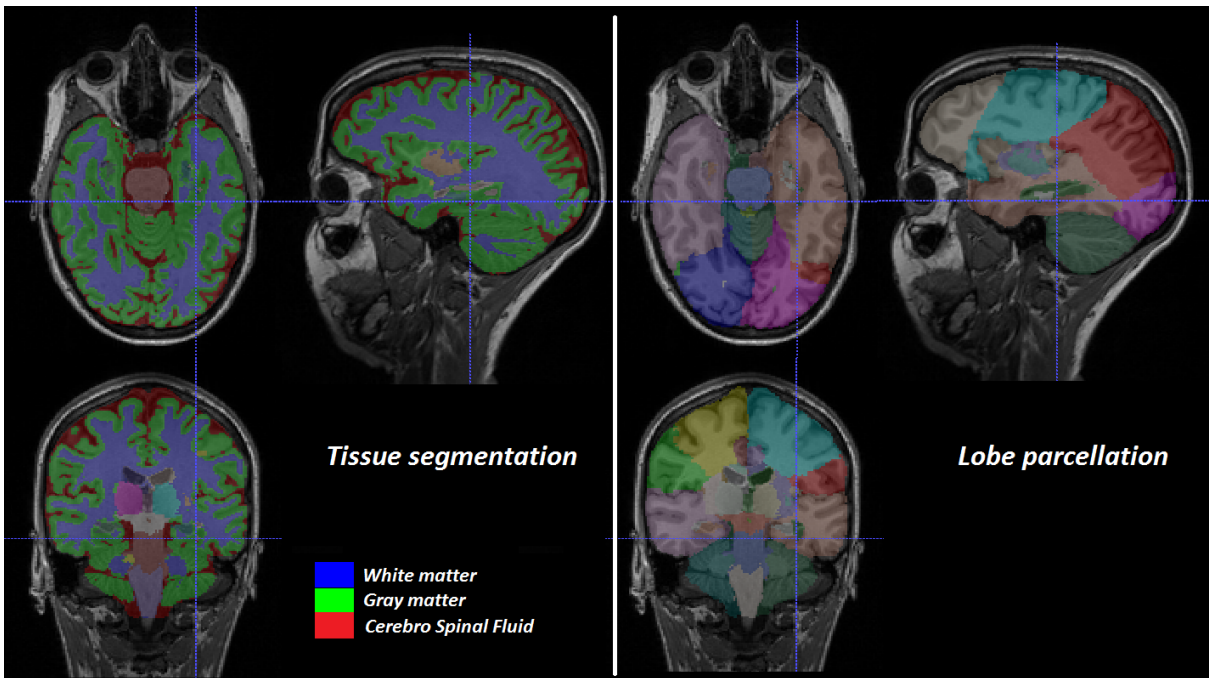


Figure 2.3: Example of tissue segmentation and lobe parcellation using in-house software MorphoBox. The segmentation was obtained using MPRAGE image as input.

2.2.6 Statistical analysis

Between-groups comparisons of subjects' demographics and clinical scores

Differences in age, gender, education, and clinical performances were assessed using a non-parametric ANOVA (Kruskal-Wallis test) among HC and MS patients.

Between-groups comparisons of multi-contrast MRI data

To assess NA tissue differences in mean T1, T2, T2*, and MTR of patients and controls, we performed a permutation-based Hotelling test with 10.000 permutations, age and gender as covariates, and family-wise error rate correction for multiple comparisons. The following null hypotheses were tested:

- (i) there are no differences in WM and GM of temporal, parietal, occipital, and frontal lobes;
- (ii) there are no differences in cerebellum WM and GM;
- (iii) there are no differences in thalamus and basal ganglia.

Lobar assessment was chosen, instead of whole brain, to take into account the local variation of quantitative relaxometry measures, as reported previously [104, 105]. In order to determine

the strength of the significance, we also calculated the Cohen's d effect size as follow:

$$d = \frac{\bar{x}_1 - \bar{x}_2}{s} \quad (2.3)$$

with \bar{x}_1 and \bar{x}_2 are the mean of the group 1 (HC) and group 2 (RRMS), and s defined as follows:

$$s = \sqrt{\frac{(n_1 - 1) \cdot s_1^2 + (n_2 - 1) \cdot s_2^2}{n_1 + n_2 - 2}} \quad (2.4)$$

Parameters s_1 and s_2 refer to the standard deviation of group 1 (HC) and group 2 (RRMS), while n_1 and n_2 are the number of samples of group 1 and 2.

For lesions analysis we normalized T1, T2, T2* and MTR value using z-score :

$$z_{T1} = \frac{1}{N} \sum I_{T1}(v) - \mu_{T1}(L, T) \sigma_{T1}(L, T) \quad (2.5)$$

where z_{T1} corresponds to the T1 lesion z-score (z), l to the lesion voxels, N to a normalisation term, I the T1 map, μ_{T1} and σ_{T1} to the mean and the standard deviation of the T1 map in the lobe L and tissue T (i.e WM or GM) in the HC group, corresponding to the lesion location. Averages of each patient's T1, T2, T2*, and MTR lesion z-scores were also performed in the whole MS group. This approach was chosen instead of the permutation-based test applied for NA tissue to account for spatial variation of relaxometry values [104, 105]. A permutation test was not feasible for each lobe as not all patients exhibited lesions in all lobes.

Between-groups comparison of volumes

To assess volumetric differences in ROIs between patients and controls, we performed a permutation-based Hotelling test with 10.000 permutations, age and gender as covariates, and family-wise error rate correction for multiple comparisons.

Linear regression of MRI parameters with clinical scores

A multivariate linear regression of clinical scores was performed using a general linear model (GLM) applied to:

- T2*, T2, T1, and MTR in the ROIs that significantly differed between patients and HC;
- T1, T2, T2*, and MTR lesion z-scores;
- Cortical/subcortical lesion count and volume.

Age, gender, educational years, anxiety, and depression scores (HAD) were considered as covariates, since they have been reported to be linked to functional performance [106, 107].

Cognitive scores were adapted using the Box-Cox transformation to satisfy the model assumption for normality [108]. EDSS scores were not considered, as they were positive only in patients. We performed seven regressions, where we used a stepwise regression approach to select the best prediction model for each dependent variable (clinical scores). Bonferroni correction was applied for multiple comparisons (seven tests). Cook's distance (Cd) was computed to assess the influence of each observation on the regression process, using $4/n$ (n : number of observations) as the threshold of significance. Robust regression was used to reduce influence of the outliers identified by Cook's distance analysis.

"Leave-one-out" (LOO) cross validation was applied to assess the prediction quality and robustness of each model. A p -value < 0.05 was considered statistically significant.

All regression analyses were performed using R software (<http://www.R-project.org>).

2.3 Results

Between-groups comparisons of subject demographics and clinical scores

No significant differences were observed between HC and MS patients in terms of age ($p = 0.3$) or gender ($p = 0.8$); however, HC had slightly higher education levels (17 ± 4 years, mean \pm standard deviation) than MS patients (15 ± 3 years, $p = 0.04$). Mean EDSS in patients was 1.6 ± 0.3 (interval: 1-2). The FSMC motor score was significantly higher in MS patients (23.1 ± 10.5) than in HC (14.8 ± 5.8 , $p < 0.02$). The FSMC cognitive scores, cognitive performance, MSFC scores, as well as anxiety and depression scores (HAD) were not significantly different between groups ($p > 0.1$).

Between-groups comparison of multi-contrast MRI data

In temporal NAWM, mean $T2^*$ and $T2$ were significantly higher in RRMS patients compared to HC ($T2^*$ rt: 55.1 ± 1.55 ms in patients and 53.4 ± 1.35 ms in HC, $d = 1.17$, $p = 0.004$; $T2$ rt: 82.0 ± 2.38 ms in patients and 79.8 ± 2.0 ms in HC, $d = 1$, $p = 0.03$) (see Figure 2.4). In order to assess whether the observed $T2^*$ increase in temporal NAWM depended on local field inhomogeneities, we also compared temporal NAWM $R2'$ between groups and found no significant differences. Additionally, parietal NAWM and cerebellar NAWM exhibited a trend toward higher $T2$ values in patients compared to HC (parietal NAWM $T2$: 83.5 ± 2.44 ms in patients compared to 81.8 ± 2.62 ms in HC; $d = 0.7$, $p = 0.05$; and cerebellar WM $T2$: 85.90 ± 1.69 ms in patients compared to 85.48 ± 1.47 ms in HC; $d = 1.62$, $p = 0.07$). Further, no differences were seen for $T1$ and MTR in NAWM and cortical NAGM, nor for $T2$ and $T2^*$ in cortical NAGM, frontal or occipital NAWM.

Finally, no significant differences between groups were found for $T1$, MTR, $T2$, or $T2^*$ in the thalamus or basal ganglia.

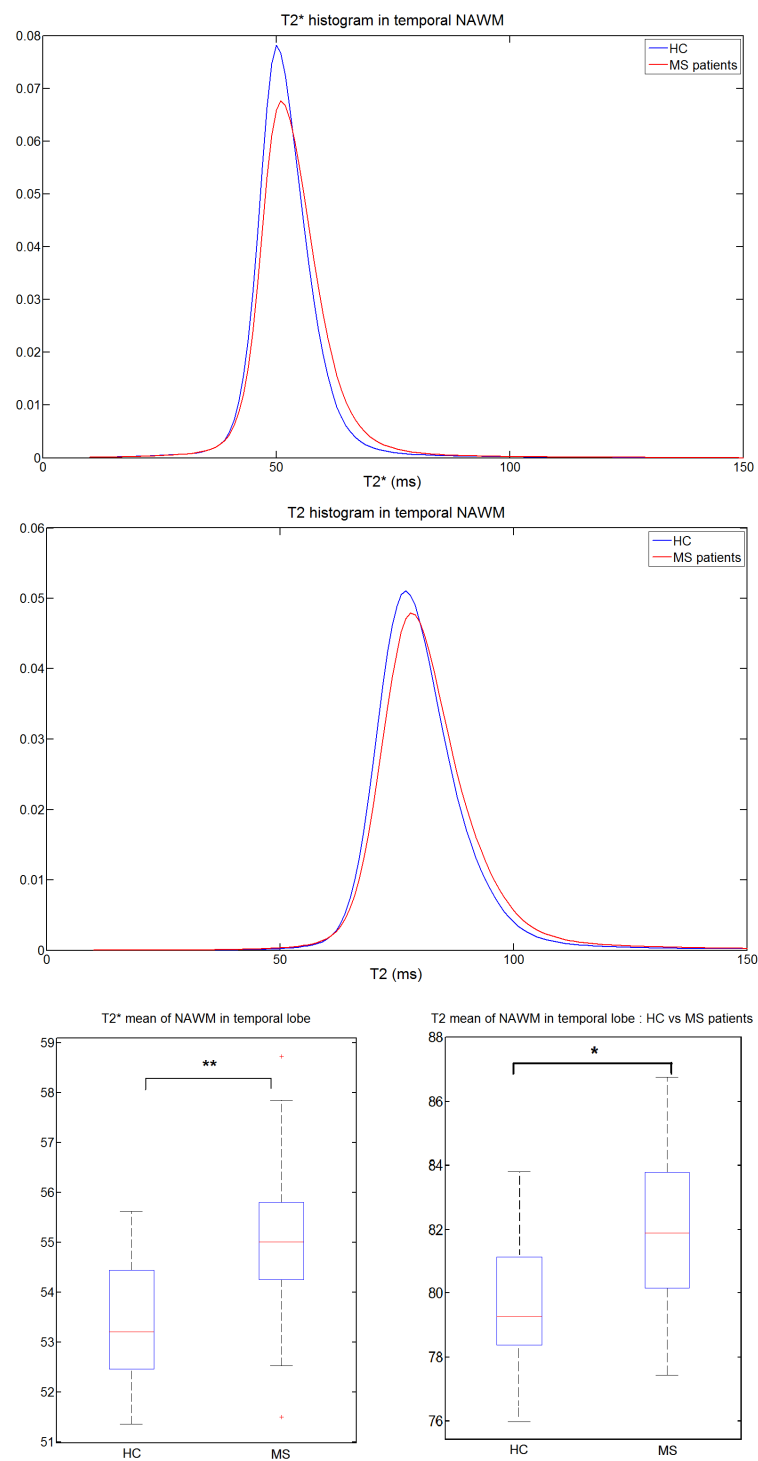


Figure 2.4: Histograms and boxplots of T2 and T2* in RRMS patients and HC. (A) (Top): T2* and T2 mean histograms in NAWM (temporal lobe) for HC (blue) and MS patients (red); (B) (Below): Boxplots of T2* and T2 in NAWM (temporal lobe) for HC (left) and MS patients (right).

Chapter 2. Multi-contrast MRI for normal appearing tissue analysis

Results of micro-structural analysis of lesions are reported in Figure 2.5. In the MS cohort, MS lesions showed a strong increase in T1 mean z-score (4.42) and an important decrease in MTR mean z-score (-4.09). T2 and T2* z-scores slightly increased (2.33 and 2.25 respectively).

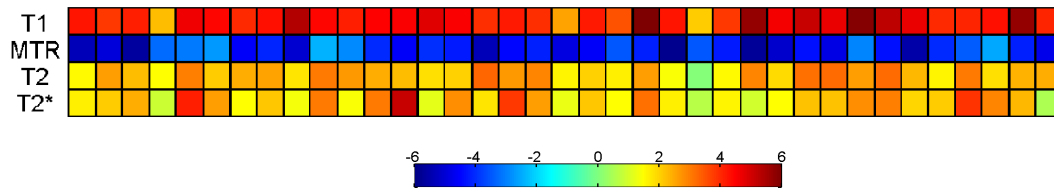


Figure 2.5: Mean z-scores of T1, MTR, T2, and T2* of MS lesions per patient. Each column represents a patient.

Between-groups comparison of volumes

No significant differences were observed in volumes between MS patients and HC; however, there was a trend ($p = 0.07$) toward smaller normalized thalamic volumes in patients (absolute volume $15.31 \pm 1.36 \text{ mm}^3$, normalized volume 0.01 ± 0.0006) compared to HC (absolute volume $16.52 \pm 2.04 \text{ mm}^3$, normalized volume 0.01 ± 0.0003).

Linear regression of MRI parameters with clinical scores

GLM using backward, stepwise regression revealed a highly significant association, confirmed by cross-validation results, between multi-contrast MRI features and four clinical scores (see Table 2.4):

- Cortical lesions count and volume, T1, T2, and T2* mean z-score of lesions, T1, T2*, and MTR mean of temporal NAWM together with gender predicted the SDMT (attention function) score ($adj-R^2 = 0.6$, $p = 0.0004$).
- T2, T2*, and MTR mean in temporal NAWM in conjunction with T1 and T2 mean z-score in lesions as well as subcortical lesion volume and educational years, gender and HAD scores predicted the MSFC (general disability) score ($adj-R^2 = 0.4$, $p = 0.03$).
- T1 and T2 mean in temporal NAWM combined with cortical lesion volume, subcortical lesion count and HADD score predicted the FSMC cognitive score ($adj-R^2 = 0.4$, $p = 0.01$).
- T1 and T2 mean in temporal NAWM combined with cortical lesion volume, subcortical lesion count, and volume with HADD score predicted the FSMC motor score ($adj-R^2 = 0.4$, $p = 0.01$).

		MSFC	SDMT	FSMC Cognitive	FSMC Motor
Stepwise regression	p-value	0.03178*	0.00051***	0.01577*	0.01250*
	Adj-R ²	0.43	0.59	0.36	0.42
Leave-one-out cross-validation	p-value	0.00080***	0.00004***	0.00696**	0.01160*
	Adj-R ²	0.24	0.44	0.26	0.24

Table 2.4: Regression analysis. Each line corresponds to the corrected p-values, and adjusted-R² of each model (n=7) subjected to regression and cross-validation analysis. (***: p< 0.001), (** : p< 0.01), (* : p< 0.05).

2.4 Discussion

The present results demonstrate that, combining multiple advanced MRI techniques it is possible to unravel the nature of subtle tissue alterations in early MS. Moreover, MRI markers of inflammation and neurodegeneration substantially improved clinical-radiological correlations compared to conventional measures.

The RRMS patients enrolled in our study exhibited significant increases in T2 and T2* in temporal NAWM, and to a lesser extent in parietal and cerebellar NAWM. These changes hint to an accumulation of extracellular water (micro-edema) and/or a reduction of macromolecular content (myelin) in affected brain tissue (see Figure 2.2). In the absence of significant changes in MTR and T1, which would support the structural explanation, the increase of both T2 and T2* most likely indicates the presence of subtle edema. Iron loss might also be responsible for a prolongation of T2 and T2*, but appears to be a less probable cause as no differences were observed in R2', which reflects local field inhomogeneities [109]. By combining multiple q/sq MRI measures, our study confirms work reporting T2 increase in NAWM in early MS [43, 44] and extends these findings by providing new insights into the pathology underlying those changes. Our data, however, contradicts studies showing a measured unimodal MTR decrease in NAWM of early MS patients attributed to myelin loss [110, 111]. These studies focused mainly on untreated patients and applied magnetization transfer imaging at lower spatial resolution and lower field strength (1.5 T) than ours. Furthermore, unimodal MTR studies in MS should be considered with caution, as magnetization transfer imaging alone cannot discriminate between myelin alterations and variation of water content in tissues [52]. Axonal degeneration in NAWM of early MS patients was also suggested by unimodal diffusion tensor imaging (DTI) studies, showing reduced fractional anisotropy (FA) [75, 76]. Nevertheless, this interpretation may be misleading since a decrease in anisotropy can derive from the loss of the branched-shape of microglia cells that is typical of their activated-inflammatory form [77]. Thus, another possible explanation is that reduced FA might point to inflammatory rather than degenerative phenomena. Several studies tried to address the limitation of unimodality studies by combining T2 relaxometry, MTR measurements [78], and DTI [79]; yet, these studies focused on selected brain structures (i.e corpus callosum [79] and corticospinal tract [78]) in

patients with advanced stages of MS [79]. Our approach overcomes the above-mentioned limits by performing a whole brain analysis of multiple q/sq assessments in early MS.

Our data also showed that both cortical and subcortical lesions were characterized by a strong increase in T1 and decrease in MTR with relatively modest positive variations of T2 and T2* (see Figure 2.5). These findings are consistent with previous MRI literature [112, 113] and histopathological studies [55, 56, 114] showing significant neurodegeneration in MS plaques. No significant micro-structural alterations were found in NA tissue belonging to the basal ganglia or thalamus in our MS cohort. Still, volumetric analyses revealed a trend toward lower regional volumes in patients ($p=0.07$), which is consistent with thalamic atrophy reported in larger and more heterogeneous patient groups [115]. Last, we showed that MRI findings of micro-structural alterations in NA tissue and lesions substantially improved the clinical-radiological correlation obtained with conventional measures, even in the presence of minor functional deficits. In fact, a variable combination of relaxometry and MTR values significantly ameliorated the prediction of cognitive performance (attention), cognitive fatigue, and general disability obtained with traditional measures of disease burden and patient covariates (see Table 2.4). Conventional MRI measures of MS disease impact provide only modest correlations with clinical performances, a phenomenon that is known as the clinico-radiological paradox. Multivariate analyses and multi-contrast, tract-specific measures were proposed to alleviate this paradox [78, 79], but suffered from the limitations of conventional protocols and partial brain analyses. Recently, ultra-high field MRI at 7T has been used to identify subtypes of cortical lesions, whose numbers showed good correlations with disability and cognitive performance in MS [116]. Extending such work, our multi-contrast approach emerges as a whole-brain MRI method at a clinically-compatible magnetic field, which produces strong clinic-radiological correlations for both cognition and disability. Future developments should aim at reducing the number of sequences required for optimal lesion detection (i.e. MP2RAGE and 3DFLAIR) as well as at applying accelerated T1-T2* relaxometry sequences to achieve a well-suited protocol for the clinical workflow.

2.5 Conclusion

In summary, in this chapter we established a methodology combining different q/sqMRI contrasts to detect subtle pathological changes in brain tissue of MS patients as well as focal alterations. We observed indeed micro-edema in NA tissue characterized by an increased of T2 and T2* in temporal NAWM, as well as prevalent tissue degeneration in MS lesions revealed by a strong increase in T1 and decrease in MTR. Last, we improved correlations between MRI data and measures of cognition and disability in early and minimally-impaired MS patients. Additional studies extending the current methods to patients at later disease stages and containing larger cohorts will be necessary in the future.

In the next chapter, we focused on the MS lesions by extended our multi-contrast approach to model the heterogeneity of tissue damage in MS lesions through a classification framework.

3 Multi-contrast MRI quantification of focal inflammation and degeneration in multiple sclerosis

Abstract

Local microstructural pathology in multiple sclerosis patients might influence their clinical performance. This study applied multi-contrast MRI to quantify inflammation and neurodegeneration in MS lesions. We explored the impact of MRI-based lesion pathology in cognition and disability. Relapsing-remitting MS subjects and healthy controls underwent neurological, cognitive, behavioural examinations and 3T MRI including: (i) advanced MR techniques for lesion count; and (ii) T1, T2, T2* relaxometry and magnetisation transfer imaging for lesion tissue characterization. Lesions were classified according to the extent of inflammation/neurodegeneration. A generalized linear model assessed the contribution of lesion groups to clinical performances. Four lesions classes were identified and characterized by (1) absence of significant alterations, (2) prevalent inflammation, (3) concomitant inflammation and microdegeneration and (4) prevalent tissue loss. Classes (1), (3), (4) strongly correlated with general disability ($Adj-R^2 = 0.6, p = 0.0005$), executive function ($Adj-R^2 = 0.5, p = 0.004$), verbal memory ($Adj-R^2 = 0.4, p = 0.02$) and attention ($Adj-R^2 = 0.5, p = 0.002$). To conclude, multi-contrast MRI provides a new approach to infer in vivo histopathology of MS plaques. Our results also support evidence that neurodegeneration is the major determinant of patients disability and cognitive dysfunction.

The content of this chapter has been published in [117].

3.1 Introduction

The hallmark of MS is the presence of multi-focal lesions or "plaques", which are characterized by variable inflammatory, degenerative and reparative processes [118, 119]. Plaques inflammation is widespread in the relapsing-remitting MS subtype, whereas important tissue loss is pronounced in progressive MS and in long-standing disease [120, 121]. In addition, new lesions are mostly characterized by inflammatory phenomena, leading to blood-brain barrier disruption, while older lesions show a higher proportion of neuro-degeneration and/or repair processes [24, 121].

Conventional magnetic resonance imaging is a valuable tool to provide information about the number, location and inflammatory "activity" of focal lesions. Nevertheless cMRI offers only limited sensitivity to focal pathology in the cortex and little insight into the nature of local damage. Non-conventional MRI techniques such as Double Inversion Recovery (DIR, Geurts Radiology 2005) and magnetization-prepared 2 rapid gradient echo (MP2RAGE, Marques Neuroimage 2010 and Kober 2012) have proven higher sensitivity to focal cortical pathology than cMRI. Similarly, the combination of multiple cMRI contrasts improved cortical lesions detection at all field strengths (1.5 T [122], 3T [123] and 7T [124]). Besides, other advanced MRI techniques have shown to be sensitive to tissue pathology in lesions, such as axonal and myelin damage (diffusion tensor imaging-DTI and magnetisation transfer imaging-MTI) and axonal metabolic deficits (magnetic resonance spectroscopy) [119, 125–128]. MRI relaxometry has also been extensively used to study normal-appearing brain tissue in multiple sclerosis patients (for review see [128, 129]), but only few works focused on lesions properties and heterogeneity [95, 130]. Yet, some recent post-mortem studies provided strong evidence of the value of MRI relaxometry techniques to study specific aspects of plaques pathology; Bagnato et al. showed that high $R2^*$ values in the periphery of white matter (WM) lesions correlated with iron accumulation in macrophages/microglia whereas high $R2^*$ inside the WM plaque had the appearance of iron aggregates typical of microbleeds [131]. Furthermore, Tardif et al. established that myelin loss within cortical lesions was associated with a concomitant increase of T1 and T2 relaxation times and a decrease of MTI measures [55].

In this chapter, we combined three relaxometry techniques (T1, T2 and T2*) and MTI (i) to classify MS cortical and WM lesions according to the extent of inflammatory and neurodegenerative phenomena, as measured by unconventional MRI and (ii) to assess the clinical impact of MRI measures of lesion pathology in a cohort of relapsing-remitting multiple sclerosis patients.

3.2 Method

3.2.1 Lesion segmentation

Cortical and WM MS lesions were manually identified in patients by an experienced neurologist (CG) and a radiologist (DR) using 3D FLAIR, 3D DIR and MP2RAGE images, as previously reported [85, 91]. Manual contours were generated for each lesion by a trained technician

for each contrast. As reported by [95] we merged the lesions extracted from FLAIR, DIR and MP2RAGE to obtain a final union lesion mask for each subject. Lesion volumes were computed and normalized by total intracranial volume using our in-house software [103]. Only lesions with more than 10 voxels size were included in the analysis. Lesion masks were then registered to MP2RAGE space using the registration parameters described in the previous chapter and mean T1, T2, T2* and MTR were calculated for each lesion.

In order to assess the mean distribution of T1, T2, T2* and MTR in HC brain tissue, we segmented lobar WM and cortical GM (frontal, parietal, occipital, temporal) as well as cerebellar WM/GM from the MPRAGE images. To compare lesion MRI properties in patients with the corresponding tissue in HC, we calculated a z-score for each contrast in each lesion (e.g. for T1 data):

$$z_{T1} = \frac{1}{N} \sum I_{T1}(v) - \mu_{T1}(L, T) \sigma_{T1}(L, T) \quad (3.1)$$

where z_{T1} corresponds to the T1 lesion z-score (z), l to the lesion voxels, N to a normalisation term, I the T1 map, μ_{T1} and σ_{T1} to the mean and the standard deviation of the T1 map in the lobe L and tissue T (i.e WM or GM) in the HC group, corresponding to the lesion location and type.

This normalisation step provide for each contrast a normalized value corresponding to the number of standard deviation measured between a lesion voxel and the corresponding healthy distribution. In this context, a negative value corresponds to a decrease of the quantitative parameter, while a positive value reflects an increase of the parameter (Figure 3.1).

3.2.2 Lesion classification

Considering the continuous distribution (without distinct cluster) of lesions z-scores in each contrast (see Appendix A.1), we classified the lesions z-score into 3 groups as follows: (i) z very low ($z < -2$), (ii) z very high ($z > 2$) and (iii) z close to the HC distribution ($-2 \leq z \leq 2$). The thresholds were chosen considering the fact that more than 95 percent of the z -scores belong in the interval $[-2, 2]$ in a normal distribution and that values beyond this interval reflect significant differences in patients compared to controls ($p < 0.05$). (Figure 3.2). Last, for each subject, all existing combinations of z were computed for all contrasts (e.g. : combination 1 = $z_{T1} > 2, z_{T2} > 2, z_{T2*} > 2, z_{MTR} < -2$; combination 2 = $z_{T1} > 2, z_{T2} > 2, -2 < z_{T2*} < 2, z_{MTR} < -2$, etc...) and mean lesion volume (MLV) was assessed for each combination (total normalized lesion volume/number of lesions).

Finally we grouped the combinations in 4 lesion types : Class 1 (Combination 1), Class 2 (Combinations 2-4), Class 3 (Combinations 5-8), Class 4 (Combinations 9-12).

Chapter 3. Multi-contrast MRI quantification of focal inflammation and degeneration in multiple sclerosis

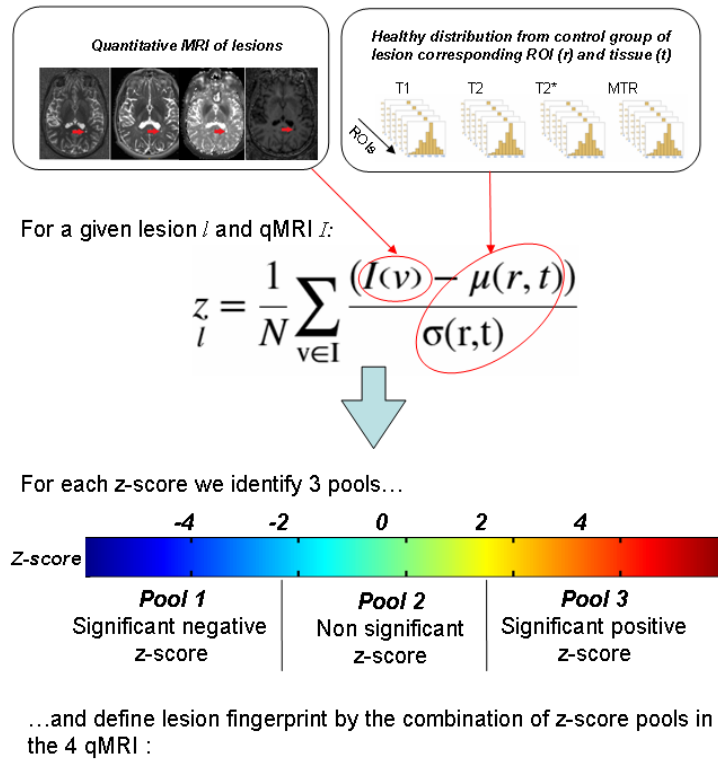


Figure 3.1: Pipeline for MS lesions classification using multi-contrast approach. Computation of lesion fingerprint using z-score measurement.

3.2.3 Statistical analysis

Regression analysis

Differences in age, gender, education, and clinical performance were assessed using a non-parametric ANOVA (Kruskal-Wallis test) among HC and MS patients. A multivariate linear regression of clinical scores was performed using a general linear model (GLM) applied to MLV in each combinations of contrasts. Age, gender, educational years, anxiety, and depression scores (HAD) were considered as covariates. Cognitive scores were adapted using Box-Cox transformation to satisfy the model assumption for normality [132].

We performed seven regressions and applied a stepwise approach to select the best prediction model for each dependent variable (clinical scores). Bonferroni correction was applied for multiple comparisons (seven tests). “Leave-one-out” (LOO) cross validation was applied to assess the prediction quality and robustness of each model. A p-value < 0.05 was considered statistically significant.

All regression analyses were performed using R software (<http://www.R-project.org>).

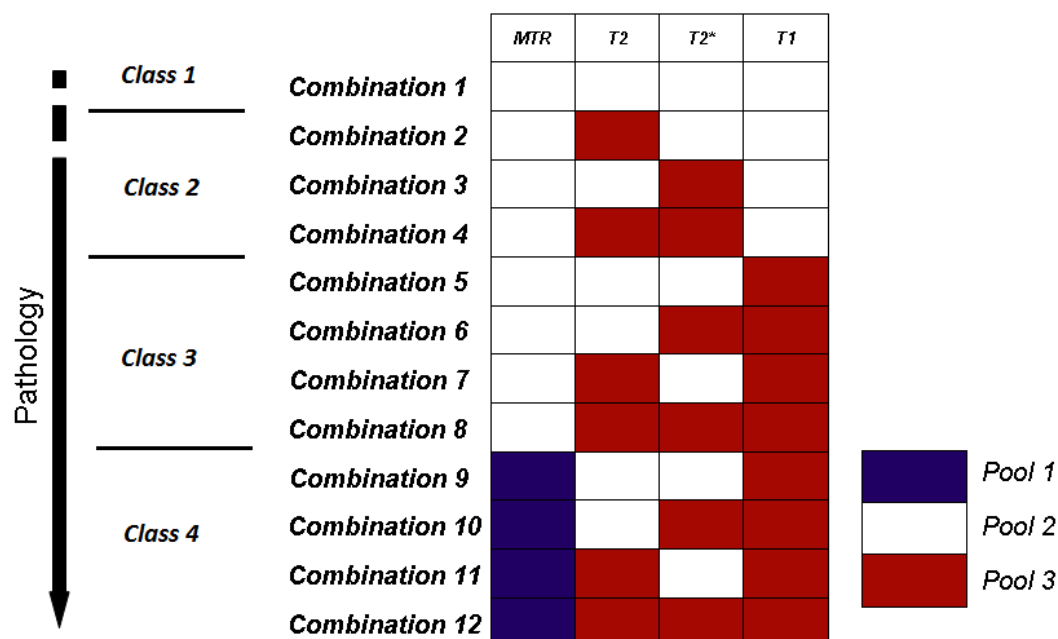


Figure 3.2: List of the 12 combinations of MS lesions z-scores for T1, T2, T2* and MTR q/sq MRI from the least (combination 1) to the most (combination 12) severe stage. The presence of irreversible tissue loss was considered a sign of higher severity than inflammation.

3.3 Results

Contrasts combinations and lesion combination distribution

We found 12 z-scores combinations in all MS lesions (1402 lesions, Figure 3.2). These combinations characterised plaques with no significant contrast changes (Class 1: combination 1, 54% cortical and 46% WM lesions), prevalent inflammatory edema (Class 2: isolated increase of T2 and/or T2* z-scores, combinations 2-4, 40% of cortical and 60% of WM lesions), microdegeneration and/or inflammatory edema (Class 3: increase in T1 and/or increase in T2/T2*, combinations 5-8, 2% cortical and 98% WM) and broad tissue loss (Class 4: strong increase in T1 and decrease in MTR z-scores, with or without increase in T2/T2*, combinations 9-12, 100% WM).

Most of the lesions (70%) showed a significantly high T1 z-score (Class 3 and 4) and only 27% of total number of lesions did not show any significant change in all contrasts (Class 1); 48% of lesions showed high T1 z-score only (Class 3), 32% exhibited high T1 z-score combined with high T2 or T2* (Class 3) and 18% were characterized by high T1 z-score combined with low MTR (Class 4). Class 2 containing lesions with high T2 and/or T2* and "non significant" T1 and MTR counted less than 3% of the total number of lesions (Figure 3.3).

The cortical lesions represented 17% of the total number of lesions; 90% were cortical lesions Type I (mixed GM/WM) and 10% Type II (GM only). They mainly belong to combination 1 (85%) and combinations 2 to 8. Most of the lesions were pure WM lesions (83%) and appeared

Chapter 3. Multi-contrast MRI quantification of focal inflammation and degeneration in multiple sclerosis

in all combinations.

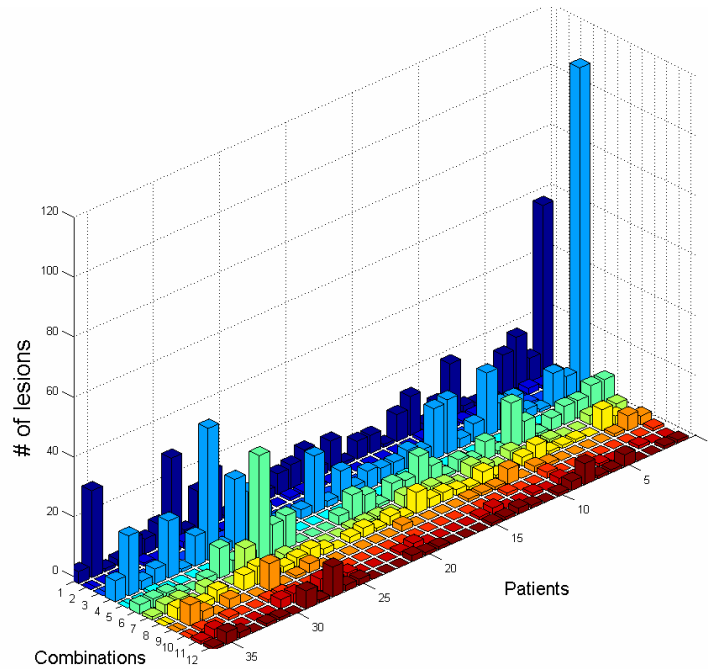


Figure 3.3: Distribution of lesions among combinations and distribution of combination among patients. Combinations 1 (non significant z-score in all contrasts) and 4 (isolated high T1 z-score) count more than 50% of all lesions and are the combinations mostly found in all patients.

Linear regression

GLM using stepwise regression revealed a highly significant association, confirmed by a cross-validation test, between lesions MRI characteristics and three clinical scores (Table 3.1):

- The MLV in combinations 8 and 9 (Class 3 and 4) together with age and depression score predicted the MSFC (general disability) score ($Adj-R^2 = 0.6, p = 0.0005$).
- The MLV in combinations 5, 6 and 9 (Class 3 and 4) in conjunction with gender predicted the FV (execution) score ($Adj-R^2 = 0.5, p = 0.002$).
- The MLV in combinations 1, 9 and 10 (Class 1 and 4) predicted the SRT (verbal memory) score ($Adj-R^2 = 0.4, p = 0.002$).
- MLV in combinations 1, 5, 6 and 9 (Class 1, 3 and 4) with age and depression score predicted the SDMT (attention function) score ($Adj-R^2 = 0.5, p = 0.004$). Nevertheless, cross-validation test revealed a possible over-fitting of the GLM (estimated score vs clinical score: $Adj-R^2 = 0.1, p = 0.09$).

		MSFC	FV	SRT	SDMT
Stepwise regression	p-value	0.00045***	0.00166**	0.01536*	0.00379**
	Adj-R ²	0.55050	0.45350	0.38040	0.48960
Leave-one-out cross-validation	p-value	0.00005***	0.00030***	0.00677**	0.09011
	Adj-R ²	0.43660	0.37490	0.25620	0.14360

Table 3.1: Regression analysis of clinical scores using lesions characteristics. Each line corresponds to the corrected p-values, and adjusted-R² of each model (n=7) subjected to regression and cross-validation analysis. (***: p< 0.001), (** : p< 0.01), (* : p< 0.05).

3.4 Discussion

Current diagnostic and prognostic criteria in MS as well as clinical trials end-points are based on conventional MRI measures of lesions number, volume and activity [133]. Nevertheless, these parameters provide only limited information about the nature and severity of tissue alterations in the central nervous system. In fact, changes in conventional T1 and T2 signals are compatible with both inflammatory and degenerative phenomena [80]; moreover, the presence of "black holes", considered to be a marker of permanent axonal/myelin loss [134, 135] might be also due to inflammatory extracellular [135] edema and activated microglia [136, 137]. Furthermore, gadolinium (Gd) enhancement, a conventional marker of active inflammation, does not detect active lesions with mild changes in blood-brain barrier (BBB) permeability [138] and disseminated inflammation due to activated microglia [139]. In addition, the presence of Gd uptake might reveal incomplete restoration of tight junction integrity and BBB function in inactive, non-inflamed, chronic lesions [2].

We previously showed the potential of advanced MRI techniques allow to unravel the nature of diffuse and focal tissue pathology in MS (Chapter 2). In this chapter, we aimed at investigating the influence of unconventional MRI metrics of lesion pathology on patients disability and cognition. In accordance with previous literature at 3T [95] we found that the majority of lesions detected in our cohort of early MS patients were located in WM (83%), a moderate number were mixed WM/GM (Cortical Lesion Type-I) (15%) and few were purely cortical and punctiform (cortical lesion Type-II) (2%). We identified twelve combinations of MRI contrasts in MS lesions, which we organized in four main groups according to the predominant underlying pathology (Figure 3.2). Class 1 was constituted by lesions that did not show any significant contrast change, possibly due to pathophysiological causes (i.e. presence of more efficient reparative processes in early stages of disease) and/or technical aspects (lack of sensitivity/spatial resolution). The other three groups were constituted by lesions exhibiting prevalent inflammation (Class 2), micro-degeneration with/without inflammation (Class 3) or predominant tissue loss (Class 4). These four groups were consistent with those reported by the histopathological "Vienna classification" of MS lesions (Class 1: Vienna lesion type-VLT 6; Class 2: VLT 2; Class 3: VLT 2/5; Class 4: VLT 5) [140]. Interestingly, we did not observe any T1/T2/T2*

Chapter 3. Multi-contrast MRI quantification of focal inflammation and degeneration in multiple sclerosis

decrease in local plaques, suggesting that no significant iron accumulation occurs in our cohort of patients. However, since we performed an average lesion analysis, this observation does not exclude the presence of local iron increase, as previously reported [131, 141].

Last, we studied the relative impact of lesion combinations/groups on clinical performance in patients. And we found that lesions with concomitant micro-degeneration/inflammation or important tissue loss had a greater impact on patients' disability, executive function and verbal memory than prevalent inflammatory lesions. This result could be due to the presence of a minority of lesions in the purely inflammatory group (Class 2), which might be due to the fact that most of the patients were benefitting of immunomodulatory/immunodepressive therapy. In addition, lesions with no significant changes in multi-contrast MRI (Class 1) played an important role in verbal memory and attention. This aspect is coherent with the fact that the majority of Class 1 lesions were located in the cortical layers; yet, it could be also due to the fact that a proportion of Class 1 lesions is located in eloquent areas. In order to elucidate this last point, an ongoing study is aiming at integrating the lesion location information in the current lesion classification.

3.5 Conclusion

In summary, this chapter provides a new approach to infer histo-pathological information from MS plaques and supports evidence that MRI measures of lesion pathology are strong determinants of patients' clinical performance in our cohort. In addition, we propose a model based on multi-contrast approach to characterized the heterogeneity of tissue damage in MS lesions through a classification framework.

The next chapter, which focuses on deep gray matter nuclei analysis, presents an innovative technique based on partial volume estimation, to disentangle the WM and GM components in deep gray matter structures, providing additional information on the micro-properties of the tissue affected by MS pathology

4 A new approach for deep gray matter analysis using partial volume estimation

Abstract

The presence of partial volume in brain regions like the deep grey matter nuclei renders quite challenging the detection and identification of pathological alterations. In this chapter, we propose a new single-contrast approach to disentangle gray and white matter (GM, WM) in the thalamus and the basal ganglia. Using a newly developed PV estimation algorithm (Roche et al. [142]) we computed tissue concentration in each voxel so as to estimate the intensity characteristic of each tissue throughout a given region of interest (ROI). The proposed methodology has been applied to a cohort of patients with early multiple sclerosis patients to assess its ability to evaluate the impact of subtle and diffuse inflammatory or neurodegenerative processes. Forty-three relapsing-remitting MS (RRMS) patients and nineteen healthy controls underwent 3T MRI including: (i) FLAIR, DIR, MPRAGE for lesion count; (ii) and T1 relaxometry for tissue characterization and concentration maps estimation. We applied a newly developed partial-volume estimation algorithm to T1 relaxometry maps (Roche et al.), and computed GM and WM tissue concentrations maps to estimate the intensity characteristic of each tissue in the thalamus and basal ganglia. Then, we performed a qualitative analysis comparing estimated concentration maps with histological data, and a quantitative analysis consisting of a group comparison based on the concentration and T1 intensity characteristic in both WM and GM. Qualitative analysis provided evidence of the precision and validity of our approach in the deep grey matter nuclei. Group comparison showed significant increase in the T1 of the GM component of the thalamus ($p=0.016$) in RRMS patients compared to HC. The presented methodology enables an in-depth characterization of deep gray matter nuclei tissue properties. This additional information holds promise to identify the presence and nature of diffuse pathology in neuroinflammatory and neurodegenerative diseases.

The content of this chapter has been submitted to *Human Brain Mapping*.

4.1 Introduction

Magnetic resonance imaging (MRI) provides in vivo information about brain tissue integrity [83]. MRI signal varies across tissue types because gray matter contains a prevalence of cell bodies (neurons, glial cells etc....) and iron, while white matter is for the majority constituted by nerve fibers (myelinated and unmyelinated axons) [143, 144]. Nevertheless, as cell bodies are common in WM, a certain amount of neuronal fibers is also present in cortical and sub-cortical gray matter (*Histology for pathologists Stacey E. Mills*).

In T1 relaxometry images for example, the globus pallidus appears with lower T1 (close to WM T1) compared with other deep gray matter nuclei (DGMN) due to an abundance of myelin [145]. On the other hand, the putamen, which is composed by packed myelinated axons [146], appears with a higher T1 (close to GM T1). The presence of several tissue types results in an intensity mixing effect known as “partial volume” (PV). In brain regions affected by important PV effects, the DGMN and the cortex (especially in the cerebellum), the identification of the tissue type affected by pathology is challenging and pathological effects might appear undetectable when tissues alterations have an opposite effect on the MRI signal. In the recent past, a number of multi-contrast MRI approaches have been proposed to image cortical myelination and differentiate the cellular component from the one constituted by neuronal fibers in the brain cortex. Glasser et al. computed the ratio between T1- and T2-weighted MR images to estimate cortical myelin content [147], while Grydeland combined this ratio with diffusion MRI information to achieve more accurate results [148]. More recently, Shafee et al. attempted at improving cortical myelin content estimation by introducing a mixture model of gray and white matter based on T1- and T2-weighted images. As to deep gray matter (DGM) structures (thalamus and basal ganglia), there have been few attempts to separate their tissue components based on advanced MRI techniques like relaxometry and magnetization transfer imaging or quantitative susceptibility mapping [149].

In this chapter, we present a new single-contrast approach, based on MP2RAGE images, to disentangle WM from GM signal components in the thalamus and the basal ganglia. Using a newly developed PV estimation algorithm (Roche et al. [142]) we computed tissue concentration in each voxel so as to estimate the intensity characteristic of each tissue throughout a given region of interest (ROI). This characteristic intensity stands for the idealized signal of a voxel composed by pure tissue. Results were evaluated qualitatively by comparing the obtained concentration maps with previously published histological data and with high-spatial resolution 7T data in healthy subjects. Next, we performed quantitative comparison by assessing differences in T1 quantitative MRI contrasts between a group of multiple sclerosis patients and of healthy subjects.

4.2 Method

4.2.1 Image processing

Extraction of regions of interest

We segmented the MPRAGE volumes using MorphoBox [103] in order to extract the following deep grey matter regions : thalamus, caudate, putamen and pallidum. MorphoBox automatically delineates regions of interest (ROIs) by performing a non-rigid registration with a template, manually defined by 3 neurologists and radiologist by consent.

Concentration map and tissue intensities

The intensity of a voxel in a MR image depends on the pulse sequence used and the type of molecules present in the voxel volume. In a T1 relaxometry map, this intensity is driven by the density and type of molecules that compose the tissue. The microstructures in the DGMN can be neurons nuclei or glial cells, mainly found in the GM, as well as axons and myelin, the main components of WM [144]. Our approach consists in grouping DGMN cells in two pools, the GM component and the WM component, and estimate their respective contributions to the T1 intensity. For each subject, we applied the PV estimation algorithm developed by Roche A. et al. [142] to the T1 relaxometry map in the extracted ROIs. This algorithm uses a PV model that describes a voxel intensity as the sum of the GM and WM pooled intensities weighted by their respective concentrations, up to Gaussian noise :

$$y_i = \mu_{GM}C_{GM} + \mu_{WM}C_{WM} + \varepsilon_i \quad \text{with } \varepsilon_i = N(0, \sigma) \quad (4.1)$$

where y_i is the intensity of a voxel i , C_{GM} and C_{WM} are the associated concentrations of GM and WM, μ_{GM} and μ_{WM} the characteristic tissue intensities, i.e. the intensities corresponding to 100% of GM and WM, respectively; ε_i represents the noise and σ its standard deviation, which is also estimated by the PV algorithm. After we initialized the vector μ by standard T1 values [85] at 3T for GM ($\mu_{GM} = 1350$ ms) and WM ($\mu_{WM} = 850$ ms), the algorithm iteratively estimated voxelwise gray and white matter concentrations and intensities within each ROI. Since the algorithm can adapt to global intensity changes, the regionally pooled GM and WM intensity estimates reflect putative T1 signal alterations due to pathology.

4.2.2 Qualitative assessment

In a first place, we qualitatively compared our results with a renowned method computing concentration maps. Images were segmented into GM, WM and CSF using SPM8 (Wellcome Trust Centre for Neuroimaging, Institute of Neurology, UCL, London, UK — <http://www.fil.ion.ucl.ac.uk/spm>), (see Figure 4.1). Then, we qualitatively compared estimated GM concentration maps with histological images reported in [150, 151]. In this work, Sadikot and Chakravarty used Nissl staining to highlight the cells bodies representing GM in red, and blue Luxol to show myelin of axons of the WM in blue (see Figure 4.3). Their images show variable concentrations of neuronal cells and myelin in the different structures of the deep gray matter. We used 3T and 7T dataset to estimate our PV maps in order to appreciate the subtle tissue concentration gradient in the different ROIs. We used whole brain estimated concentration maps to ease visual inspection of the data. In practice global tissue concentration maps turned out qualitatively

similar to their ROI-based counterparts.

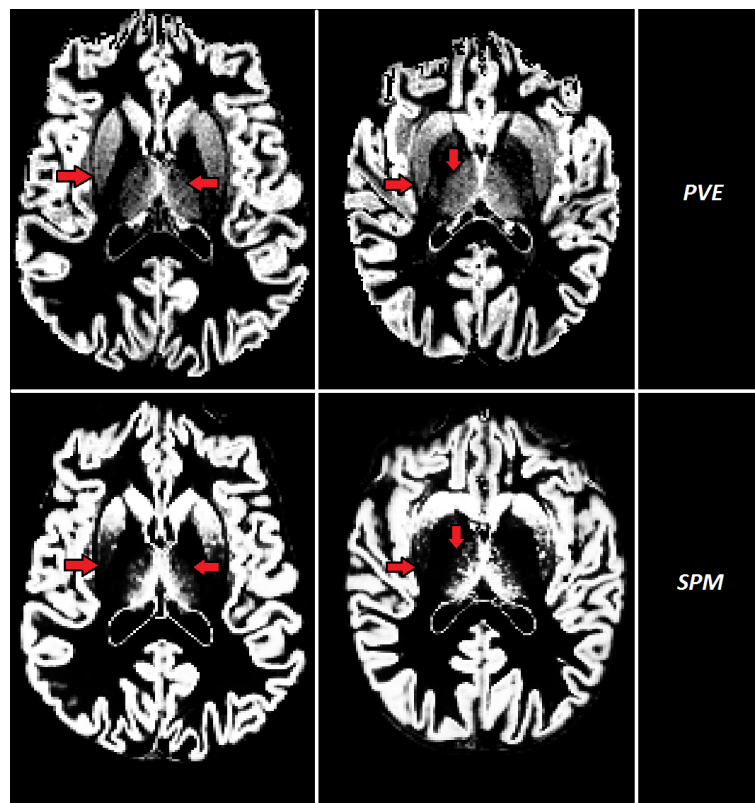


Figure 4.1: Comparison between 2 axial slices of GM concentration maps (first row) and Statistical Parametric Mapping (SPM) GM probabilistic maps (second row) at 3T. The SPM map mainly shows binary concentrations, and some parts (pointed out by red arrows) of the thalamus and putamen disappear compared with concentration maps.

4.2.3 Quantitative assessment

We performed a group analysis to compare RRMS patients and controls for each ROI. We computed the T1 averaged across each ROI in RRMS patients and controls, and applied a two-tailed permutation-based two sample t-tests with age and gender as covariates. Then we performed the same analysis on ROIs revealing significant differences between the two groups, based on the estimated pooled T1 intensity in GM and WM, as well as the logarithm of the ratio between GM and WM concentration. A family-wise error rate correction was used for multiple comparisons correction. Both concentration and intensity tests were corrected simultaneously.

4.3 Results

4.3.1 Qualitative assessment

The observation of GM concentration maps using SPM showed similarities with our PV estimated maps. Nevertheless, the SPM maps appeared mostly binary than our PVE maps and did not represent parts of the thalamus as well as a large part of the putamen (red arrows) (see Figure 4.1). These results reflect the additional information provided by our method compared with SPM in deep gray matter regions. Then, we qualitatively compared the results from the concentration maps obtained from 3T data of 3 healthy subjects with two histological slices obtained from Sadikot and Chakravarty [150, 151]. The first slice shows the histology of the thalamus, the caudate and the putamen (see Figure 4.2): neurons nuclei in red, and myelin in blue. While the concentration of nuclei in the putamen and caudate appears homogeneous, the thalamus shows a variable amount of cells nuclei which gradually increase towards the ventricles. The concentration maps estimated from the T1 map at 3T show very similar homogeneity in the GM concentration of the caudate (delineated in green) and putamen (delineated in yellow), while the thalamus (delineated in blue) exhibits an increase of GM concentration going from the border of the structure to its center. The red coloration in the histological slice shows a higher concentration of neurons nuclei in the caudate than in the putamen. The GM concentration map reflects this difference as the caudate appears brighter than the putamen for the 3 subjects. We also noticed the difference in GM concentrations between the thalamus and caudate, reflecting the presence of myelin, as shown in the histological data. Furthermore, the concentration maps visualized the red nucleus (Ru) and the locus niger (Ni), as reported by histological data.

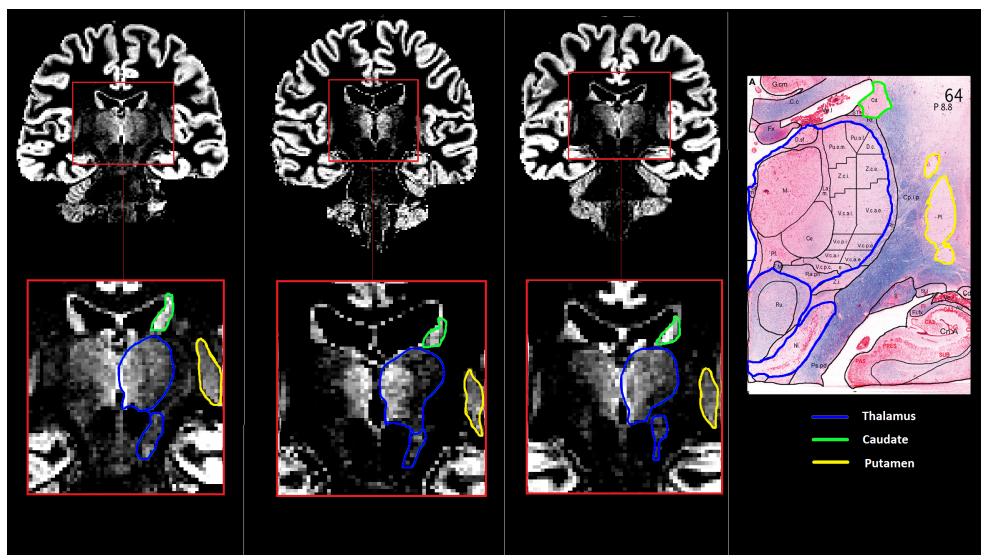


Figure 4.2: GM concentration map using T1 maps of 3 healthy subjects at 3T and histological slice with an outline of nuclei of the thalamus on a coronal Myelin-Nissl-stained section (right).

Chapter 4. A new approach for deep gray matter analysis using partial volume estimation

Similar observations are made in others coronal slices from estimated concentration maps of 3 healthy subjects scanned at 7T MRI compared with histological stainings [151] (see Figure 4.3). Owing to the higher spatial resolution than 3T data, 7T images showed additional detail: a GM bridge between the caudate and putamen which is clearly observable on stained images. The qualitative assessment showed multiple similarities in terms of nuclei structures and relative concentration of each DGMN between histological data and concentration maps.

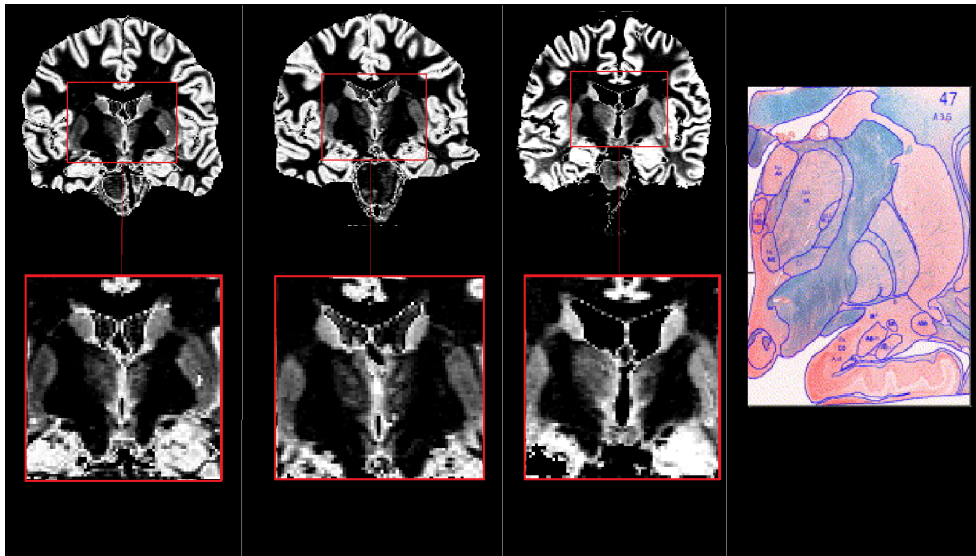


Figure 4.3: Comparison between GM concentration map of 3 healthy subjects at 7T and an histological slice from a healthy human subject . The concentration map were estimated using the whole-brain T1 map. In the zoomed area of GM concentration map we can observe the gray matter bridge present in the histological slice between the caudate and the putamen.

4.3.2 Quantitative group comparison using global ROI averaging, T1 tissue intensities and concentrations

The multivariate analysis of T1 pooled intensities and concentration ratios revealed a significant difference in the thalamus of RRMS patients ($p=0.0016$). The analysis of the tissue T1 intensities and concentrations showed a significant increase of 3% of the GM T1 in the RRMS patients (Controls: $\mu_{GM} = 1389 \pm 47$ ms; Patients: $\mu_{GM} = 1427 \pm 40$ ms; $p = 0.016$), while the WM T1 (0.6%) and the concentration ratio (-1%) were not found significantly different (Controls: $\mu_{WM} = 912 \pm 18$ ms, $\mu_{ratio} = 0.62 \pm 0.08$; Patients: $\mu_{WM} = 918 \pm 14$ ms, $\mu_{ratio} = 0.61 \pm 0.07$) (see Figure 4.4).

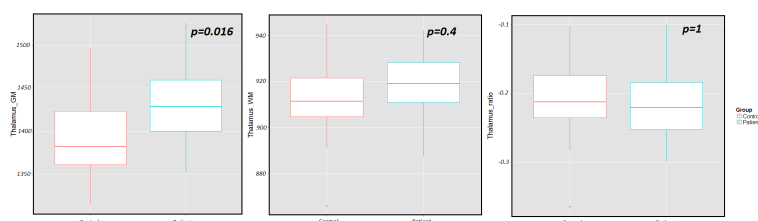


Figure 4.4: Boxplots of the WM and GM of the thalamus for RRMS patients and controls using the proposed PV method. It shows significant increase in the T1 of the GM components between the RRMS patients and HC.

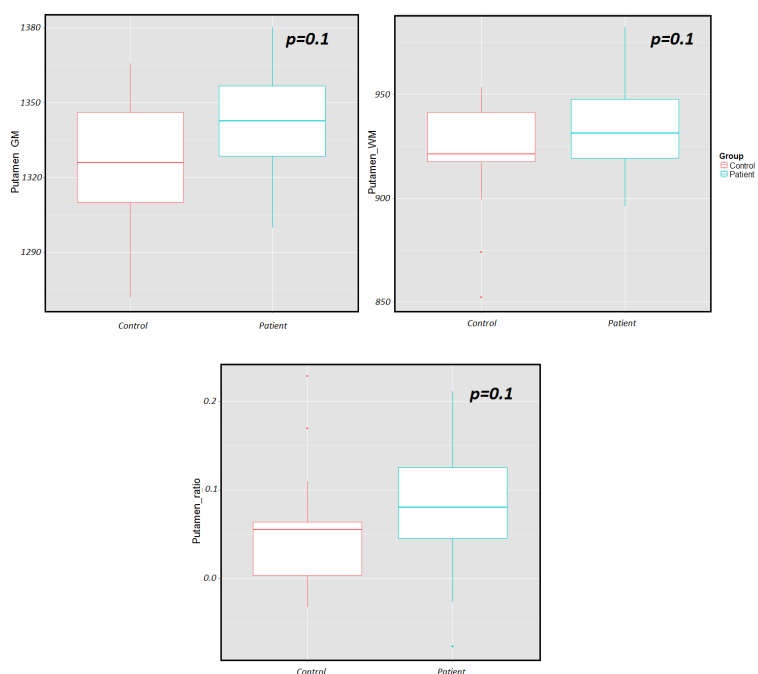


Figure 4.5: Boxplots of the WM and GM of the putamen for RRMS patients and controls using PV method. This method showed no significant increase in the T1 of the GM and WM components neither concentration ratio between the RRMS patients and HC.

The putamen, caudate and pallidum did not show any significant changes between RRMS patients and HC using the multivariate analysis (see Figure 4.5). The global averaging analysis showed significant differences in the thalamus but also in the putamen between RRMS patients and HC. In both structures, we observed a significant T1 increase in RRMS patients compared with HC (thalamus: $p = 0.038$; HC : $\mu T1 = 1094 \pm 33$ ms; RRMS : $\mu T1 = 1110 \pm 22$ ms ; putamen: $p = 0.026$; HC : $\mu T1 = 1136 \pm 35$ ms; RRMS : $\mu T1 = 1156 \pm 27$ ms, see Figure 4.6).

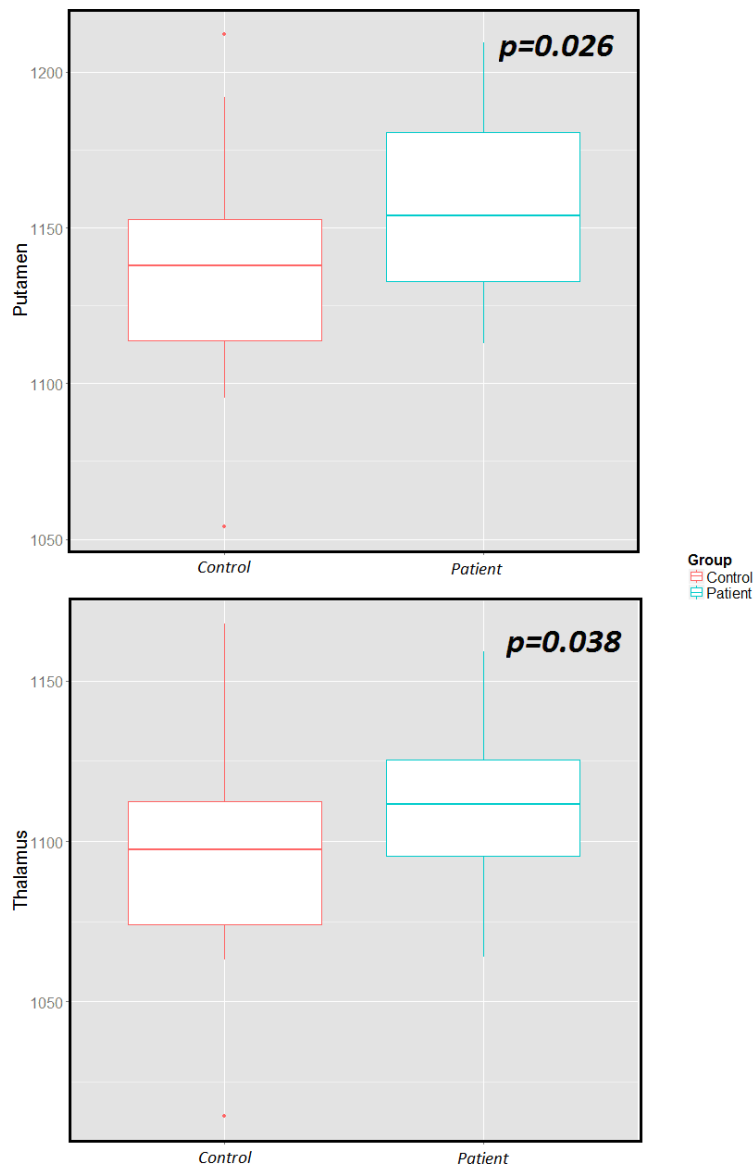


Figure 4.6: Boxplot of mean T1 in the thalamus and putamen using global averaging method. This method showed significant increase of T1 in both ROIs in RRMS patients compared with HC.

4.4 Discussion

This study presents a new approach to disentangle GM and WM in regions affected by PV like the thalamus and the basal ganglia. The proposed methodology provides quantitative estimations of GM and WM voxelwise concentrations and pooled intensity values that are characteristic of GM and WM within a particular region, opening new perspectives to evaluate

the impact and the nature of pathological processes in these brain regions.

The comparison with concentration maps estimated using a publically available software (SPM8) revealed similarities and some differences. Specifically, SPM maps had an overall comparable global appearance with the one obtained with our method, though our maps visualize parts of the thalamus and putamen, which were not visible on SPM maps. In parallel, the qualitative comparison of estimated tissue concentration maps with histological data showed remarkable similarities. The heterogeneity of cells nuclei concentration in the thalamus, as well as the variable amount of myelin among the DGMN, could indeed be observed in GM concentration maps as shown in the histological slices. Also, the concentration maps estimated from 7T MRI data showed subtle structure such a GM bridge between the caudate nucleus and the putamen in addition to the detailed microstructure already revealed by 3T maps. All together therefore, these findings provide qualitative validation of the PV estimation technique, recently proposed by Roche et al. [142].

Furthermore, group analysis showed a significant changes between MS patients and controls in the thalamus ($p=0.038$) and putamen ($p=0.026$). The changes in the thalamus were mainly reflected by an increase of the intrinsic T1 value of the GM in RRMS patients ($p=0.016$), with no significant changes in the T1 of the WM component nor in the concentration ratio. At the same time, the analysis of the putamen did not show significant changes in the T1 of the GM and WM nor concentration ratio, but revealed an increase in the 3 components. These results suggest that the pathology in the thalamus seems to mainly affect the microstructure elements composing the GM pool, while in the putamen the WM and GM pools appeared less but equally affected.

From a patho-physiological viewpoint, these findings imply the presence of a diffuse alteration of the tissue in the thalamus and putamen, which may be due to a loss of tissue or an increase in water component. This might reflect a stage preceding atrophy, which has been already reported in the thalamus since the early stages of the MS [152]. Our approach provided additional information and improved our understanding of the underlying processes involved in brain tissue alteration in ROIs affected by PV. Although global averaging method remains sensitive to compare MR intensities in ROIs, our method may also reveal changes in DGMN in a more sensitive way. In fact, a multivariate analysis (e.g. MANOVA) may be more appropriate in case of larger cohort, to detect subtle changes.

Yet, our approach suffers from some limitations. Concerning the intensity model we used, it considers that the characteristic intensity of a tissue is homogeneous over the whole region of interest. This hypothesis is questionable for large regions of interest such as the cortical gray matter, and may limit the validity of our method to small regions such as the DGMN. Moreover, the estimation of the PV becomes ambiguous when the tissue is so altered that its intensity is drastically changed. Consequently, focal alterations such as lesions, could be confused with voxels with high GM concentration in T1 maps for example. Therefore, an exclusion of the lesions should be considered before estimating concentration maps.

4.5 Conclusion

In summary, our study proposed a single-contrast approach which provides novel and relevant characteristics of brain tissue in regions affected by partial voluming. In this context, the analysis of basal nuclei and thalamus which are involved in the physiopathology of various neurodegenerative diseases [153], may be improved and lead to new perspectives to understand underlying processes of the pathology. Additional studies extending the PV approach to other regions (lobes, cerebellum) and other qMRI would provide whole-brain concentration map, and allow to compute spatial comparison map between individual and control group (see Conclusion : Perspectives).

In the next chapter we present the results of a longitudinal analysis based on our q/sq multi-contrast approach, and we show the potential of our methodology to monitor disease over 2 years.

5 Longitudinal analysis of multi-contrast advanced MRI

Abstract

Clinical monitoring of RRMS patients evolution and therapy efficacy plays a key role in MS since a number of treatments have been shown to substantially reduce the number of clinical relapses and disability, as well as the extent of local inflammation and brain volume loss [154]. Recently, a number of non-conventional MRI techniques have been applied to disease follow-up, to overcome the limitations of conventional MRI due to their low sensitivity to diffuse and subtle changes in brain tissue. In this chapter, we used longitudinal MRI data acquired over 2 years to assess (i) the sensitivity of multi-contrast MRI (mcMRI) to longitudinal changes in normal appearing brain tissue and lesions, and (ii) the prognostic value of baseline mcMRI metrics to predict motor and cognitive performance at 2 years in MS patients. Results showed significant changes in normal brain tissue due to aging effect characterized by an increase of T1 and a decrease of MTR in MS patient and controls. Lesions analysis revealed significant changes suggesting reparative processes such as remyelination and scar formation. Finally the combination of quantitative MR measurements of focal and diffuse pathology from the first time-point showed strong correlation with clinical score of the second time-point.

5.1 Introduction

To date, there is no cure for RRMS but a number of treatments have been shown to substantially reduce the number of clinical relapses and disability, as well as the extent of local inflammation and brain volume loss [154]. Clinical monitoring of RRMS patients evolution and therapy efficacy relies on neurological and disability assessment, which is often insensitive to mild and subclinical disease progression. On the other hand, conventional magnetic resonance imaging (MRI), such as T2-weighted and gadolinium enhanced MRI, provide quantitative measurements of local MS pathology (lesion number and volume) as well as on inflammatory activity [155]. In addition, conventional T1-weighted MRI is sensitive to the presence of severe local tissue loss ("black holes") [155], and provides the basis for volumetric estimations and brain atrophy assessment [28, 156]. Yet, conventional MRI has low sensitivity to diffuse and subtle brain alterations, and provides with metrics that only partially correlate with patients function and disability [157–159]).

In this context, a number of non-conventional MRI techniques have been applied to overcome the limitations of conventional MRI, such as Magnetisation Transfer Imaging, Diffusion Tensor Imaging, relaxometry and spectroscopy [160]. Nevertheless, single contrast approaches provides only limited knowledge about the nature of measured alteration. We recently showed that advanced multicontrast MRI (mcMRI) provides metrics to quantify the extent and the nature of focal and diffuse pathology in MS, with higher specificity than single contrast approaches; besides, we determined that metrics of tissue microstructural integrity as obtained with cMRI improved the clinico-radiological correlations obtained with conventional measures only (lesion number and volume).

In this chapter, we assessed (i) the sensitivity of mcMRI to assess longitudinal changes in brain tissue properties of a cohort of MS patients compared to healthy controls, that we followed-up for 2 years; and (ii) the prognostic value of baseline mcMRI metrics to predict motor and cognitive performance at 2 years in MS patients.

5.2 Methods

Thirty RRMS patients out of 36 and 9 HC out of 20 were enrolled for a second scan session 24 months after the first scan. Seven patients and one control were discarded because one or more datasets were artefactual.

The cohort of interest consisted therefore of 23 RRMS patients (17 women / 6 men, age = 35.7 ± 11.8 years) and 8 HC (2 women / 6 men, age = 34.3 ± 9.2 years). The MRI protocol was the same for the 2 time-points as well as the cognitive, behavioural and motor tests applied (see Chapter 2.2.3).

As to therapy, thirty patients (83%) were under immunomodulatory treatment (high dosage IFN beta or fingolimod) for at least 3 months. No patient had received corticosteroid therapy within the three months preceding the enrollment.

5.2.1 Tissue and lesions segmentation and images registration

Morphobox [103] was used to segment tissues and structures (lobes, deep gray mater nuclei etc...) on MPRAGE images for both time-points. Images were registered to the MP2RAGE space using the same approach presented in Chapter 2.

Lesions were manually segmented on 3D FLAIR, DIR and MP2RAGE images also for the second time-point by an expert technician, who reviewed also the first time-point for consistency. The lesions masks of the second time-point were all registered with lesions masks of the first time-point (TP1) so we could match the same lesions identification number.

5.2.2 Image processing and lesions classification

For both time-points, we extracted mean T1, T2, T2* and MTR in the gray and white matter components of the following ROIs: frontal lobe, temporal lobe, parietal lobe, occipital lobe, cerebellum, thalamus and basal ganglia. Normal appearing tissue was obtained in each ROI by subtracting the lesions union mask.

The lesions were processed separately using the methodology presented in chapter 3. We computed T1, T2 and MTR z-scores for all lesions and we assigned each lesions to its corresponding combination and group (see Chapter 3.2.2).

5.2.3 Statistical analysis

Normal appearing tissue and volumetry

MANOVA was used to study the influence of a number of independent variables (age, gender, patients group, MRI sequence and time-points) on the four dependent variables represented by T1, T2, T2* and MTR mean in each brain ROI (WM, GM, cerebellum, thalamus and basal ganglia).

Based on the MANOVA results, we then performed a number of ANOVA tests to assess the influence of the time-points and of the group, on each MRI sequence (T1, T2 and MTR).

Time-point 1 vs. Time-point 2

In order to analyse the changes over 2 years, we performed paired t-tests for each contrast and group. This analysis considered multiple pairs of observations (mean of the corresponding contrast and region) to assess the following H0 hypotheses:

- There are no differences in the mean T1, T2 and MTR of the GM and WM of the temporal, frontal, parietal and occipital lobes between TP1 and TP2.
- There are no differences in the mean of the T1, T2 and MTR of the GM and WM of the cerebellum between TP1 and TP2.
- There are no differences in the mean of the T1, T2 and MTR of the thalamus, caudate,

putamen and pallidum between TP1 and TP2.

All tests were corrected for multiple comparison using Bonferroni.

Patients vs. Controls Group

In order to differentiate normal aging and pathological effects, we computed the difference between the time-points in each contrast for all patients and controls, and performed two-sampled t-tests to assess the following H0 hypotheses:

- There are no differences in the evolution of the T1, T2 and MTR of the GM and WM of the temporal, frontal, parietal and occipital lobes between the control and patient group.
- There are no differences in the evolution of the T1, T2 and MTR of the GM and WM of the cerebellum between the control and patient group.
- There are no differences in the evolution of the T1, T2 and MTR of the thalamus, caudate, putamen and pallidum between the control and patient group.

All tests were corrected for multiple comparison using Bonferroni.

Volumetry

We performed two-sampled t-tests analysis to measure the difference of normalized volume of the global GM and WM, as well as the thalamus and basal ganglia between patients and controls groups. All tests were corrected for multiple comparison using Bonferroni.

Lesions

In order to detect changes in lesions evolution, we measured changes in lesions combinations and groups. We grouped the 12 combinations in 4 main groups and we performed a paired two-sampled t-tests in each group. Results were corrected for multiple comparisons using Bonferroni.

In order to assess the potential of mcMRI to predict the appearance of new lesions or lesions expansion, we computed the mean T1, T2 and MTR value at TP1 of the region corresponding to new lesions and expanding lesions at TP2. Then we performed a two-sampled t-test for each contrast between the mean value of the region defined previously and the mean value of the healthy tissue in the corresponding lobe. Last, we repeated the analysis by replacing healthy tissue mean value by the normal appearing tissue characteristic T1, T2, T2* and MTR at TP1.

Regression analysis

A multivariate linear regression of clinical scores was performed using a general linear model (GLM) on TP1 MRI data (regressors) and TP2 clinical scores (predicted variables). Age, gender and educational years were considered as covariates.

Due to the small cohort of subjects, we considered global measurements and not lobe-wise mean. We also added T1, T2, T2* and MTR lesion z-scores to assess their prediction potential in clinical scores. Cognitive scores were adapted using Box-Cox transformation to satisfy model assumption for normalization. EDSS scores were not considered, as they were positive only in patients. We performed seven regressions, where we used a stepwise approach to select the best prediction model for each dependent variable (clinical scores). Bonferroni correction was applied for multiple comparisons (seven tests).

“Leave-one-out” cross validation (LOOV) was applied to assess the prediction quality and robustness of each model. This last analysis extracted a correlation coefficient between the predicted value and the real one. All regression analyses were performed using R software (<http://www.R-project.org>).

5.3 Results

5.3.1 Normal appearing tissue and volume analysis

The MANOVA showed that the time-points, the group and the age significantly influenced the evolution of all contrasts. Therefore we performed ANOVA on time-points and group effect separately considering age as a covariates.

Time-points effects

In patients normal appearing tissue, we observed a significant increase in the T1 in the WM of the occipital and lobe frontal lobes (occipital : $p = 1.2e-04$, frontal : $p = 0.012$), as well as in the WM and GM of the temporal lobe (WM : $p = 5.86e-05$; GM : $p = 0.011$) between the 2 time-points Figure 1-a. We also measured an increase in T1 in the WM of the cerebellum ($p = 0.016$) and a significant decrease in the pallidum ($p = 0.0089$).

We observed a decrease of T2-rt in the WM of the occipital and parietal lobes (occipital : $p = 3.2e-07$; parietal : $p = 3.99e-06$), as well as the GM of the frontal lobe ($p=0.026$) between the 2 time-points. We also measured a decrease in T2-rt in the pallidum and putamen (pallidum : $p = 0.0206$; putamen : $p = 0.04$), and an increase in T2 in the caudate ($p = 0.039$).

T2* was greatly increased in the frontal and temporal lobes of MS patients vs controls (frontal : $p = 1.37e-04$; temporal : $p = 3.60e-10$), nevertheless we mainly attributed those differences to strong distortion artefact that we observed in these regions at TP2. In the cerebellum, we found a significant increase of T2* in WM ($p = 0.027$) as well as in the caudate ($p = 0.002$) and the putamen ($p = 0.0003$). The MTR showed a significant decrease in the GM of the occipital

Chapter 5. Longitudinal analysis of multi-contrast advanced MRI

lobe ($p = 0.003$).

Significant changes were also measured in normal appearing tissue of controls with an increase of the T1 of the temporal WM ($p = 0.0002$), and a decrease of the T2 of the parietal WM ($p = 0.007$). We measured significant decrease of the T2 in the putamen of controls ($p = 0.0012$), as well as an increase of T2* in the caudate ($p = 0.023$) and putamen ($p = 0.044$).

All graphs illustrating changes in T1, T2, T2* and MTR are in Appendix A.3-A.7.

	GM			WM				
	Occipital	Frontal	Temporal	Parietal	Occipital	Frontal	Temporal	Cerebellum
T1	n.s	n.s	0.011*	n.s	0.00012**	0.012*	5.86e-05***	0.016*
T2	n.s	0.026*	n.s	3.99e-06***	3.2e-07***	0.007*	n.s	n.s
T2*	n.s	n.s	n.s	n.s	n.s	n.s	n.s	0.027*
MTR	0.003*	n.s	n.s	n.s	n.s	n.s	n.s	n.s
				Caudate	Putamen	Pallidum		
T1				n.s	n.s	0.0089*		
T2				0.039*	0.04*	0.0206*		
T2*				0.002*	0.0003**	n.s		
MTR				n.s	n.s	n.s		

Table 5.1: Paired two-sampled t-tests p-values for RRMS patients in significant ROIs for all contrast between TP1 and TP2. n.s : non significant.

	WM		CN	
	Parietal	Temporal	Caudate	Putamen
T1	n.s	n.s	n.s	0.0002**
T2	0.007*	n.s	n.s	0.0012*
T2*	n.s	n.s	0.023*	0.044*

Table 5.2: Paired two-sampled t-tests p-values for controls in significant ROIs for all contrast between TP1 and TP2. n.s : non significant.

Groups effects

We did not find any significant difference between changes observed in RRMS patients and control group. The volumetric analysis did not show any significant group differences in the observed changes in T1, T2, T2* relaxation times and MTR between time-points.

5.3.2 Lesions

The paired t-tests on lesions revealed significant decrease of T1-rt and T2-rt and an increase of MTR (T1 : $p = 6.18e-43$; T2 : $p = 6.54e-04$; MTR : $p = 1.60e-04$) Figure A.8. The analysis of the longitudinal evolutions of lesions combinations and groups showed different effects in the

four groups. The first group, composed by lesion with no difference in T1, T2, T2* and MTR with healthy tissue, showed no significant changes between the time-points ($p = 0.5$). This group counted for 35% of the total number of lesions at the TP1, and 45% at TP2. Most of the lesions from this group (88%) remained in the same group, while the rest equally divided in the Class2 (6%), Class3 (4%) and Class4 (2%) Figure(5.1).

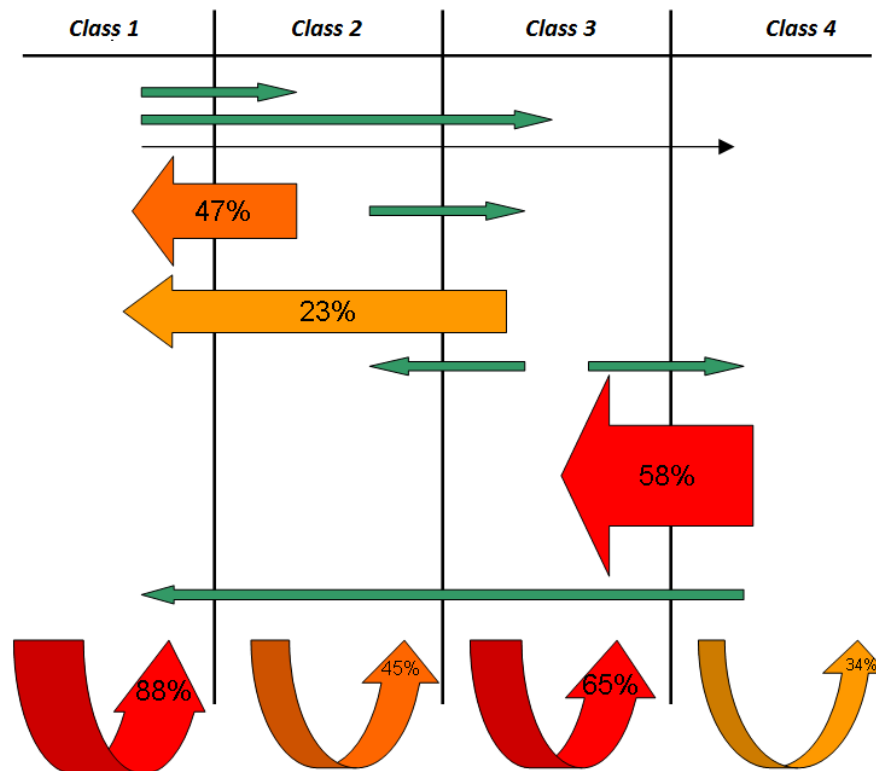


Figure 5.1: Evolution of lesions among the different group based on qMRI combination.

Also the second group, composed by lesions exhibiting prevalent inflammation, did not show any significant changes between the two time-points ($p = 0.3$). This group counted for 6% of the total number of lesions at TP1 and increase to 20% of the lesions of TP2. 45% of the lesions of this group remained in the same group, while 47% evolved to the Class1 and the rest evolved to Class3 (8%) Figure(5.1).

The third group of lesions, including lesions with micro-degeneration with or without inflammation showed significant changes ($p = 6e-06$), characterized by an evolution toward combinations reflecting milder tissue alterations. This group counted for 50% of the total number of lesions at TP1 and increased to 53% at TP2. Twenty-three percent of the lesions of this group evolved to Class1 (23%) and few of them in Class2 (6%) and Class4 (6%), while more than the half of the lesions (65%) remained in the same group Figure(5.1).

Similarly the Class4, composed by lesion with predominant tissue loss, showed significant changes between the two time-points ($p = 3.06e-09$) (Figure 4). This group counted for 8% of

the total number of lesions at TP1, and decreased to 7% at TP2. Most of the lesions evolved to Class3 lesions (58%) and few to Class1 lesions (8%), while the rest remained in the same group (34%) Figure(5.1).

Finally, the analysis of the tissue in TP1 where new lesions will appear on TP2, showed a significant increase in T1 ($p = 1.24e-05$) and T2 ($p = 1.24e-06$) in patients compared with healthy tissue as well as with normal appearing tissue surrounding the analyzed regions (T1 : $p = 0.018$; T2 : $p = 5e-04$). We also observed a significant decrease of MTR compared with healthy tissue ($p = 0.005$), but no changes with normal appearing tissue ($p = 0.4$). Figure A.9. Likewise, the regions where lesions expanded also showed significant increase of T1 compared with healthy tissue ($p = 1e-56$) and with NA tissue ($p = 1e-46$), as well as an increase of T2 (healthy tissue : $p = 2.8e-71$; NA : $p = 7.7e-54$) and T2* (healthy tissue : $p = 4.07e-13$; NA : $p = 1.05e-05$), and a decrease of MTR (healthy tissue : $p = 7.7e-41$; NA : $p = 1.07e-36$) Figure 5.2, Figure A.10.

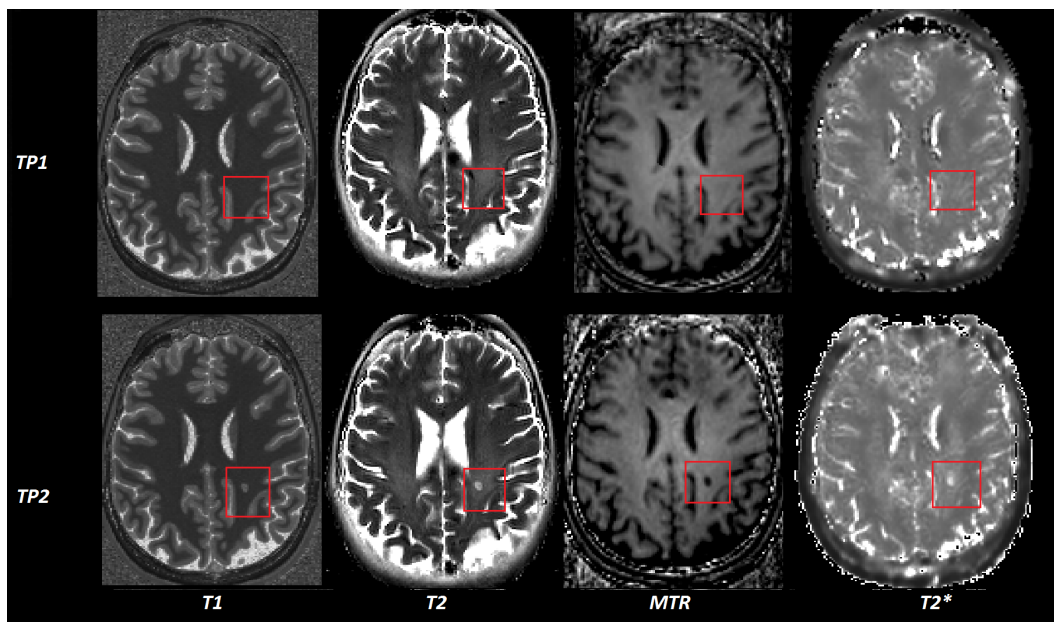


Figure 5.2: Example of new lesions on q/sq MRI contrasts. Though we found significant difference between normal appearing tissue and HC in regions where lesions will appear (red square), we can not see any evidence of changes in q/sq MRI before lesions appearance.

5.3.3 Regression analysis

GLM using stepwise regression revealed a highly significant association, confirmed by cross-validation results, between multi-contrast MRI features and three clinical scores (Table 2):

- T1, T2 mean z-score of lesions and T1, T2, T2*, and MTR mean of NAWM and NAGM together with age and education predicted the word list generation (memory function)

score ($Adj-R^2: 0.97, p = 0.0001; LOOV: 0.28$).

- T1, T2, T2* and MTR mean z-score of lesions and T1, T2, T2*, and MTR mean of NAWM and NAGM together with age, gender and education predicted the FSMC cognitive (fatigue) score ($Adj-R^2: 0.97, p = 0.006; LOOV: 0.61$).
- T1 T1, T2, T2* and MTR mean z-score of lesions and T1, T2, T2*, and MTR mean of NAWM and NAGM together with age, gender and education predicted the FSMC motor (fatigue) score ($Adj-R^2: 0.93, p = 0.01; LOOV: 0.41$).

	Word list generation	FSMC cognitive	FSMC motor
<i>p-value</i>	1.27e-04 ^{***}	0.006 [*]	0.0105 ^{***}
Adj-R ²	0.9795	0.9750	0.9391
Leave-one-out	0.28	0.61	0.41

Table 5.3: Regression results using MRI data from Time-point 1 to predict clinical scores from Time-point 2.

5.4 Discussion

Our longitudinal study shows that multicontrast quantitative and semiquantitative MRI is sensitive to local and diffuse pathology evolution in a group of RRMS patients under immunomodulatory and immunodepressive therapy. In addition, multi-contrast MRI metrics provided strong predictors of memory function and fatigue at two years follow-up.

In RRMS patients, we observed a small difference between time-points in mean T1, T2, T2* and MTR in normal appearing tissue. These minor parametric variations (<3%) over two years follow-up are compatible with changes observed during normal aging processes. In fact, Callaghan et al. observed similar T1 increases in several regions of the brain (1% to 1.6% over one year [161]). Likewise, the same authors and several others studies [162–164] reported a decrease of quantitative MT value between 1.5% and 2.5% in one year, while we measured a decrease of MTR around 5% in two years.

The changes in T1 are associated with degenerative changes on myelin sheaths due to normal aging [38, 165]. The decrease of MT ratio in GM may reflect neuronal or nerve fibers loss [166]. We also observed an increase of T2*-rt in the caudate and putamen (<5%) over the two years, which was accompanied by an increase in T1-rt and T2-rt in the caudate, and a decrease of T1 and T2 in the putamen. This effect might originate from iron loss due to degenerative changes in the basal ganglia [161] but since changes in the other parameters were quite modest (<5%), the interpretation of these findings remain challenging. Future studies in

larger cohorts, including patients at more advanced disease stages, may help distangling the pathophysiological mechanisms T2* changes in the basal ganglia.

The analysis of T1, T2 and MTR of lesions showed an improvement revealed by a significant global decrease of T1-rt and T2-rt, and combined with a global increase of MTR. These results suggest a repair activity within the lesions. The individual analysis of MS lesions revealed changes in all lesion groups though only changes in Class3 (lesion with both inflammation and degeneration) and Class4 (lesions with predominant degeneration) reached significance. A significant part of Class3 ($p=6e-06$) and Class4 ($p=3.06e-09$) lesions evolved to lesions with milder alterations (Classes 1-3). In Class3, we observed a decrease of T1, T2 and or T2* reflected by an evolution of the lesions toward Class1 (20%) and Class2(6%). This changes might indicate an attenuation of inflammatory and degenerative phenomena. Nonetheless, most of Class3 lesions (65%) remained in the same group suggesting that micro-degeneration is counterbalanced by remyelination process [118]. Only few lesions from Class3 evolved to more advanced stage in Class4 (6%) where MTR decrease reveal a destruction of tissue and may suggest an acute phase of the lesions. In group 4, we observed an increase of MTR in lesions that evolved to Class3 (58%). These changes suggest a reparative activity characterized by remyelination and/or scar tissue formation [118, 167]. A third of Class4 lesions remained in the same group, providing evidence that repair mechanisms did not counter-balanced the tissue loss.

Although we did not measured significant changes in lesions from Class1 ($p=0.5$) and Class2 ($p=0.3$), a minority of Class1 lesions (12%) evolved toward more advanced stages including inflammatory and degenerative activity. As to Class2, a very small number (8%) showed evidence of micro-degeneration or tissue loss after 2 years, but almost half of Class2 lesions even evolved toward milder stage, which may be due to reabsorption of inflammatory oedema [118]. In summary, therefore, the analysis of lesions evolution revealed different underlying processes that modified tissue microstructure, and that reflect the balance between injury and repair capacity of the brain.

Interestingly, the analysis of the normal tissue at TP1 that evolved into lesion tissue at 2 years follow-up showed a significant increase of T1-rt and T2-rt and a decrease of MTR when compared with healthy tissue in HC and tissue surrounding the lesions in patients. This suggests an increase in water content of the pre-lesion tissue and/or tissue loss. Filippi and Pike previously observed MTR abnormalities up to 2 years before lesions appearance, suggesting primary myelin damage before inflammatory mediated brain-blood barrier disruption [168, 169]. Fazekas et al. also measured a significant drop of MTR six month before lesions appearance, combined with an increase of T1 native relaxation time [170]. Though MTR decrease was interpreted as demyelination, it could actually suggest water accumulation in the form of micro-oedema, which is what we observed in a previous study [80].

Last, relaxation times and MTR in NA tissue combined with mean lesions z-scores at the first MRI strongly predict patients cognitive ($Adj-R^2: 0.97, p = 0.006$) and motor fatigue ($Adj-R^2:$

0.97, $p = 0.0001$) as well as memory ($Adj-R^2: 0.97, p = 0.01$) at 2 years follow-up. This study extends results obtained at TP1 (Chapter 2), by showing the longitudinal predictive power of mcMRI even in patients with mild clinical deficits.

5.5 Conclusion

In conclusion, mcMRI provided sensitive measures to assess longitudinal changes of diffuse and focal brain tissue abnormalities, over 2 years. We also measured quantitative T1 and T2 abnormalities preceding lesions appearance suggesting presence of micro-edema. Finally, we provided evidence of the strong prognostic value of baseline mcMRI metrics to predict motor and cognitive performance at 2 years in MS patients. Future studies should confirm and extend our findings in other MS disease subtypes and with longer follow-up.

6 Conclusion : Achievements and Perspectives

This thesis aimed at studying the micro-properties of brain tissue in MS patients using new advanced techniques in MRI. Initially, we established a methodology combining different q/sqMRI contrasts to detect diffuse subtle pathological changes in brain tissue of MS patients as well as focal alterations. We also showed how to take advantage of the complementarity of q/sqMRI sensitivity (i.e. changes in water, macro-molecules, iron...), to identify the physiopathological process underlying tissue microstructure alterations in MS. Then, we extended our multi-contrast approach to model the heterogeneity of tissue damage in MS lesions through a classification framework. We also presented an innovative technique based on partial volume estimation, to disentangle the WM and GM components in deep gray matter structures, providing additional information on the micro-properties of the tissue affected by MS pathology. Last, we showed the potential of our approach to monitor MS patients over a 2 years period, and particularly to identify repair and degeneration activity in brain tissue.

6.1 Achievements

The results we reported in this thesis may have potential impact both at a methodological and clinical application level.

On a methodological level, we established that multi-contrast q/sq MRI provides higher sensitivity and specificity than single contrast approaches.

- We showed the sensitivity of q/sqMRI to subtle changes in large regions as well as in focal areas and provided metrics to estimate the physiopathology of observed tissue alterations.
- Based on these metrics, we proposed a new classification method of MS lesions pathology and their evolution, which recalls histopathological data in MS patients.
- Last, we revealed the potential of a partial volume approach based on T1 relaxometry contrast, to detect subtle pathological and tissue-specific effect in the deep gray matter

nuclei.

In term of clinical applications, the constant development of MR technology and the acceleration of MR sequences acquisition might render q/sq MRI clinically compatible in a near future. Of course, extension to more advanced and bigger MS cohorts as well as reproducibility studies in a multi-centre settings are required before foreseen the introduction of q/sq MRI in clinical protocols; however, the current work sets the basis for future investigations.

6.2 Perspectives

In this thesis, we performed a comparison between MS patients and healthy controls groups. Yet, clinical applications are based on single-patients evaluations. Therefore, we conceived a pipeline model to perform analysis of tissue microstructure in a single MS patients. Specifically, we created a voxel-wise deviation map of an individual by computing z-score maps for each q/sq contrast. We then incorporated the partial volume estimation technique in the pipeline to identify the WM and GM components in each brain structure.

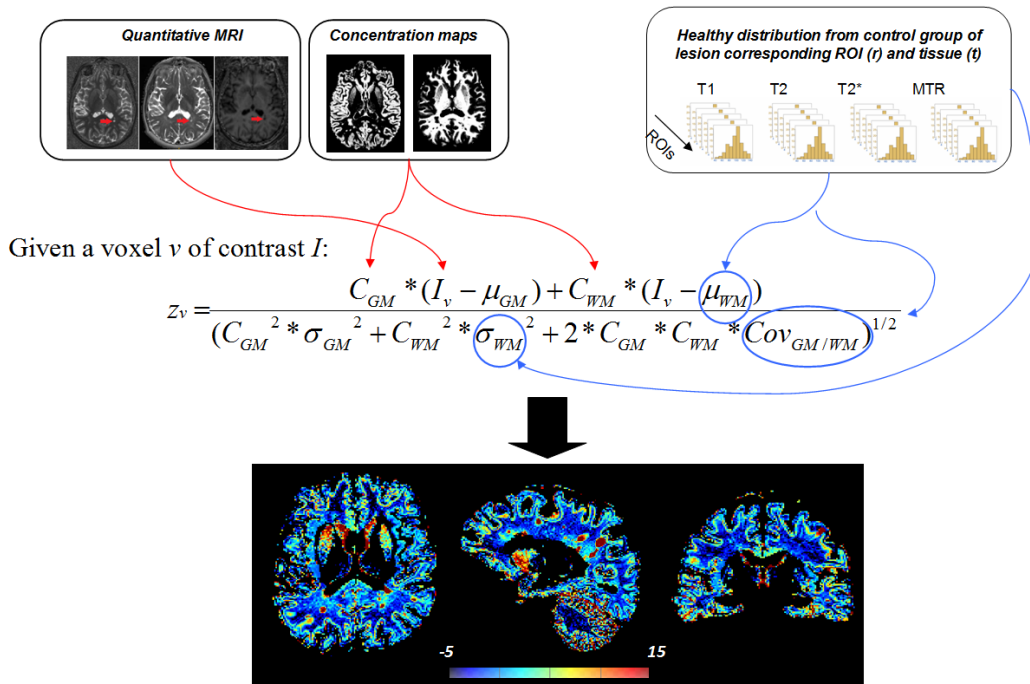


Figure 6.1: Pipeline for deviation maps computation. The inputs are the q/sq MRI concentration maps, as well as the normative ranges of WM and GM in each brain structure.

Subsequently, we computed the normative ranges of 3 contrasts (T1, T2, MTR) in all brain regions (lobes, basal ganglia, cerebellum) for each tissue (GM, WM) in the control population (n=18). Then, we computed the z-score map of the 3 contrasts from the concentration maps for each a single patient. Figure 6.1.

We performed our pipeline on T1, T2 and MTR contrasts. The results show relevant representation of diffuse changes, particularly in the T2 relaxation time Figure 6.2. The analysis of lesions show strong changes in T1, T2 and MTR inside the lesions but also in the surrounding area. Our maps provide evidence of diffuse alteration of the tissue characterized by T2 and MTR variations. These results may help to improve our understanding of tissue alterations, and should help to identify more precisely areas where pathology occurs.

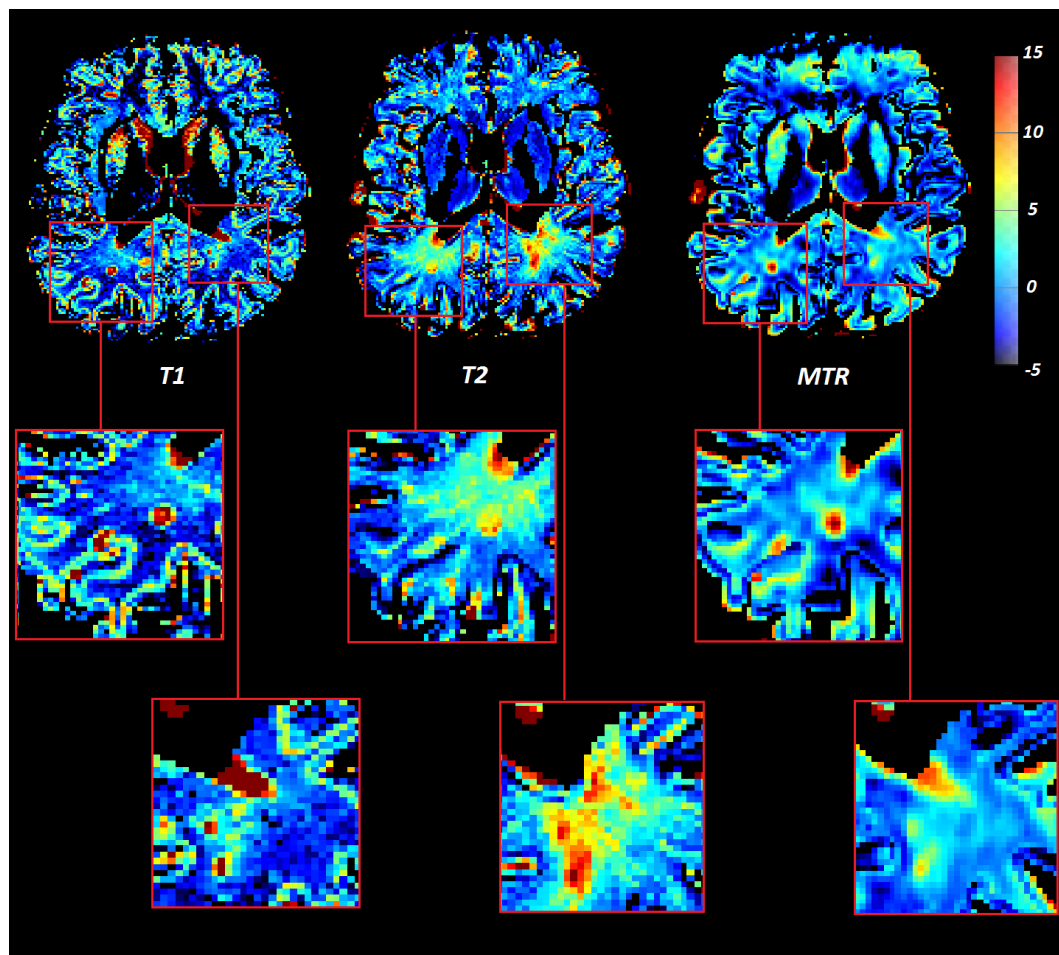


Figure 6.2: Deviation maps of T1, T2 and MTR contrast. In order to adapt the colormap to the T1 and T2 contrasts, the MTR deviation map shows the opposite of the MTR z-score ($z_{MTR} = -z$). The color code shows in dark blue the negative z-scores (decrease of T1, T2 and an increase of MTR), in light blue a positive z-score, and in yellow to red a high z-score (increase of T1, T2 and decrease of MTR). Based on this color code, the analysis of the lesions shows strong changes in T1, T2 and MTR z-scores within the lesions but also in the surrounding area.

This technique which showed promising preliminary results, presents advantages compared with existing methods such as voxel based morphometry. First of all, this methodology is based on brain tissue identification (GM, WM, CSF) and comparison with normative ranges which does not require any inter-subject registration. This technique combined with partial volume method giving precise tissue concentration information, may also allow a finer analysis of

Chapter 6. Conclusion : Achievements and Perspectives

challenging areas such cortex and cerebellum. Nevertheless, this approach requires a large cohort of healthy subjects to correctly set the normative ranges. In addition, lesions masks are required rendering this approach only feasible when an automatic and reliable lesion detection tool is available.

In summary, we set up a method that we foresee can be easily applied in the future to provide a visual map of brain tissue pathology in single MS patients. Future work should focus in building up robust normative ranges in the healthy population as well as integrating automatic lesion assessment algorithms in the current pipeline.

A Appendix

A.1 Preliminary analysis on lesions classification

In a preliminary analysis of MS lesions, we performed correlation analysis between the z-score distribution of each contrast (Figure A.1). We also analysed outliers and the association between distribution of lesions z-score among the 4 q/sqMRI with lesions size, type (GM, WM, mixed GM/WM), and location (Figure A.2). Finally we performed an automatic classification of lesions according to their 4 z-scores using a simple K-mean algorithm.

As expected, we noticed a strong positive correlation between T1 and T2 z-scores, as well as a negative correlation between T1 and MTR z-scores (Figure A.1). The analysis of the outlier pointed out segmentation issue in periventricular lesions, where CSF is wrongly include in the lesions leading to very high z-score. In fact it compared wrong tissue type. The distribution of lesions z-score did not show any significant association with lesions size, type or location. Finally, the K-mean algorithm showed no significant results, reflecting absence of cluster in the data. The distribution of lesions z-scores appear indeed continuous in the 4 contrasts.

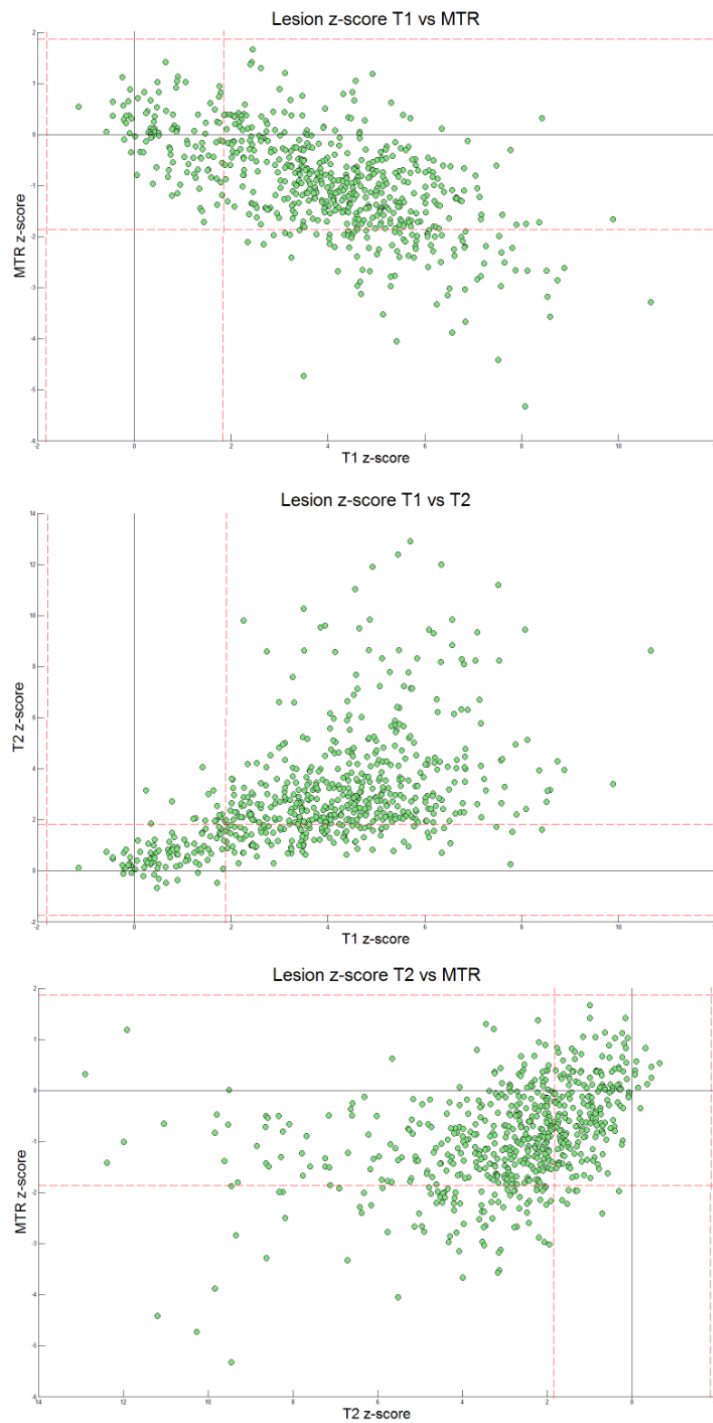


Figure A.1: Distribution of all lesions according to their T1, T2 and MTR z-score. The distribution shows no cluster. The red dashed lines delimit the threshold manually set for lesion classification.

A.1. Preliminary analysis on lesions classification

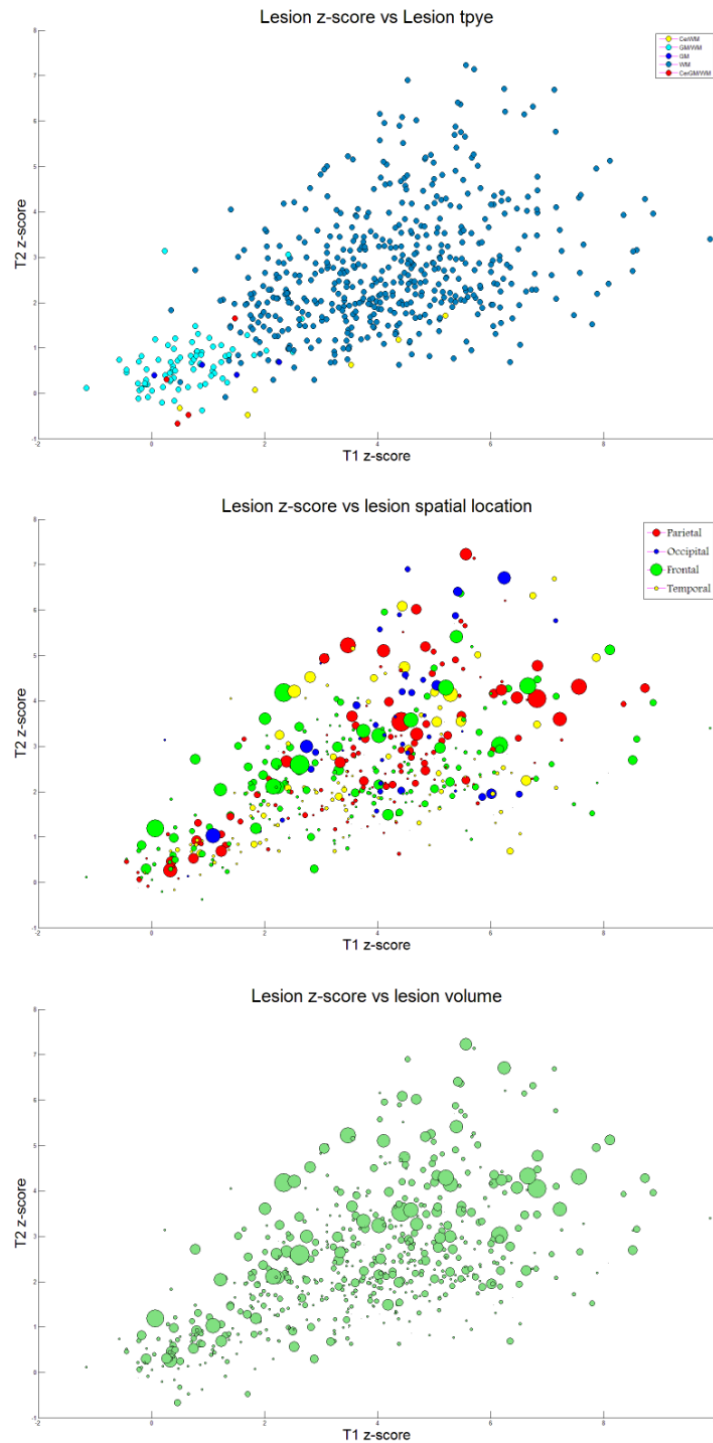


Figure A.2: Distribution of lesions z-scores according to their type, size and location. Cortical lesions appeared to have lower z-score, due to their low contrast. No sign of correlation between T1, T2, T2* and MTRz-score value and lesions size and location.

A.2 Longitudinal analysis of RRMS patients and controls

We present here the figures illustrating the changes in T1, T2, T2* and MTR in the regions were it appeared significant.

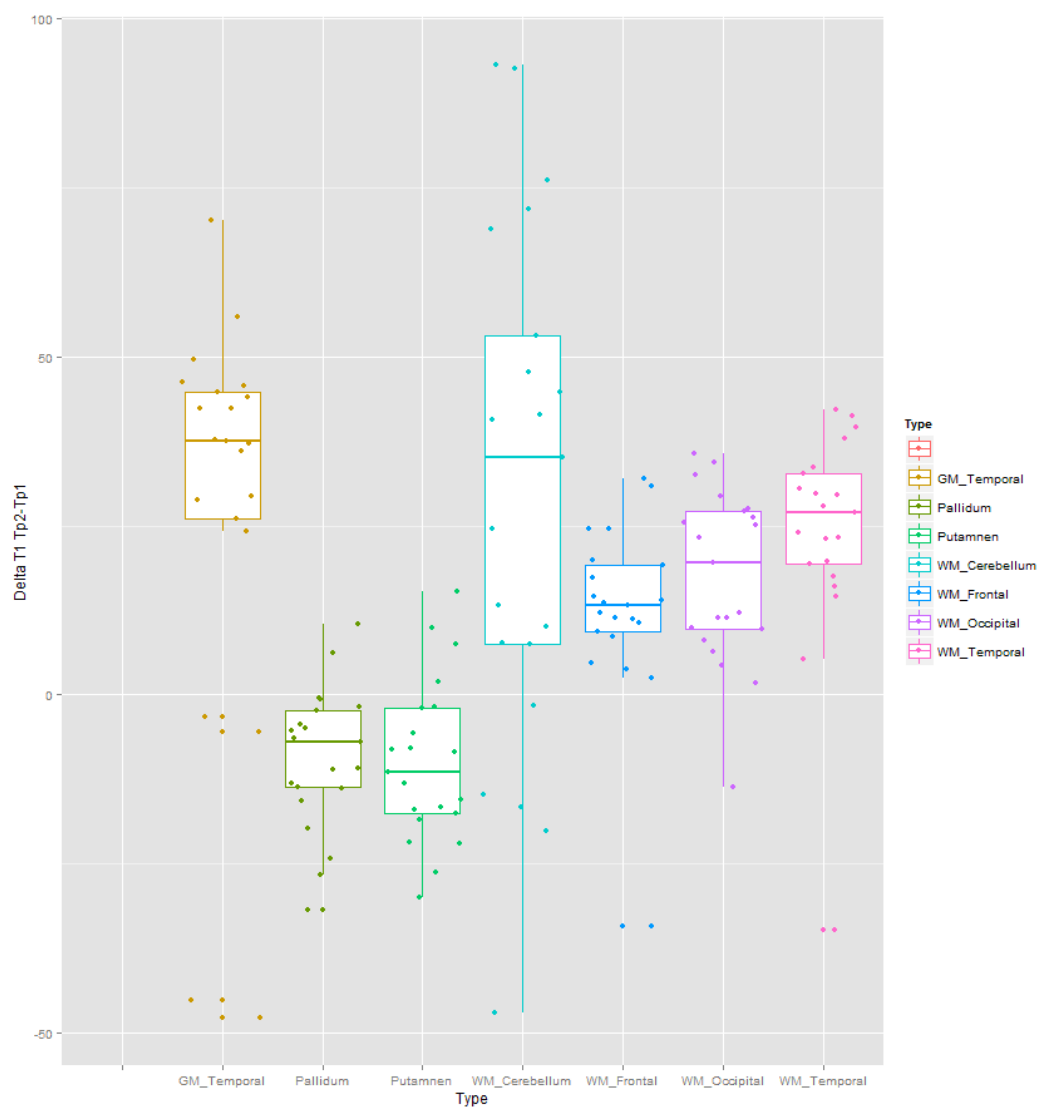


Figure A.3: Boxplot of the difference of T1 of normal appearing tissue in patients between time-points. T1 relaxation times increase in WM and GM of the temporal lobe and in the WM of the cerebellum.

A.2. Longitudinal analysis of RRMS patients and controls

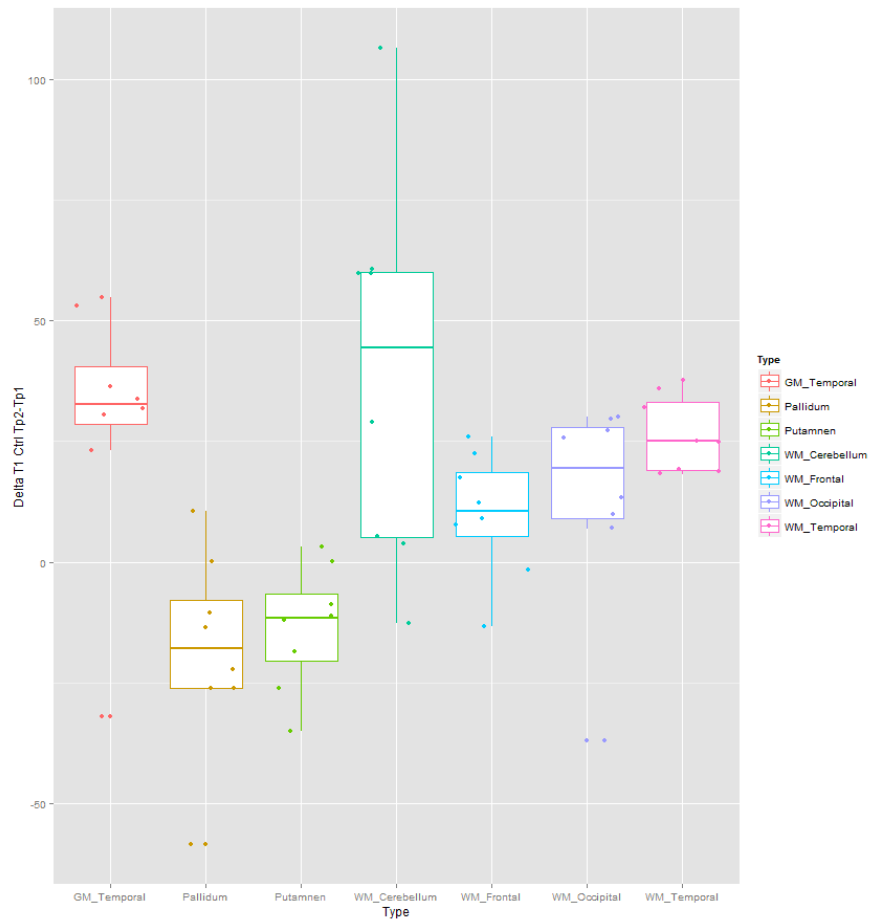


Figure A.4: Boxplot of the difference of T1 of normal appearing tissue of controls between time-points. T1 relaxation times increase in WM and GM of the temporal lobe and in the WM of the cerebellum.

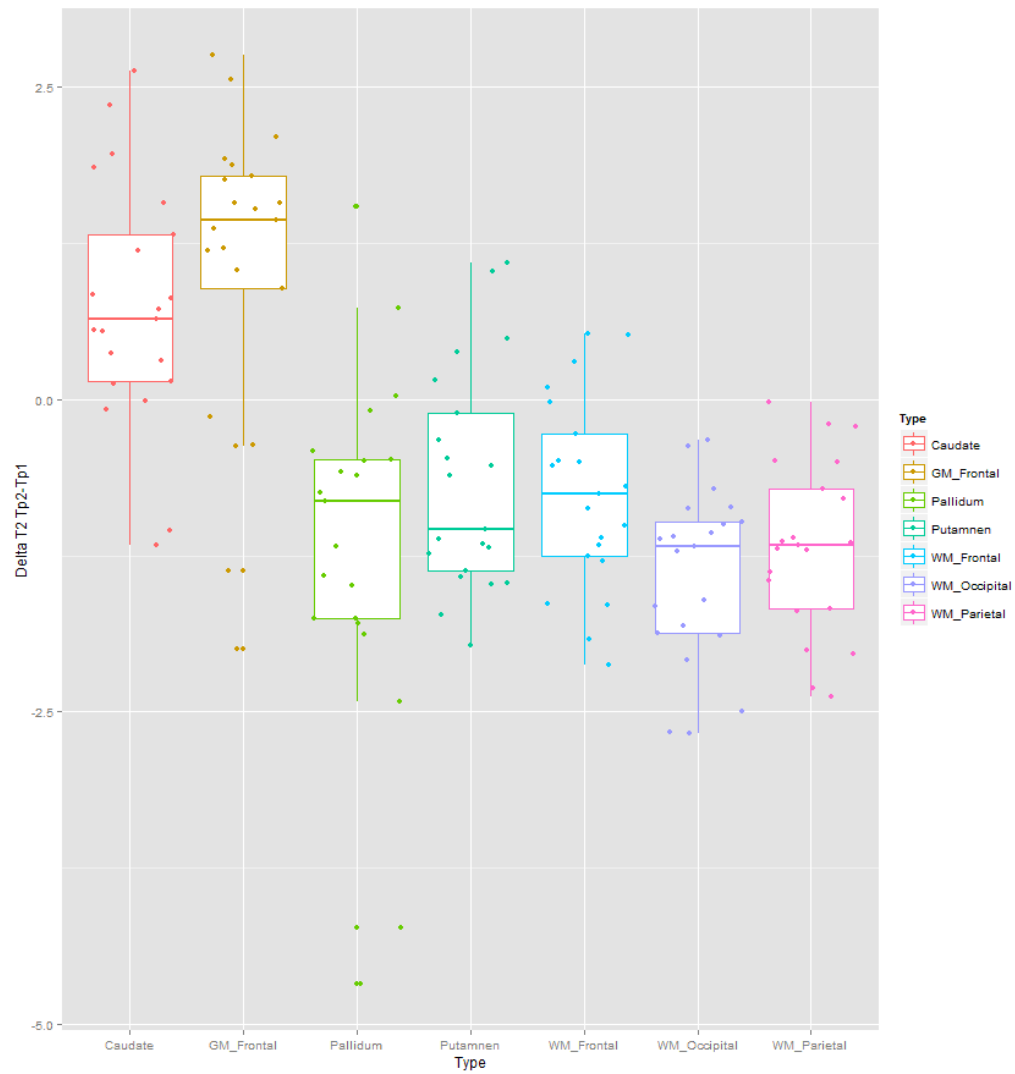


Figure A.5: Boxplot of T2 difference of normal appearing tissue in patients between time-points. T2 relaxation times decrease in pallidum, putamen and WM of the parietal, frontal and parietal lobes but increases in the caudate and MG of the frontal lobe.

A.2. Longitudinal analysis of RRMS patients and controls

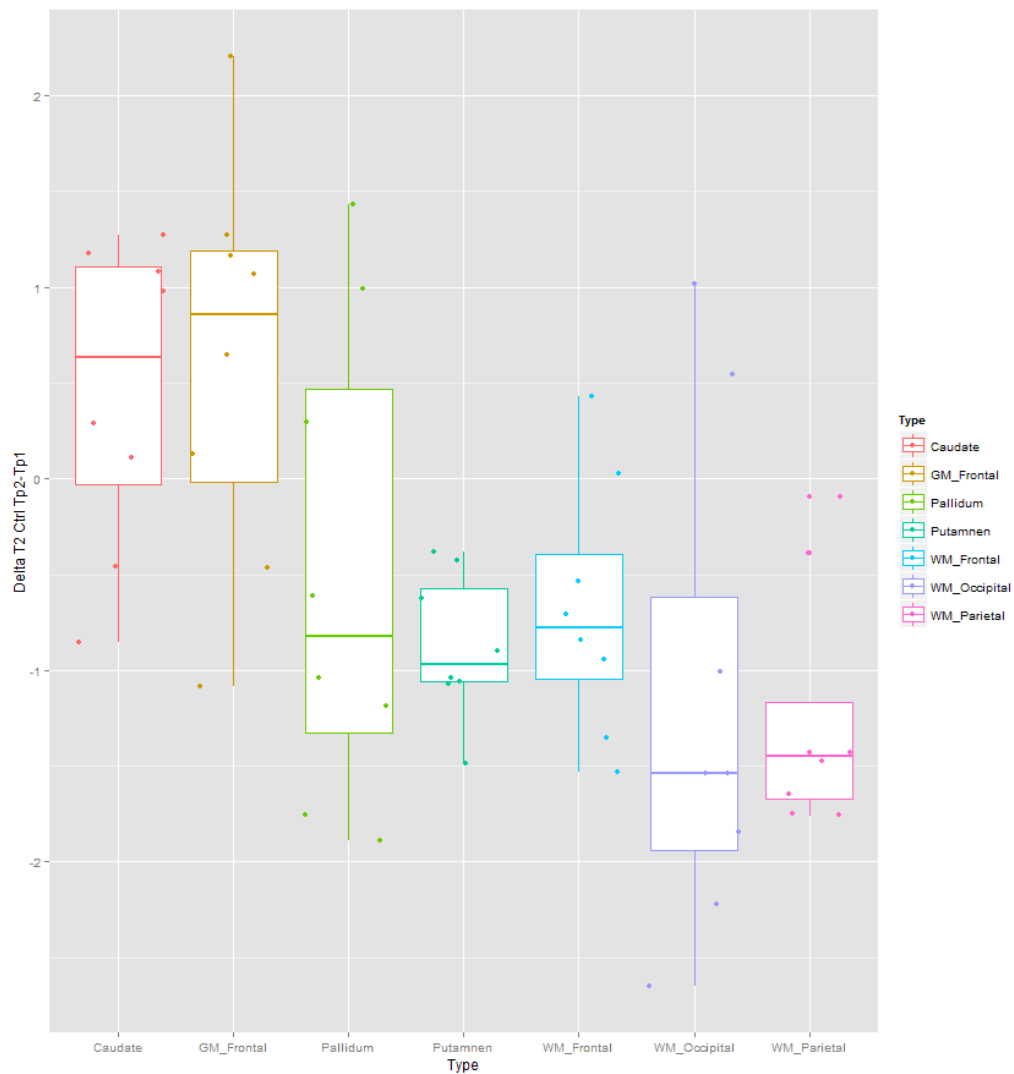


Figure A.6: Boxplot of T2 difference of normal appearing tissue in controls between time-points. T2 relaxation times decrease in pallidum, putamen and WM of the parietal, frontal and parietal lobes but increases in the caudate and MG of the frontal lobe.

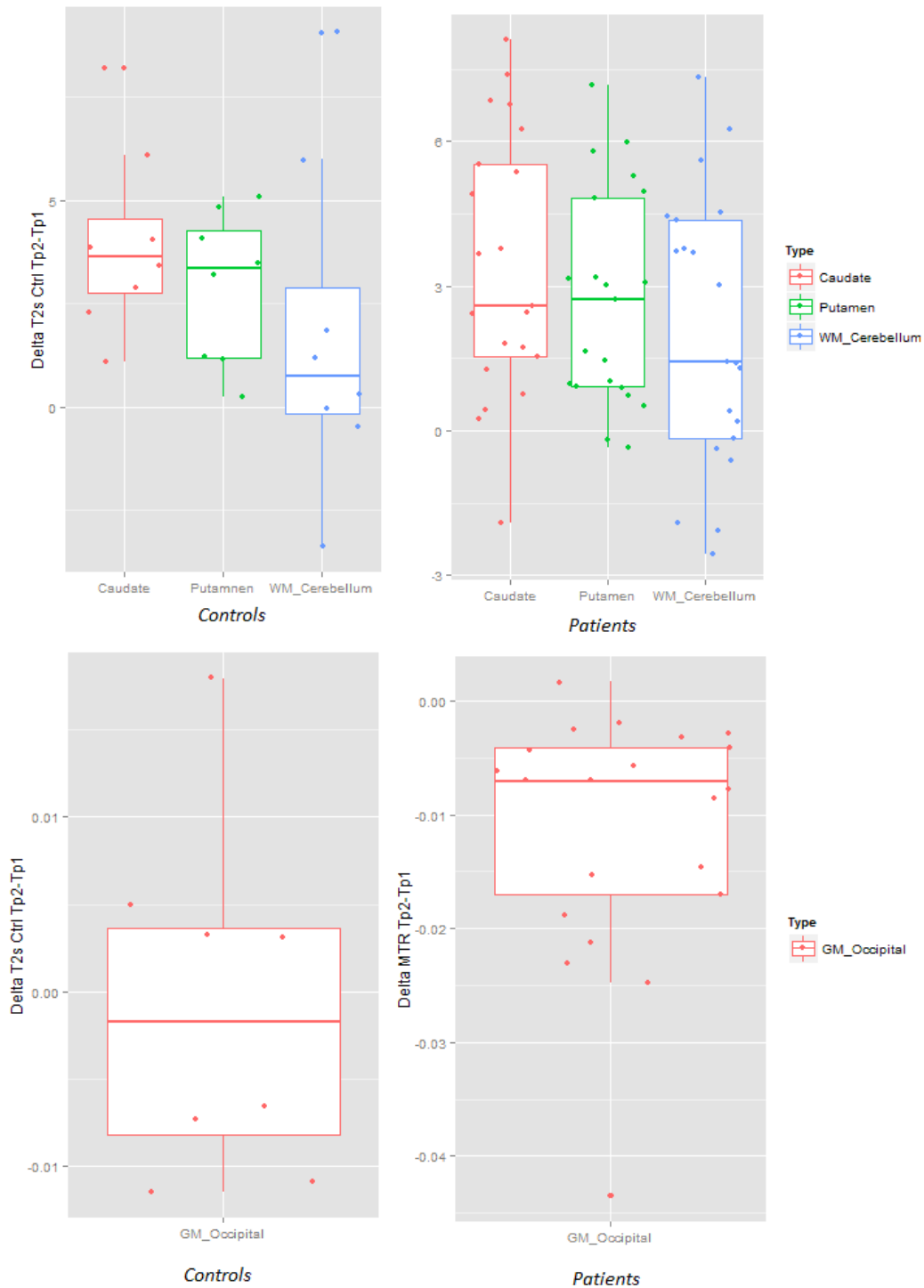


Figure A.7: Boxplot of T2* and MTR differences of normal appearing tissue between time-points. T2* relaxation times increases in caudate, putamen and WM of the cerebellum, while MTR decreases in the GM of the occipital lobe.

A.2. Longitudinal analysis of RRMS patients and controls

The following figures illustrate the evolution of T1, T2 and MTRz-scores in MS lesions, as well as in regions where lesions will appear or expand.

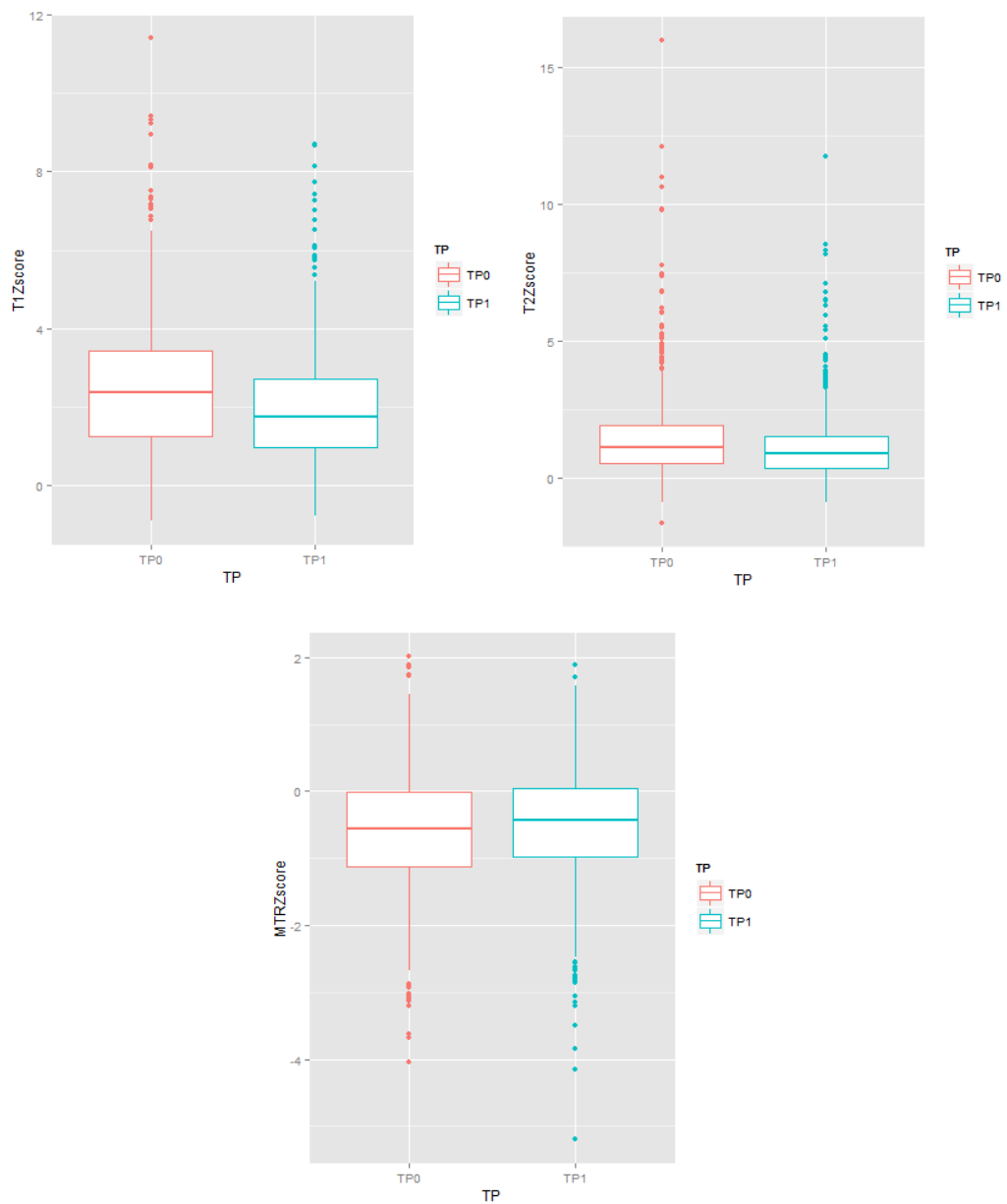


Figure A.8: Evolution of lesions among the different group based on qMRI combination.

Appendix A. Appendix

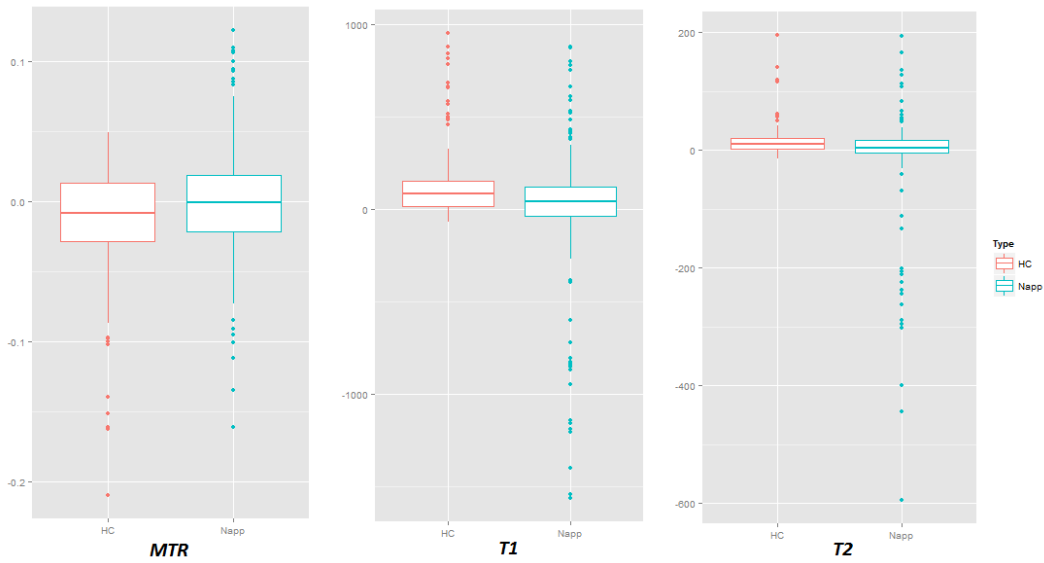


Figure A.9: Difference between T1, T2 and MTR in RRMS patients at TP1 in regions where lesions appear at TP2 and T1, T2, MTR of the healthy normal appearing tissue in the corresponding lobes (HC), and T1, T2, MTR at TP1 in the normal appearing tissue surrounding the region (NA).

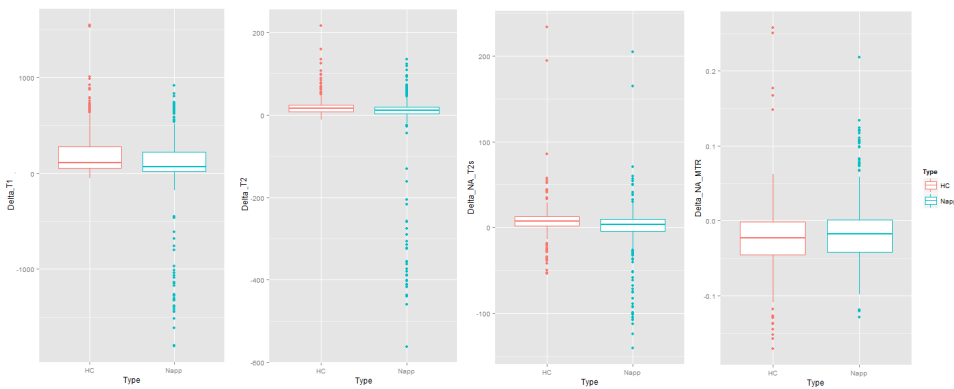


Figure A.10: Difference between T1, T2, T2* and MTR in RRMS patients at TP1 in regions where lesions expand at TP2 and the T1, T2, T2* and MTR in healthy normal appearing tissue in the corresponding lobes (HC) and T1, T2, T2* and MTR in the normal appearing tissue surrounding the region (NA).

Bibliography

- [1] I. Loma and R. Heyman, "Multiple sclerosis: Pathogenesis and treatment," vol. 9, no. 3, pp. 409–416.
- [2] S. Leech, J. Kirk, J. Plumb, and S. McQuaid, "Persistent endothelial abnormalities and blood–brain barrier leak in primary and secondary progressive multiple sclerosis," vol. 33, no. 1, pp. 86–98.
- [3] R. Gandhi, A. Laroni, and H. L. Weiner, "Role of the innate immune system in the pathogenesis of multiple sclerosis," vol. 221, no. 1, pp. 7–14.
- [4] A. Bitsch, J. Schuchardt, S. Bunkowski, T. Kuhlmann, and W. Brück, "Acute axonal injury in multiple sclerosis. correlation with demyelination and inflammation," vol. 123 (Pt 6), pp. 1174–1183.
- [5] T. Kuhlmann, G. Lingfeld, A. Bitsch, J. Schuchardt, and W. Brück, "Acute axonal damage in multiple sclerosis is most extensive in early disease stages and decreases over time," vol. 125, pp. 2202–2212.
- [6] A. Diestel, O. Aktas, D. Hackel, I. Hake, S. Meier, C. S. Raine, R. Nitsch, F. Zipp, and O. Ullrich, "Activation of microglial poly(ADP-ribose)-polymerase-1 by cholesterol breakdown products during neuroinflammation: a link between demyelination and neuronal damage," vol. 198, no. 11, pp. 1729–1740.
- [7] C. Bjartmar, R. P. Kinkel, G. Kidd, R. A. Rudick, and B. D. Trapp, "Axonal loss in normal-appearing white matter in a patient with acute MS," vol. 57, no. 7, pp. 1248–1252.
- [8] C. Lappe-Siefke, S. Goebbels, M. Gravel, E. Nicksch, J. Lee, P. E. Braun, I. R. Griffiths, and K.-A. Nave, "Disruption of *cnp1* uncouples oligodendroglial functions in axonal support and myelination," vol. 33, no. 3, pp. 366–374.
- [9] C. Lucchinetti, W. Brück, J. Parisi, B. Scheithauer, M. Rodriguez, and H. Lassmann, "Heterogeneity of multiple sclerosis lesions: implications for the pathogenesis of demyelination," vol. 47, no. 6, pp. 707–717.
- [10] B. F. G. Popescu, I. Pirko, and C. F. Lucchinetti, "Pathology of multiple sclerosis: Where do we stand?," vol. 19, no. 4, pp. 901–921.

Bibliography

- [11] L. Bø, C. A. Vedeler, H. I. Nyland, B. D. Trapp, and S. J. Mørk, "Subpial demyelination in the cerebral cortex of multiple sclerosis patients," vol. 62, no. 7, pp. 723–732.
- [12] J. J. G. Geurts, L. Bö, P. J. W. Pouwels, J. A. Castelijns, C. H. Polman, and F. Barkhof, "Cortical lesions in multiple sclerosis: combined postmortem MR imaging and histopathology," vol. 26, no. 3, pp. 572–577.
- [13] D. Kidd, F. Barkhof, R. McConnell, P. R. Algra, I. V. Allen, and T. Revesz, "Cortical lesions in multiple sclerosis," vol. 122, no. 1, pp. 17–26.
- [14] C. F. Lucchinetti, B. F. G. Popescu, R. F. Bunyan, N. M. Moll, S. F. Roemer, H. Lassmann, W. Brück, J. E. Parisi, B. W. Scheithauer, C. Giannini, S. D. Weigand, J. Mandrekar, and R. M. Ransohoff, "Inflammatory cortical demyelination in early multiple sclerosis," vol. 365, no. 23, pp. 2188–2197.
- [15] A. Kutzelnigg, C. F. Lucchinetti, C. Stadelmann, W. Brück, H. Rauschka, M. Bergmann, M. Schmidbauer, J. E. Parisi, and H. Lassmann, "Cortical demyelination and diffuse white matter injury in multiple sclerosis," vol. 128, pp. 2705–2712.
- [16] C. H. Polman, S. C. Reingold, B. Banwell, M. Clanet, J. A. Cohen, M. Filippi, K. Fujihara, E. Havrdova, M. Hutchinson, L. Kappos, F. D. Lublin, X. Montalban, P. O'Connor, M. Sandberg-Wollheim, A. J. Thompson, E. Waubant, B. Weinshenker, and J. S. Wolinsky, "Diagnostic criteria for multiple sclerosis: 2010 revisions to the McDonald criteria," vol. 69, no. 2, pp. 292–302.
- [17] P. A. Brex, O. Ciccarelli, J. I. O'Riordan, M. Sailer, A. J. Thompson, and D. H. Miller, "A longitudinal study of abnormalities on MRI and disability from multiple sclerosis," vol. 346, no. 3, pp. 158–164.
- [18] X. Montalban, M. Tintoré, J. Swanton, F. Barkhof, F. Fazekas, M. Filippi, J. Frederiksen, L. Kappos, J. Palace, C. Polman, M. Rovaris, N. de Stefano, A. Thompson, T. Youstry, A. Rovira, and D. H. Miller, "MRI criteria for MS in patients with clinically isolated syndromes," vol. 74, no. 5, pp. 427–434.
- [19] F. D. Lublin and S. C. Reingold, "Defining the clinical course of multiple sclerosis: results of an international survey. national multiple sclerosis society (USA) advisory committee on clinical trials of new agents in multiple sclerosis," vol. 46, no. 4, pp. 907–911.
- [20] J. F. Kurtzke, "Rating neurologic impairment in multiple sclerosis: an expanded disability status scale (EDSS)," vol. 33, no. 11, pp. 1444–1452.
- [21] M. A. van Walderveen, W. Kamphorst, P. Scheltens, J. H. van Waesberghe, R. Ravid, J. Valk, C. H. Polman, and F. Barkhof, "Histopathologic correlate of hypointense lesions on t1-weighted spin-echo MRI in multiple sclerosis," vol. 50, no. 5, pp. 1282–1288.
- [22] M. Filippi, M. A. Rocca, F. Barkhof, W. Brück, J. T. Chen, G. Comi, G. DeLuca, N. De Stefano, B. J. Erickson, N. Evangelou, F. Fazekas, J. J. G. Geurts, C. Lucchinetti, D. H. Miller,

- D. Pelletier, B. F. G. Popescu, H. Lassmann, and Attendees of the Correlation between Pathological MRI findings in MS workshop, "Association between pathological and MRI findings in multiple sclerosis," vol. 11, no. 4, pp. 349–360.
- [23] M. Filippi, "Enhanced magnetic resonance imaging in multiple sclerosis," vol. 6, no. 5, pp. 320–326.
- [24] D. S. Meier, H. L. Weiner, and C. R. G. Guttmann, "MR imaging intensity modeling of damage and repair in multiple sclerosis: Relationship of short-term lesion recovery to progression and disability," vol. 28, no. 10, pp. 1956–1963.
- [25] Y. Duan, P. G. Hildenbrand, M. P. Sampat, D. F. Tate, I. Csapo, B. Moraal, R. Bakshi, F. Barkhof, D. S. Meier, and C. R. G. Guttmann, "Segmentation of subtraction images for the measurement of lesion change in multiple sclerosis," vol. 29, no. 2, pp. 340–346.
- [26] N. De Stefano, M. Battaglini, and S. M. Smith, "Measuring brain atrophy in multiple sclerosis," vol. 17 Suppl 1, pp. 10S–15S.
- [27] E. Radü, K. Bendfeldt, N. Mueller-Lenke, S. Magon, and T. Sprenger, "Brain atrophy: an in-vivo measure of disease activity in multiple sclerosis,"
- [28] R. A. Bermel and R. Bakshi, "The measurement and clinical relevance of brain atrophy in multiple sclerosis," vol. 5, no. 2, pp. 158–170.
- [29] M. Sailer, B. Fischl, D. Salat, C. Tempelmann, M. A. Schönfeld, E. Busa, N. Bodammer, H.-J. Heinze, and A. Dale, "Focal thinning of the cerebral cortex in multiple sclerosis," vol. 126, pp. 1734–1744.
- [30] A. Charil, A. Dagher, J. P. Lerch, A. P. Zijdenbos, K. J. Worsley, and A. C. Evans, "Focal cortical atrophy in multiple sclerosis: relation to lesion load and disability," vol. 34, no. 2, pp. 509–517.
- [31] G. Tedeschi, L. Lavorgna, P. Russo, A. Prinster, D. Dinacci, G. Savettieri, A. Quattrone, P. Livrea, C. Messina, A. Reggio, V. Bresciamorra, G. Orefice, M. Paciello, A. Brunetti, G. Coniglio, S. Bonavita, A. Di Costanzo, A. Bellacosa, P. Valentino, M. Quarantelli, F. Patti, G. Salemi, E. Cammarata, I. L. Simone, M. Salvatore, V. Bonavita, and B. Alfano, "Brain atrophy and lesion load in a large population of patients with multiple sclerosis," vol. 65, no. 2, pp. 280–285.
- [32] J. W. Peterson, L. Bö, S. Mörk, A. Chang, and B. D. Trapp, "Transected neurites, apoptotic neurons, and reduced inflammation in cortical multiple sclerosis lesions," vol. 50, no. 3, pp. 389–400.
- [33] W. Brück, "Inflammatory demyelination is not central to the pathogenesis of multiple sclerosis," vol. 252 Suppl 5, pp. v10–15.

Bibliography

- [34] C. Oreja-Guevara, S. Noval, J. Alvarez-Linera, L. Gabaldón, B. Manzano, B. Chamorro, and E. Diez-Tejedor, "Clinically isolated syndromes suggestive of multiple sclerosis: An optical coherence tomography study," vol. 7, no. 3, p. e33907.
- [35] C. M. Dalton, D. T. Chard, G. R. Davies, K. A. Miszkiel, D. R. Altmann, K. Fernando, G. T. Plant, A. J. Thompson, and D. H. Miller, "Early development of multiple sclerosis is associated with progressive grey matter atrophy in patients presenting with clinically isolated syndromes," vol. 127, pp. 1101–1107.
- [36] H.-L. M. Cheng, N. Stikov, N. R. Ghugre, and G. A. Wright, "Practical medical applications of quantitative MR relaxometry," vol. 36, no. 4, pp. 805–824.
- [37] N. Weiskopf, J. Suckling, G. Williams, M. M. Correia, B. Inkster, R. Tait, C. Ooi, E. T. Bullmore, and A. Lutti, "Quantitative multi-parameter mapping of r_1 , PD^* , MT , and r_2^* at 3t: a multi-center validation," vol. 7.
- [38] R. J. Ogg and R. G. Steen, "Age-related changes in brain t_1 are correlated with iron concentration," vol. 40, no. 5, pp. 749–753.
- [39] C. Schenker, D. Meier, W. Wichmann, P. Boesiger, and A. Valavanis, "Age distribution and iron dependency of the t_2 relaxation time in the globus pallidus and putamen," vol. 35, no. 2, pp. 119–124.
- [40] S. Ropele, W. de Graaf, M. Khalil, M. P. Wattjes, C. Langkammer, M. A. Rocca, A. Rovira, J. Palace, F. Barkhof, M. Filippi, and F. Fazekas, "MRI assessment of iron deposition in multiple sclerosis," vol. 34, no. 1, pp. 13–21.
- [41] M. A. Rocca, R. Messina, and M. Filippi, "Multiple sclerosis imaging: recent advances," vol. 260, no. 3, pp. 929–935.
- [42] S. C. L. Deoni, "Magnetic resonance relaxation and quantitative measurement in the brain," vol. 711, pp. 65–108.
- [43] M. Neema, D. Goldberg-Zimring, Z. D. Guss, B. C. Healy, C. R. Guttmann, M. K. Houtchens, H. L. Weiner, M. A. Horsfield, D. B. Hackney, D. C. Alsop, and R. Bakshi, "3t MRI relaxometry detects t_2 prolongation in the cerebral normal-appearing white matter in multiple sclerosis," vol. 46, no. 3, pp. 633–641.
- [44] K. P. Whittall, A. L. MacKay, D. K. B. Li, I. M. Vavasour, C. K. Jones, and D. W. Paty, "Normal-appearing white matter in multiple sclerosis has heterogeneous, diffusely prolonged t_2 ," vol. 47, no. 2, pp. 403–408.
- [45] R. Bakshi, R. H. B. Benedict, R. A. Bermel, S. D. Caruthers, S. R. Puli, C. W. Tjoa, A. J. Fabiano, and L. Jacobs, "T2 hypointensity in the deep gray matter of patients with multiple sclerosis: a quantitative magnetic resonance imaging study," vol. 59, no. 1, pp. 62–68.

- [46] H. Vrenken, J. J. G. Geurts, D. L. Knol, C. H. Polman, J. A. Castelijns, P. J. W. Pouwels, and F. Barkhof, "Normal-appearing white matter changes vary with distance to lesions in multiple sclerosis," vol. 27, no. 9, pp. 2005–2011.
- [47] F. Manfredonia, O. Ciccarelli, Z. Khaleeli, D. J. Tozer, J. Sastre-Garriga, D. H. Miller, and A. J. Thompson, "Normal-appearing brain t1 relaxation time predicts disability in early primary progressive multiple sclerosis," vol. 64, no. 3, pp. 411–415.
- [48] I. E. Ormerod, A. Bronstein, P. Rudge, G. Johnson, D. Macmanus, A. M. Halliday, H. Barratt, E. P. D. Boulay, B. E. Kendal, and I. F. Moseley, "Magnetic resonance imaging in clinically isolated lesions of the brain stem.," vol. 49, no. 7, pp. 737–743.
- [49] G. Helms and A. Piringner, "Simultaneous measurement of saturation and relaxation in human brain by repetitive magnetization transfer pulses," vol. 18, no. 1, pp. 44–50.
- [50] S. Graham, G. Stanisz, A. Kecojevic, M. Bronskill, and R. Henkelman, "Analysis of changes in MR properties of tissues after heat treatment," vol. 42, no. 6, pp. 1061–1071.
- [51] J. C. McGowan, M. Filippi, A. Campi, and R. I. Grossman, "Magnetisation transfer imaging: theory and application to multiple sclerosis," vol. 64 Suppl 1, pp. S66–69.
- [52] I. M. Vavasour, C. Laule, D. K. B. Li, A. L. Traboulsee, and A. L. MacKay, "Is the magnetization transfer ratio a marker for myelin in multiple sclerosis?," vol. 33, no. 3, pp. 713–718.
- [53] H. Vrenken, P. J. W. Pouwels, S. Ropele, D. L. Knol, J. J. G. Geurts, C. H. Polman, F. Barkhof, and J. A. Castelijns, "Magnetization transfer ratio measurement in multiple sclerosis normal-appearing brain tissue: limited differences with controls but relationships with clinical and MR measures of disease," vol. 13, no. 6, pp. 708–716.
- [54] I. Catalaa, R. I. Grossman, D. L. Kolson, J. K. Udupa, L. G. Nyul, L. Wei, X. Zhang, M. Polansky, L. J. Mannon, and J. C. McGowan, "Multiple sclerosis: magnetization transfer histogram analysis of segmented normal-appearing white matter," vol. 216, no. 2, pp. 351–355.
- [55] C. L. Tardif, B. J. Bedell, S. F. Eskildsen, D. L. Collins, and G. B. Pike, "Quantitative magnetic resonance imaging of cortical multiple sclerosis pathology," vol. 2012, p. e742018.
- [56] I. R. Levesque, P. S. Giacomini, S. Narayanan, L. T. Ribeiro, J. G. Sled, D. L. Arnold, and G. B. Pike, "Quantitative magnetization transfer and myelin water imaging of the evolution of acute multiple sclerosis lesions," vol. 63, no. 3, pp. 633–640.
- [57] P. J. Basser, "Inferring microstructural features and the physiological state of tissues from diffusion-weighted images," vol. 8, no. 7, pp. 333–344.
- [58] J. P. Mottershead, K. Schmierer, M. Clemence, J. S. Thornton, F. Scaravilli, G. J. Barker, P. S. Tofts, J. Newcombe, M. L. Cuzner, R. J. Ordidge, W. I. McDonald, and D. H. Miller, "High field MRI correlates of myelin content and axonal density in multiple sclerosis—a post-mortem study of the spinal cord," vol. 250, no. 11, pp. 1293–1301.

Bibliography

- [59] K. Schmierer, C. A. Wheeler-Kingshott, P. A. Boulby, F. Scaravilli, D. R. Altmann, G. J. Barker, P. S. Tofts, and D. H. Miller, "Diffusion tensor imaging of post mortem multiple sclerosis brain," vol. 35, no. 2, pp. 467–477.
- [60] P. Christiansen, P. Gideon, C. Thomsen, M. Stubgaard, O. Henriksen, and H. B. Larsson, "Increased water self-diffusion in chronic plaques and in apparently normal white matter in patients with multiple sclerosis," vol. 87, no. 3, pp. 195–199.
- [61] M. Filippi, M. Cercignani, M. Inglese, M. A. Horsfield, and G. Comi, "Diffusion tensor magnetic resonance imaging in multiple sclerosis," vol. 56, no. 3, pp. 304–311.
- [62] U. S. A Castriota-Scanderbeg, "Diffusion of water in large demyelinating lesions: a follow-up study.," vol. 44, no. 9, pp. 764–7.
- [63] A. G. Droogan, C. A. Clark, D. J. Werring, G. J. Barker, W. I. McDonald, and D. H. Miller, "Comparison of multiple sclerosis clinical subgroups using navigated spin echo diffusion-weighted imaging," vol. 17, no. 5, pp. 653–661.
- [64] M. A. Rocca, M. Cercignani, G. Iannucci, G. Comi, and M. Filippi, "Weekly diffusion-weighted imaging of normal-appearing white matter in MS," vol. 55, no. 6, pp. 882–884.
- [65] A. O. Nusbaum, C. Y. Tang, T. Wei, M. S. Buchsbaum, and S. W. Atlas, "Whole-brain diffusion MR histograms differ between MS subtypes," vol. 54, no. 7, pp. 1421–1427.
- [66] M. Inglese and M. Bester, "Diffusion imaging in multiple sclerosis: research and clinical implications," vol. 23, no. 7, pp. 865–872.
- [67] M. Rovaris, G. Iannucci, M. Falautano, F. Possa, V. Martinelli, G. Comi, and M. Filippi, "Cognitive dysfunction in patients with mildly disabling relapsing-remitting multiple sclerosis: an exploratory study with diffusion tensor MR imaging," vol. 195, no. 2, pp. 103–109.
- [68] P. A. Narayana, "Magnetic resonance spectroscopy in the monitoring of multiple sclerosis," vol. 15, no. 4, pp. 46S–57S.
- [69] P. A. Narayana, J. S. Wolinsky, S. B. Rao, R. He, M. Mehta, and PROMiSe Trial MRSI Group, "Multicentre proton magnetic resonance spectroscopy imaging of primary progressive multiple sclerosis," vol. 10 Suppl 1, pp. S73–78.
- [70] P. A. Narayana, T. J. Doyle, D. Lai, and J. S. Wolinsky, "Serial proton magnetic resonance spectroscopic imaging, contrast-enhanced magnetic resonance imaging, and quantitative lesion volumetry in multiple sclerosis," vol. 43, no. 1, pp. 56–71.
- [71] I. Mader, U. Seeger, R. Weissert, U. Klose, T. Naegele, A. Melms, and W. Grodd, "Proton MR spectroscopy with metabolite-nulling reveals elevated macromolecules in acute multiple sclerosis," vol. 124, pp. 953–961.

- [72] J. L. Ruiz-Peña, P. Piñero, G. Sellers, J. Argente, A. Casado, J. Foronda, A. Uclés, and G. Izquierdo, "Magnetic resonance spectroscopy of normal appearing white matter in early relapsing-remitting multiple sclerosis: correlations between disability and spectroscopy," vol. 4, p. 8.
- [73] A. Tourbah, J. L. Stievenart, O. Gout, B. Fontaine, R. Liblau, C. Lubetzki, E. A. Cabanis, and O. Lyon-Caen, "Localized proton magnetic resonance spectroscopy in relapsing remitting versus secondary progressive multiple sclerosis," vol. 53, no. 5, pp. 1091–1097.
- [74] M. Filippi and F. Agosta, "Imaging biomarkers in multiple sclerosis," vol. 31, no. 4, pp. 770–788.
- [75] W. Rashid, A. Hadjiprocopis, G. Davies, C. Griffin, D. Chard, M. Tiberio, D. Altmann, C. Wheeler-Kingshott, D. Tozer, A. Thompson, and D. H. Miller, "Longitudinal evaluation of clinically early relapsing-remitting multiple sclerosis with diffusion tensor imaging," vol. 255, no. 3, pp. 390–397.
- [76] C. S. Yu, F. C. Lin, Y. Liu, Y. Duan, H. Lei, and K. C. Li, "Histogram analysis of diffusion measures in clinically isolated syndromes and relapsing-remitting multiple sclerosis," vol. 68, no. 2, pp. 328–334.
- [77] N. M. Moll, A. M. Rietsch, S. Thomas, A. J. Ransohoff, J.-C. Lee, R. Fox, A. Chang, R. M. Ransohoff, and E. Fisher, "Multiple sclerosis normal-appearing white matter: pathology-imaging correlations," vol. 70, no. 5, pp. 764–773.
- [78] D. S. Reich, S. A. Smith, K. M. Zackowski, E. M. Gordon-Lipkin, C. K. Jones, J. A. D. Farrell, S. Mori, P. C. M. van Zijl, and P. A. Calabresi, "Multiparametric magnetic resonance imaging analysis of the corticospinal tract in multiple sclerosis," vol. 38, no. 2, pp. 271–279.
- [79] K. M. Hasan, I. S. Walimuni, H. Abid, J. S. Wolinsky, and P. A. Narayana, "Multi-modal quantitative MRI investigation of brain tissue neurodegeneration in multiple sclerosis," vol. 35, no. 6, pp. 1300–1311.
- [80] B. Guillaume, "Advanced MRI unravels the nature of tissue alterations in early multiple sclerosis," pp. 1–20.
- [81] M. Filippi, "Multiple sclerosis: a white matter disease with associated gray matter damage," vol. 185, no. 1, pp. 3–4.
- [82] M. Calabrese, M. Filippi, and P. Gallo, "Cortical lesions in multiple sclerosis," vol. 6, no. 8, pp. 438–444.
- [83] A. L. Alexander, S. A. Hurley, A. A. Samsonov, N. Adluru, A. P. Hosseinbor, P. Mossahebi, D. P. Tromp, E. Zakszewski, and A. S. Field, "Characterization of cerebral white matter properties using quantitative magnetic resonance imaging stains," vol. 1, no. 6, pp. 423–446.

Bibliography

- [84] T. J. Sumpf, M. Uecker, S. Boretius, and J. Frahm, "Model-based nonlinear inverse reconstruction for t2 mapping using highly undersampled spin-echo MRI," vol. 34, no. 2, pp. 420–428.
- [85] J. P. Marques, T. Kober, G. Krueger, W. van der Zwaag, P.-F. Van de Moortele, and R. Gruetter, "MP2rage, a self bias-field corrected sequence for improved segmentation and t1-mapping at high field," vol. 49, no. 2, pp. 1271–1281.
- [86] S. M. Rao, G. J. Leo, L. Bernardin, and F. Unverzagt, "Cognitive dysfunction in multiple sclerosis. i. frequency, patterns, and prediction," vol. 41, no. 5, pp. 685–691.
- [87] A. S. Zigmond and R. P. Snaith, "The hospital anxiety and depression scale," vol. 67, no. 6, pp. 361–370.
- [88] I. K. Penner, C. Raselli, M. Stöcklin, K. Opwis, L. Kappos, and P. Calabrese, "The fatigue scale for motor and cognitive functions (FSMC): validation of a new instrument to assess multiple sclerosis-related fatigue," vol. 15, no. 12, pp. 1509–1517.
- [89] J. S. Fischer, R. A. Rudick, G. R. Cutter, and S. C. Reingold, "The multiple sclerosis functional composite measure (MSFC): an integrated approach to MS clinical outcome assessment. national MS society clinical outcomes assessment task force," vol. 5, no. 4, pp. 244–250.
- [90] C. Granziera, D. Romascano, A. Daducci, A. Roche, M. Vincent, G. Krueger, and N. Hadjikhani, "Migraineurs without aura show microstructural abnormalities in the cerebellum and frontal lobe," vol. 12, no. 6, pp. 812–818.
- [91] C. Granziera, A. Daducci, S. Simioni, M. Cavassini, A. Roche, D. Meskaldji, T. Kober, M. Metral, A. Calmy, G. Helms, B. Hirschel, F. Lazeyras, R. Meuli, G. Krueger, and R. A. Du Pasquier, "Micro-structural brain alterations in aviremic HIV+ patients with minor neurocognitive disorders: A multi-contrast study at high field," vol. 8, no. 9.
- [92] C. Granziera, A. Daducci, D. Romascano, A. Roche, G. Helms, G. Krueger, and N. Hadjikhani, "Structural abnormalities in the thalamus of migraineurs with aura: A multi-parametric study at 3 t,"
- [93] P. M. Robson, A. K. Grant, A. J. Madhuranthakam, R. Lattanzi, D. K. Sodickson, and C. A. McKenzie, "Comprehensive quantification of signal-to-noise ratio and g-factor for image-based and k-space-based parallel imaging reconstructions," vol. 60, no. 4, pp. 895–907.
- [94] C. N. Wiens, S. J. Kisch, J. D. Willig-Onwuachi, and C. A. McKenzie, "Computationally rapid method of estimating signal-to-noise ratio for phased array image reconstructions," vol. 66, no. 4, pp. 1192–1197.
- [95] T. Kober, C. Granziera, D. Ribes, P. Browaeys, M. Schlupe, R. Meuli, R. Frackowiak, R. Gruetter, and G. Krueger, "MP2rage multiple sclerosis magnetic resonance imaging at 3 t," vol. 47, no. 6, pp. 346–352.

- [96] D. A. Yablonskiy, A. L. Sukstanskii, J. Luo, and X. Wang, "Voxel spread function method for correction of magnetic field inhomogeneity effects in quantitative gradient-echo-based MRI," vol. 70, no. 5, pp. 1283–1292.
- [97] chemsedinne Fatnassi, Meuli Reito, and O'brien Kieran, "Non linear correction of r2*maps from macroscopic field inhomogeneities,"
- [98] P. Irarrazabal, C. H. Meyer, D. G. Nishimura, and A. Macovski, "Inhomogeneity correction using an estimated linear field map," vol. 35, no. 2, pp. 278–282.
- [99] H. An and W. Lin, "Impact of intravascular signal on quantitative measures of cerebral oxygen extraction and blood volume under normo- and hypercapnic conditions using an asymmetric spin echo approach," vol. 50, no. 4, pp. 708–716.
- [100] R. I. Grossman, "Magnetization transfer in multiple sclerosis," vol. 36 Suppl, pp. S97–99.
- [101] S. Klein, M. Staring, K. Murphy, M. A. Viergever, and J. P. W. Pluim, "elastix: a toolbox for intensity-based medical image registration," vol. 29, no. 1, pp. 196–205.
- [102] A. Roche, D. Ribes, M. Bach-Cuadra, and G. Krüger, "On the convergence of EM-like algorithms for image segmentation using markov random fields," vol. 15, no. 6, pp. 830–839.
- [103] D. Schmitter, A. Roche, B. Maréchal, D. Ribes, A. Abdulkadir, M. Bach-Cuadra, A. Daducci, C. Granziera, S. Klöppel, P. Maeder, R. Meuli, and G. Krueger, "An evaluation of volume-based morphometry for prediction of mild cognitive impairment and alzheimer's disease," vol. 7, pp. 7–17.
- [104] K. M. Hasan, I. S. Walimuni, L. A. Kramer, and P. A. Narayana, "Human brain iron mapping using atlas-based t2 relaxometry," vol. 67, no. 3, pp. 731–739.
- [105] C. S. Georgiades, R. Itoh, X. Golay, P. C. M. v. Zijl, and E. R. Melhem, "MR imaging of the human brain at 1.5 t: Regional variations in transverse relaxation rates in the cerebral cortex," vol. 22, no. 9, pp. 1732–1737.
- [106] J. DeLuca, S. K. Johnson, D. Beldowicz, and B. H. Natelson, "Neuropsychological impairments in chronic fatigue syndrome, multiple sclerosis, and depression.," vol. 58, no. 1, pp. 38–43.
- [107] L. J. Phillips and A. K. Stuijbergen, "The relevance of depressive symptoms and social support to disability in women with multiple sclerosis or fibromyalgia," vol. 33, no. 2, pp. 142–150.
- [108] O. JW., "Improving your data transformations: Applying box-cox transformations as a best practice. .," vol. 15, pp. 1–9.

Bibliography

- [109] E. M. Haacke, M. Makki, Y. Ge, M. Maheshwari, V. Sehgal, J. Hu, M. Selvan, Z. Wu, Z. Latif, Y. Xuan, O. Khan, J. Garbern, and R. I. Grossman, "Characterizing iron deposition in multiple sclerosis lesions using susceptibility weighted imaging," vol. 29, no. 3, pp. 537–544.
- [110] N. De Stefano, M. Battaglini, M. L. Stromillo, V. Zipoli, M. L. Bartolozzi, L. Guidi, G. Siracusa, E. Portaccio, A. Giorgio, S. Sorbi, A. Federico, and M. P. Amato, "Brain damage as detected by magnetization transfer imaging is less pronounced in benign than in early relapsing multiple sclerosis," vol. 129, pp. 2008–2016.
- [111] C. M. Griffin, D. T. Chard, G. J. M. Parker, G. J. Barker, A. J. Thompson, and D. H. Miller, "The relationship between lesion and normal appearing brain tissue abnormalities in early relapsing remitting multiple sclerosis," vol. 249, no. 2, pp. 193–199.
- [112] P. Sati, A. H. Cross, J. Luo, C. F. Hildebolt, and D. A. Yablonskiy, "In vivo quantitative evaluation of brain tissue damage in multiple sclerosis using gradient echo plural contrast imaging technique," vol. 51, no. 3, pp. 1089–1097.
- [113] J. Luo, D. A. Yablonskiy, C. F. Hildebolt, S. Lancia, and A. H. Cross, "Gradient echo magnetic resonance imaging correlates with clinical measures and allows visualization of veins within multiple sclerosis lesions," vol. 20, no. 3, pp. 349–355.
- [114] H. Lassmann, "Pathology and disease mechanisms in different stages of multiple sclerosis," vol. 333, no. 1, pp. 1–4.
- [115] S. Batista, R. Zivadinov, M. Hoogs, N. Bergsland, M. Heininen-Brown, M. G. Dwyer, B. Weinstock-Guttman, and R. H. B. Benedict, "Basal ganglia, thalamus and neocortical atrophy predicting slowed cognitive processing in multiple sclerosis," vol. 259, no. 1, pp. 139–146.
- [116] A. S. Nielsen, R. P. Kinkel, N. Madigan, E. Tinelli, T. Benner, and C. Mainero, "Contribution of cortical lesion subtypes at 7t MRI to physical and cognitive performance in MS," vol. 81, no. 7, pp. 641–649.
- [117] G. Bonnier, A. Roche, D. Romascano, S. Simioni, D. E. Meskaldji, D. Rotzinger, Y.-C. Lin, G. Menegaz, M. Schlupe, R. Du Pasquier, T. J. Sumpff, J. Frahm, J.-P. Thiran, G. Krueger, and C. Granziera, "Multicontrast MRI quantification of focal inflammation and degeneration in multiple sclerosis,"
- [118] A. Rovira, C. Auger, and J. Alonso, "Magnetic resonance monitoring of lesion evolution in multiple sclerosis," vol. 6, no. 5, pp. 298–310.
- [119] H. Lassmann, "The pathologic substrate of magnetic resonance alterations in multiple sclerosis," vol. 18, no. 4, pp. 563–576, ix.
- [120] P. M. Matthews, E. Piore, S. Narayanan, N. De Stefano, L. Fu, G. Francis, J. Antel, C. Wolfson, and D. L. Arnold, "Assessment of lesion pathology in multiple sclerosis using

- quantitative MRI morphometry and magnetic resonance spectroscopy,” vol. 119 (Pt 3), pp. 715–722.
- [121] D. S. Meier, H. L. Weiner, and C. R. G. Guttmann, “Time-series modeling of multiple sclerosis disease activity: a promising window on disease progression and repair potential?,” vol. 4, no. 3, pp. 485–498.
- [122] B. Moraal, S. D. Roosendaal, P. J. W. Pouwels, H. Vrenken, R. A. van Schijndel, D. S. Meier, C. R. G. Guttmann, J. J. G. Geurts, and F. Barkhof, “Multi-contrast, isotropic, single-slab 3d MR imaging in multiple sclerosis,” vol. 18, no. 10, pp. 2311–2320.
- [123] M. Archambault-Wallenburg, D. Arnold, S. Narayanan, G. B. Pike, and D. L. Collins, “Cortical surface analysis of multi-contrast MR data to improve detection of cortical pathology in multiple sclerosis,” in *Multimodal Brain Image Analysis* (L. Shen, T. Liu, P.-T. Yap, H. Huang, D. Shen, and C.-F. Westin, eds.), no. 8159 in Lecture Notes in Computer Science, pp. 138–149, Springer International Publishing.
- [124] W. L. de Graaf, I. D. Kilsdonk, A. Lopez-Soriano, J. J. M. Zwanenburg, F. Visser, C. H. Polman, J. A. Castelijns, J. J. G. Geurts, P. J. W. Pouwels, P. R. Luijten, F. Barkhof, and M. P. Wattjes, “Clinical application of multi-contrast 7-t MR imaging in multiple sclerosis: increased lesion detection compared to 3 t confined to grey matter,” vol. 23, no. 2, pp. 528–540.
- [125] N. Nathoo, V. W. Yong, and J. F. Dunn, “Using magnetic resonance imaging in animal models to guide drug development in multiple sclerosis,” vol. 20, no. 1, pp. 3–11.
- [126] S. Boretius, A. Escher, T. Dallenga, C. Wrzos, R. Tammer, W. Brück, S. Nessler, J. Frahm, and C. Stadelmann, “Assessment of lesion pathology in a new animal model of MS by multiparametric MRI and DTI,” vol. 59, no. 3, pp. 2678–2688.
- [127] E. Fisher, A. Chang, R. J. Fox, J. A. Tkach, T. Svarovsky, K. Nakamura, R. A. Rudick, and B. D. Trapp, “Imaging correlates of axonal swelling in chronic multiple sclerosis brains,” vol. 62, no. 3, pp. 219–228.
- [128] A. Ceccarelli, R. Bakshi, and M. Neema, “MRI in multiple sclerosis: a review of the current literature,” vol. 25, no. 4, pp. 402–409.
- [129] S. Ropele, C. Langkammer, C. Enzinger, S. Fuchs, and F. Fazekas, “Relaxation time mapping in multiple sclerosis,” vol. 11, no. 3, pp. 441–450.
- [130] P. Brex, G. Parker, S. Leary, P. Molyneux, G. Barker, C. Davie, A. Thompson, and D. Miller, “Lesion heterogeneity in multiple sclerosis: a study of the relations between appearances on t1 weighted images, t1 relaxation times, and metabolite concentrations,” vol. 68, no. 5, pp. 627–632.
- [131] F. Bagnato, S. Hametner, B. Yao, P. van Gelderen, H. Merkle, F. K. Cantor, H. Lassmann, and J. H. Duyn, “Tracking iron in multiple sclerosis: a combined imaging and histopathological study at 7 tesla,” vol. 134, pp. 3602–3615.

Bibliography

- [132] “Box cox transformation.”
- [133] M. Filippi, P. Preziosa, and M. A. Rocca, “Magnetic resonance outcome measures in multiple sclerosis trials: time to rethink?,” vol. 27, no. 3, pp. 290–299.
- [134] W. Brück, A. Bitsch, H. Kolenda, Y. Brück, M. Stiefel, and H. Lassmann, “Inflammatory central nervous system demyelination: correlation of magnetic resonance imaging findings with lesion pathology,” vol. 42, no. 5, pp. 783–793.
- [135] M. A. van Walderveen, L. Truyen, B. W. van Oosten, J. A. Castelijns, G. J. Lycklama à Nijeholt, J. H. van Waesberghe, C. Polman, and F. Barkhof, “Development of hypointense lesions on t1-weighted spin-echo magnetic resonance images in multiple sclerosis: relation to inflammatory activity,” vol. 56, no. 3, pp. 345–351.
- [136] S. Nessler, S. Boretius, C. Stadelmann, A. Bittner, D. Merkler, H.-P. Hartung, T. Michaelis, W. Brück, J. Frahm, N. Sommer, and B. Hemmer, “Early MRI changes in a mouse model of multiple sclerosis are predictive of severe inflammatory tissue damage,” vol. 130, pp. 2186–2198.
- [137] P. Giannetti, M. Politis, P. Su, F. Turkheimer, O. Malik, S. Keihaninejad, K. Wu, R. Reynolds, R. Nicholas, and P. Piccini, “Microglia activation in multiple sclerosis black holes predicts outcome in progressive patients: An in vivo [(11)c](r)-PK11195-PET pilot study,” vol. 65, pp. 203–210.
- [138] D. Soon, D. J. Tozer, D. R. Altmann, P. S. Tofts, and D. H. Miller, “Quantification of subtle blood-brain barrier disruption in non-enhancing lesions in multiple sclerosis: a study of disease and lesion subtypes,” vol. 13, no. 7, pp. 884–894.
- [139] M. Bradl and H. Lassmann, “Progressive multiple sclerosis,” vol. 31, no. 4, pp. 455–465.
- [140] B. Ferguson, M. K. Matyszak, M. M. Esiri, and V. H. Perry, “Axonal damage in acute multiple sclerosis lesions,” vol. 120 (Pt 3), pp. 393–399.
- [141] K. E. Hammond, M. Metcalf, L. Carvajal, D. T. Okuda, R. Srinivasan, D. Vigneron, S. J. Nelson, and D. Pelletier, “Quantitative in vivo magnetic resonance imaging of multiple sclerosis at 7 tesla with sensitivity to iron,” vol. 64, no. 6, pp. 707–713.
- [142] A. Roche, F. Forbes, and Alzheimer’s Disease Neuroimaging Initiative, “Partial volume estimation in brain MRI revisited,” vol. 17, pp. 771–778.
- [143] K. B. Walhovd, H. Johansen-Berg, and R. T. Káradóttir, “Unraveling the secrets of white matter – bridging the gap between cellular, animal and human imaging studies,” vol. 276, pp. 2–13.
- [144] R. H. Garman, “Histology of the central nervous system,” vol. 39, no. 1, pp. 22–35.
- [145] J. Kiernan and R. Rajakumar, *Barr’s The Human Nervous System: An Anatomical Viewpoint*. Lippincott Williams & Wilkins.

- [146] E. A. Accolla, J. Dukart, G. Helms, N. Weiskopf, F. Kherif, A. Lutti, R. Chowdhury, S. Hetzer, J.-D. Haynes, A. A. Kühn, and B. Draganski, “Brain tissue properties differentiate between motor and limbic basal ganglia circuits,” vol. 35, no. 10, pp. 5083–5092.
- [147] M. F. Glasser and D. C. V. Essen, “Mapping human cortical areas in vivo based on myelin content as revealed by t1- and t2-weighted MRI,” vol. 31, no. 32, pp. 11597–11616.
- [148] H. Grydeland, K. B. Walhovd, C. K. Tamnes, L. T. Westlye, and A. M. Fjell, “Intracortical myelin links with performance variability across the human lifespan: results from t1- and t2-weighted MRI myelin mapping and diffusion tensor imaging,” vol. 33, no. 47, pp. 18618–18630.
- [149] A. Deistung, A. Schäfer, F. Schweser, U. Biedermann, R. Turner, and J. R. Reichenbach, “Toward in vivo histology: A comparison of quantitative susceptibility mapping (QSM) with magnitude-, phase-, and r2*-imaging at ultra-high magnetic field strength,” vol. 65, pp. 299–314.
- [150] A. F. Sadikot, M. M. Chakravarty, G. Bertrand, V. V. Rymar, F. Al-Subaie, and D. L. Collins, “Creation of computerized 3d MRI-integrated atlases of the human basal ganglia and thalamus,” vol. 5.
- [151] M. M. Chakravarty, G. Bertrand, C. P. Hodge, A. F. Sadikot, and D. L. Collins, “The creation of a brain atlas for image guided neurosurgery using serial histological data,” vol. 30, no. 2, pp. 359–376.
- [152] A. Minagar, M. H. Barnett, R. H. B. Benedict, D. Pelletier, I. Pirko, M. A. Sahraian, E. Frohman, and R. Zivadinov, “The thalamus and multiple sclerosis: modern views on pathologic, imaging, and clinical aspects,” vol. 80, no. 2, pp. 210–219.
- [153] A. A. Utter and M. A. Basso, “The basal ganglia: An overview of circuits and function,” vol. 32, no. 3, pp. 333–342.
- [154] R. M. Ransohoff, D. A. Hafler, and C. F. Lucchinetti, “Multiple sclerosis—a quiet revolution,” vol. 11, no. 3, pp. 134–142.
- [155] S. Markovic-Plese and H. F. McFarland, “Immunopathogenesis of the multiple sclerosis lesion,” vol. 1, no. 3, pp. 257–262.
- [156] D. H. Miller, F. Barkhof, J. A. Frank, G. J. M. Parker, and A. J. Thompson, “Measurement of atrophy in multiple sclerosis: pathological basis, methodological aspects and clinical relevance,” vol. 125, pp. 1676–1695.
- [157] R. H. B. Benedict and R. Zivadinov, “Risk factors for and management of cognitive dysfunction in multiple sclerosis,” vol. 7, no. 6, pp. 332–342.
- [158] S. Messina and F. Patti, “Gray matters in multiple sclerosis: Cognitive impairment and structural MRI,” vol. 2014, p. e609694.

Bibliography

- [159] R. Zivadinov, J. Sepcic, D. Nasuelli, R. De Masi, L. M. Bragadin, M. A. Tommasi, S. Zambito-Marsala, R. Moretti, A. Bratina, M. Ukmar, R. S. Pozzi-Mucelli, A. Grop, G. Cazzato, and M. Zorzon, "A longitudinal study of brain atrophy and cognitive disturbances in the early phase of relapsing-remitting multiple sclerosis," vol. 70, no. 6, pp. 773–780.
- [160] P. S. Giacomini and D. L. Arnold, "Non-conventional MRI techniques for measuring neuroprotection, repair and plasticity in multiple sclerosis," vol. 21, no. 3, pp. 272–277.
- [161] M. F. Callaghan, P. Freund, B. Draganski, E. Anderson, M. Cappelletti, R. Chowdhury, J. Diedrichsen, T. H. B. FitzGerald, P. Smittenaar, G. Helms, A. Lutti, and N. Weiskopf, "Widespread age-related differences in the human brain microstructure revealed by quantitative magnetic resonance imaging," vol. 35, no. 8, pp. 1862–1872.
- [162] P. Hofman, G. Kemerink, J. Jolles, and J. Wilmlink, "Quantitative analysis of magnetization transfer images of the brain: Effect of closed head injury, age and sex on white matter," vol. 42, no. 4, pp. 803–806.
- [163] N. C. Silver, G. J. Barker, D. G. MacManus, P. S. Tofts, and D. H. Miller, "Magnetisation transfer ratio of normal brain white matter: a normative database spanning four decades of life.," vol. 62, no. 3, pp. 223–228.
- [164] M. Rovaris, G. Iannucci, M. Cercignani, M. P. Sormani, N. De Stefano, S. Gerevini, G. Comi, and M. Filippi, "Age-related changes in conventional, magnetization transfer, and diffusion-tensor MR imaging findings: Study with whole-brain tissue histogram analysis1," vol. 227, no. 3, pp. 731–738.
- [165] J. D. Yeatman, B. A. Wandell, and A. A. Mezer, "Lifespan maturation and degeneration of human brain white matter," vol. 5.
- [166] L. Marner, J. R. Nyengaard, Y. Tang, and B. Pakkenberg, "Marked loss of myelinated nerve fibers in the human brain with age," vol. 462, no. 2, pp. 144–152.
- [167] M. Filippi and F. Agosta, "Magnetization transfer MRI in multiple sclerosis," vol. 17 Suppl 1, pp. 22S–26S.
- [168] G. B. Pike, N. De Stefano, S. Narayanan, K. J. Worsley, D. Pelletier, G. S. Francis, J. P. Antel, and D. L. Arnold, "Multiple sclerosis: magnetization transfer MR imaging of white matter before lesion appearance on t2-weighted images," vol. 215, no. 3, pp. 824–830.
- [169] M. Filippi, M. A. Rocca, G. Martino, M. A. Horsfield, and G. Comi, "Magnetization transfer changes in the normal appearing white matter precede the appearance of enhancing lesions in patients with multiple sclerosis," vol. 43, no. 6, pp. 809–814.
- [170] F. Fazekas, S. Ropele, C. Enzinger, T. Seifert, and S. Strasser-Fuchs, "Quantitative magnetization transfer imaging of pre-lesional white-matter changes in multiple sclerosis," vol. 8, no. 6, pp. 479–484.

Guillaume Bonnier

Name: Guillaume BONNIER
Date of birth: 23.03.1983
Citizenship: French
Family Status: in partnership, one child
Email: guillaume.bonnier@unil.ch;
Phone: + 41 77 4419591

PROFILE

Reliable, creative and motivated engineer with research experience in advanced neuroimaging methods and computer vision. I possess excellent communication skills and can work independently or as part of a team.

PROFESSIONAL EXPERIENCE

- 2011-2015 :** Research engineer, PhD student in **Advanced Clinical Imaging** Technology, Siemens-EPFL, Lausanne.
- **Advanced magnetic resonance imaging (MRI) techniques** to study the physiopathology of multiple sclerosis.
 - Web application development to process MRI images
- 2007-2011 :** Computer vision research engineer in **Computer Vision Laboratory** at EPFL.
- **2D tracking** of level of Hydroptere's foils immersion.
 - **Software development.**
 - **3D reconstruction of deformable object** from monocular images.
- 2005-2006 :** Work placement at **Cybernetix SA** (specialist in **robotic** and industrial plants)
- **Image processing** (rails space measurement)
 - Embedded software development
 - **Teamwork, communication and time management**

EDUCATION

- 2011-2015 :** **PhD**, Advanced Clinical Imaging Technology Laboratory, Siemens-EPFL, Lausanne. Advisor: Pr J.P Thiran. Universtiy of Lausanne. Dpt of Biologie and medicine (thesis defense scheduled on 22.05.2015).
- 2007 :** **Master diploma** from ESCPE Lyon in **Electronic, Telecommunication and computer science.**
- 2006-2007 :** ERASMUS student at EPFL (Ecole Polytechnique Fédérale de Lausanne) in the **Computer and Communication Science** section.
- 2003-2005 :** Engineer student at ESCPE Lyon in **Electronic/Telecommunication/Computer science** section.
- 2001-2003 :** **Classes préparatoires** in **Math/Physique** in Lycée Thiers of Marseille.
- 2001 :** **French Baccalaureate S (equivalent to A-levels)** (with honor).

SCIENTIFIC ACTIVITY:

Original Articles:

1. **Bonnier G.**, Roche A., Romascano D., Simioni S., Meskaldji D., Rotzinger D., Lin Y.C., Menegaz G., Schlupe M., Du Pasquier R., Sumpf T.J., Frahm J., Thiran J.P., Krueger G., Granziera C. Advanced MRI unravels the nature of tissue alterations in early multiple sclerosis. *Annals of Clinical and Translational Neurology*, 2014 Jun;1(6):423-32.
2. Simioni S., Amaru F., **Bonnier G.**, Roche A., Kober T., Rotzinger D., Schlupe M., Dupasquier R., Meuli R., Sbarbati A., Thiran J.P., Krueger G. and Granziera C. MP2RAGE provides new clinically-compatible correlates of mild cognitive deficits in early multiple sclerosis. *Journal of Neurology*, 2014 Jun 10.
3. Romascano D., Meskaldji D.E., **Bonnier G.**, Simioni S., Rotzinger D., Lin Y., Menegaz G., Roche A., Schlupe M., Du Pasquier R., Richiardi J., Van De Ville D., Daducci A., Sumpf T.J., Frahm J., A. Thiran J.P., Krueger G., and Granziera C. Multi-contrast *connectometry*: a new tool to assess cerebellum alterations in early relapsing-remitting multiple sclerosis. *Human Brain Mapping*, 2014 Nov 24.
4. **Bonnier G.**, Roche A., Romascano D., Simioni S., Meskaldji D., Rotzinger D., Lin Y.C., Menegaz G., Schlupe M., Du Pasquier R., Sumpf T.J., Frahm J., Thiran J.P., Krueger G., Granziera C. Multi-contrast MRI quantification of focal inflammation and degeneration in multiple sclerosis. *BioMed International*, 2014 in press.
5. Granziera C., Daducci A., **Bonnier G.**, Romascano D., Roche A., Bach Cuadra M., Schmitter D., Kloeppe S., Meuli R., von Gunten A. and Krueger G. A multi-contrast MRI study of microstructural brain damage in patients with mild cognitive impairment. *Neurobiol of Aging*, under revision.
6. Fartaria M. J., **Bonnier G.**, Roche A., Kober T., Meuli R., Rotzinger D., R. Frackowiak, Schlupe M., Du Pasquier R., Thiran J.-P., Krueger G., Bach Cuadra M., Granziera C. Automated detection of white matter and cortical lesions in early-stages of multiple sclerosis based on advanced magnetic resonance imaging. *Neuroimage*, under revision.

Conference abstracts:

1. **Bonnier, G.**, Sumpf T., Romascano D., Roche A., Schlupe M., Dupasquier R., G. Krueger and Granziera C. Ultrafast T2-mapping of multiple sclerosis pathology in early disease. ISMRM 2013 (Salt Lake City, USA), Electronic poster.
2. O' Brian K., **Bonnier, G.**, Roche A., Kober T. Lazeyras F., G. Krueger and Granziera C. Feasibility of whole brain high-resolution quantitative T1 and T2* at 7T: regional investigation of pathology in early multiple sclerosis. 4th annual symposium of Ultra High Field Magnetic Resonance Imaging 2013 (Berlin, Germany).
3. **Bonnier G.**, Roche A., Romascano D., Simioni S., Meskaldji D., Rotzinger D., Lin Y.C., Menegaz G., Schlupe M., Dupasquier R., Sumpf T.J., Frahm J., Thiran J.P., Krueger G. and Granziera C. Multicontrats MRI improved the clinico-radiological correlation in early multiple sclerosis patients with minor deficits. ISMRM 2014 (Milan, Italy), Traditional poster.
4. **Bonnier G.**, Roche A., Romascano D., Simioni S., Meskaldji D., Rotzinger D., Lin Y.C., Menegaz G., Schlupe M., Dupasquier R., Sumpf T.J., Frahm J., Thiran J.P., Krueger G. and Granziera C. Multiple Sclerosis lesion fingerprint using multicontrast MRI ISMRM 2014 (Milan, Italy), Traditional poster.
5. Romascano D., Meskaldji, **Bonnier G.**, Simioni S., Rotzinger D., Lin Y.C., Menegaz G., Roche A., Schlupe M., Du Pasquier R., Richiardi J., Van De Ville D., Daducci A., Sumpf T.J., Frahm J., Thiran J.P., Krueger G. and Granziera C. "Cerebellar connectomics provides new biomarkers in early multiple sclerosis. ISMRM 2014 (Milan, Italy), Electronic poster.

6. **Bonnier G.** Mortamet B. Thiran J.P., Krueger G., Kober T. and Granziera C.. Longitudinal analysis of advanced and conventional magnetic resonance imaging measures of disease impact in multiple sclerosis. ISMRM 2015 (Toronto, Canada). Traditionnal poster.

7. **Bonnier G.**, Thiran J.P., Krueger G. , Kober T., Granziera C. and Roche A.. Concentration maps improve detection of gray matter alteration in cerebellum and deep gray matter structures. ISMRM 2015 (Toronto, Canada). Traditionnal poster.

8. Babayeva M., Falkovskiy P., Hilbert T., **Bonnier G.**, Maréchal B., Meuli R., Thiran J.P., Gruetter, R. Krueger G., and Kober T. . Prospective motion correction with FID-triggered image navigators. ISMRM 2015 (Toronto, Canada). Oral presentation.